AD_____

Award Number: DAMD17-00-1-0415

TITLE: Functional Analysis of the ErbB4 Receptor Tyrosine Kinase

PRINCIPAL INVESTIGATOR: David J. Riese

CONTRACTING ORGANIZATION: Purdue Research Foundation
West Lafayette, Indiana 47907

REPORT DATE: July 2001

TYPE OF REPORT: Annual Summary

PREPARED FOR: U.S. Army Medical Research and Materiel Command
Fort Detrick, Maryland 21702-5012

REPORT DOCUMENTATION PAGE

Form Approved
OMB No. 074-0188

1. AGENCY USE ONLY (Leave blank)	2. REPORT DATE	3. REPORT TYPE AND DATES COVERED
	July 2001	Annual Summary (1 Jul 00 - 30 Jun 01)

4. TITLE AND SUBTITLE
Functional Analysis of the ErbB4 Receptor Tyrosine Kinase

5. FUNDING NUMBERS
DAMD17-00-1-0415

6. AUTHOR(S)
David J. Riese

7. PERFORMING ORGANIZATION NAME(S) AND ADDRESS(ES)

Purdue Research Foundation
West Lafayette, Indiana 47907

E-Mail: driese@purdue.edu

8. PERFORMING ORGANIZATION REPORT NUMBER

9. SPONSORING / MONITORING AGENCY NAME(S) AND ADDRESS(ES)

U.S. Army Medical Research and Materiel Command
Fort Detrick, Maryland 21702-5012

10. SPONSORING / MONITORING AGENCY REPORT NUMBER

11. SUPPLEMENTARY NOTES

12a. DISTRIBUTION / AVAILABILITY STATEMENT
Approved for Public Release; Distribution Unlimited

12b. DISTRIBUTION CODE

13. Abstract ***(Maximum 200 Words)*** *(abstract should contain no proprietary or confidential information)*

This career development award is supporting a multi-faceted, multidisciplinary approach to elucidate the roles of EGF (epidermal growth factor) family hormones and ErbB receptors in breast cancer and to develop novel strategies to target these hormones and receptors. We have four major efforts underway. (1) We have been assaying novel quinazolines and analogs of lavendustin A for inhibition of EGFR tyrosine kinase activity. The goal is to identify potential breast tumor imaging agents and breast tumor chemotherapeutics that target the EGFR. (2) We have constructed a constitutively active mutant of the ErbB4 receptor tyrosine kinase. The activities of this mutant suggest that ErbB4 may be coupled to mammary tumor cell growth arrest and mammary tumor suppression. (3) We have identified the ErbB family receptors that are activated by four novel EGF family hormones. This is the first step in determining the role that these hormones may play in mammary tumorigenesis. (4) We have identified amino acid residues in the EGF family hormone Neuregulin2beta that are critical for activation of ErbB4 signaling by this hormone. This is the first step in developing potential breast cancer therapeutics that specifically target ErbB4.

14. SUBJECT TERMS

15. NUMBER OF PAGES
157

16. PRICE CODE

17. SECURITY CLASSIFICATION OF REPORT	18. SECURITY CLASSIFICATION OF THIS PAGE	19. SECURITY CLASSIFICATION OF ABSTRACT	20. LIMITATION OF ABSTRACT
Unclassified	Unclassified	Unclassified	Unlimited

Table of Contents

Cover	1
SF 298	2
Table of Contents	3
Introduction	4
Body	5 - 7
Key Research Accomplishments	8
Reportable Outcomes	9 - 10
Conclusions	11
References	11
Appendices	11 - 155

Introduction

This career development award is partially supporting a multifaceted, multidisciplinary approach to elucidate the roles of EGF (epidermal growth factor) family hormones and ErbB family receptor tyrosine kinases in breast cancer and to develop novel strategies to target these hormones and receptors. We have a number of efforts underway: (1) we are screening novel small molecules to identify potent specific ErbB family receptor tyrosine kinase inhibitors; (2) we have generated a constitutively-active mutant of the ErbB4 receptor tyrosine kinase and we are using this mutant to elucidate ErbB4 function; (3) we have identified the ErbB family receptors that are activated by novel EGF family hormones; (4) we have used genetic strategies to identify amino acid residues in EGF family hormones that are critical for ErbB receptor activation; (5) we are screening an oligonucleotide library for aptamer ligands for EGFR/ErbB1 (epidermal growth factor receptor), ErbB2/HER2/Neu, and ErbB4.

Report Body

1. Characterize putative inhibitors of ErbB family receptor tyrosine kinases. We have screened novel quinazolines and novel analogs of lavendustin A to identify novel, specific inhibitors of ErbB family receptor tyrosine kinases. This is the first step in developing novel breast tumor imaging agents that identify the most aggressive tumors by targeting tumor cells that overexpress EGFR or ErbB2. These experiments are being performed in collaboration with the laboratory of Dr. Mark Cushman at Purdue University and the laboratory of Dr. Henry VanBrocklin at the Lawrence Berkeley National Laboratory.

We have identified a number of novel EGFR tyrosine kinase inhibitors, some of which are quite potent. The results of the screen of the lavendustin A analogs are described in a research article published in the *Journal of Medicinal Chemistry*. A copy of this article can be found in the appendix (Mu, *et al*). Dr. Van Brocklin is preparing a manuscript that describes the results of the screen of the quinazoline analogs.

While we have identified some potent inhibitors of the EGFR tyrosine kinase, none of the molecules identified to date are suitable tumor imaging agents; the ^{18}F-labeled analogs of these compounds are readily metabolized in the liver. Dr. VanBrocklin is preparing a manuscript that describes the results of these experiments.

These experiments have been supported in part by an NIH grant to Dr. Riese (R21CA80770). However, this grant expired 3/31/01 and this grant is not renewable. Dr. VanBrocklin and Dr. Cushman have grant proposals to generate and screen additional tyrosine kinase inhibitors under consideration at NIH/NCI. Dr. Riese is named as a co-investigator on these proposals and his laboratory will receive support from these grants should they be funded. Continued pursuit of this avenue of research is dependent on receiving this additional funding.

2. Define ErbB4 coupling to biological responses. We have generated three constitutively-active mutants of the ErbB4 receptor tyrosine kinase. We are expressing these mutants in variety of cellular and organismal contexts to define the functional role of ErbB4 signaling. Obviously, we are particularly interested in the role of ErbB4 signaling in breast cancer.

These mutants, unlike constitutively-active ErbB2/HER2/Neu mutants, do NOT cause anchorage independence, increased growth rates, increased saturation densities, or a loss of contact inhibition in fibroblast cell lines. These results are described in a draft of a manuscript being prepared for submission. A copy of this draft can be found in the appendix (Penington, *et al*). These data suggest that ErbB2 and ErbB4 play distinct roles in mammary tumorigenesis. Indeed, we have generated preliminary data indicating that one of our constitutively-active ErbB4 mutants is coupled to reduced colony formation and reduced cell proliferation in mammary and prostate tumor cell lines. These data suggest that ErbB4 may be a tumor suppressor and that reduced ErbB4 expression and signaling plays a causative role in mammary and prostate tumorigenesis. Additional experiments to evaluate the effect of ErbB4 signaling on mammary and prostate tumor cell line proliferation, differentiation, and malignant phenotype are underway. Moreover, in collaboration with Dr. William Muller at McMaster University, we are generating transgenic mice that express the constitutively-active ErbB4 mutants in the mammary epithelium. These mice will enable us to test our ErbB4 tumor suppressor hypothesis.

Report Body (continued)

These experiments are being supported by a USAMRMC BCRP Idea grant (DAMD-17-00-0416) as well as by undergraduate research fellowships to Mr. Eric Williams and Ms. Ianthe Bryant. Dr. Riese has submitted an application for a USAMRMC PCRP grant to support these experiments and Dr. Shruti Shukla has submitted an application for a USAMRMC BCRP postdoctoral fellowship.

3. Characterize biological responses to recombinant neuregulins. We have developed a system to express and purify novel recombinant neuregulins, which are members of the EGF family of peptide hormones. We have identified the patterns of ErbB family receptor tyrosine phosphorylation and signaling that are activated by each of these four recombinant neuregulins. Neuregulin 2alpha (NRG2α) and neuregulin2beta (NRG2β) are both ErbB3 agonists, but neuregulin3 (NRG3) and neuregulin4 (NRG4) are not. NRG2β is the most potent ErbB4 agonist whereas NRG3 and NRG4 are more modest ErbB4 agonists and NRG2α is a weak ErbB4 agonist. Figures 1 and 2 in the appendix to this report show examples of our data. These results are described in a draft of a manuscript being prepared for submission. These experiments have been supported in part by an NIH grant to Dr. Riese (R21CA80770). However, this grant expired 3/31/01 and this grant is not renewable.

4. Identify and characterize the ErbB4 binding domain of neuregulin2β (NRG2β). NRG2α and NRG2β are splicing isoforms of the same gene. NRG2β is a potent ErbB4 agonist, whereas NRG2α is not (Figure 2). We have generated mutants of NRG2α and NRG2β to identify amino acid residues that are sufficient and necessary for activation of ErbB4 signaling by NRG2 isoforms. We have determined that Phe45 of NRG2β is necessary and sufficient for activation of ErbB4 tyrosine phosphorylation by NRG2. Figures 3 and 4 in the appendix to this report show examples of our data. These results are described in a draft of a manuscript being prepared for submission. These give us important clues as to how binding of EGF family hormones to ErbB4 is specified. These clues are the first steps in our attempts to generate specific synthetic or recombinant ErbB4 agonists and antagonists. Such molecules will be useful in probing ErbB4 function and may be useful in staging or treating breast and prostate cancers. These experiments have been supported in part by an NIH grant to Dr. Riese (R21CA80770) and an NIH sabbatical leave fellowship to Dr. Robert P. Hammer of Louisiana State University (F33CA85049). However, both of these grants have expired and neither is renewable. This winter we intend to submit a new application for an NIH/NCI R01 grant to support these experiments.

Report Body (continued)

5. Screen an oligonucleotide library for aptamer ligands for EGFR, ErbB2, and ErbB4. In collaboration with Dr. Henry VanBrocklin at the Lawrence Berkeley National Laboratory, our goal is to generate synthetic oligonucleotide (aptamer) ligands for EGFR, ErbB2, and ErbB4. We will use these aptamers to develop imaging agents that will be used in positron emission tomography (PET) scanning to noninvasively assess EGFR, ErbB2, and ErbB4 expression levels in normal and malignant tissues *in vivo*. Such imaging agents should permit noninvasive staging of tumor aggressiveness and aggressive tumor metastases.

We have expressed and purified a secreted, recombinant form of the human ErbB2 extracellular domain. We have coupled this protein to nickel ion beads and shown that this affinity reagent retains the epitopes of the native ErbB2 extracellular domain. We have used this affinity reagent to identify conditions for screening the oligonucleotide library, including aptamer binding, aptamer elution and recovery, and aptamer amplification. These results are described in a draft of a manuscript being prepared for submission. A copy of this draft can be found in the appendix (Riese, *et al*). These studies are being supported by a grant from NIH (R21CA89274) to Dr. Riese.

In the near future we will be beginning to screen an oligonucleotide library for ErbB2 aptamer ligands. We are also expressing and purifying a secreted, recombinant form of the EGFR and ErbB4 extracellular domains. We will use these proteins to screen an oligonucleotide library for EGFR and ErbB4 aptamer ligands.

Key Research Accomplishments

Task 1

- Screened novel lavendustin A analogs for inhibition of EGFR, ErbB2, and ErbB4 tyrosine kinase activity and for inhibition of EGFR coupling to cell proliferation.
- Screened novel quinazolines for inhibition of EGFR, ErbB2, and ErbB4 tyrosine kinase activity and for inhibition of EGFR coupling to cell proliferation.

Task 2

- Generated a set of three constitutively-active ErbB4 mutants and demonstrated that these mutants do not malignantly transform the growth of a rodent fibroblast cell line.
- In preliminary experiments, we have demonstrated that one of the constitutively-active ErbB4 mutants appears to be coupled to reduced colony formation and reduced cell proliferation in a panel of human mammary and prostate tumor cell lines. Additional experiments to evaluate the consequences of ErbB4 signaling on cellular function are underway.

Task 3

- Developed a system to express and purify recombinant neuregulins.
- Assayed recombinant neuregulins for stimulation of ErbB family receptor tyrosine phosphorylation.

Task 4

- Generated putative NRG2α "gain of function" and NRG2β "loss of function" mutants.
- Assayed NRG2α and NRG2β mutants for activation of ErbB4 tyrosine phosphorylation.
- Determined that NRG2β Phe45 is sufficient and necessary (within the context of NRG2) for activation of ErbB4 tyrosine phosphorylation.

Task 5

- Expressed a recombinant, secreted form of the ErbB2 extracellular domain.
- Coupled this recombinant protein to nickel ion beads to form an affinity matrix suitable for screening libraries for ErbB2 ligands.
- Validated this affinity reagent as being suitable for screening libraries for ErbB2 ligands.
- Began developing conditions and protocols for screening oligonucleotide libraries for ErbB2 aptamer ligands using this affinity reagent.

Reportable Outcomes

Task 1

- We published a manuscript that describes the results of our screen of the lavendustin A analogs. A copy of this publication is included in the appendix of this report (Mu, *et al*).
- We submitted a pending grant application to NCI/NIH for additional funding to support our efforts to synthesize and screen novel lavendustin A analogs (Dr. Mark Cushman, PI).
- We submitted a pending grant application to NCI/NIH for additional funding to support our efforts to synthesize and screen novel quinazolines (Dr. Henry VanBrocklin, PI).

Task 2

- We prepared a manuscript that describes the construction and analysis of our constitutively-active ErbB4 mutants. A copy of the manuscript draft is included in the appendix of this report (Penington, *et al*).
- Mr. Desi Penington wrote and successfully defended a master's degree thesis entitled "Construction and analysis of constitutively-active mutants of the ErbB4 receptor tyrosine kinase" that is based on the results of the studies described in Task 2. A copy of Mr. Penington's thesis is included in the appendix of this report. Mr. Penington will receive his M.S. in August 2001.
- We submitted a pending grant application to the USAMRMC PCRP for additional funding to support our efforts to analyze ErbB4 function in prostate cancer cells (Dr. David J. Riese II, PI).
- We were awarded an undergraduate research fellowship by the American Association of Colleges of Pharmacy to support our efforts to analyze ErbB4 function in prostate cancer cells (Mr. Eric Williams, PI; Dr. David J. Riese II , mentor).
- We submitted a pending postdoctoral fellowship application to the USAMRMC BCRP for additional funding to support our efforts to analyze ErbB4 function in breast cancer cells (Dr. Shruti Shukla, PI; Dr. David J. Riese II, mentor).
- We were awarded an undergraduate research fellowship by the American Society for Microbiology to support our efforts to analyze ErbB4 function in breast and prostate cancer cells (Ms. Ianthe Bryant, PI; Dr. David J. Riese II, mentor).

Task 3

- We are preparing a manuscript that describes the expression and purification of recombinant neuregulins. This manuscript will also describe the patterns of ErbB family receptor signaling that are stimulated by each neuregulin.

Task 4

- We are preparing a manuscript that describes the construction and functional analyses of the NRG2 mutants.

Reportable Outcomes (continued)

Task 5

- We prepared a manuscript that describes the expression and purification of the recombinant ErbB2 extracellular domain. This manuscript describes the validation of this recombinant protein as an affinity reagent suitable for screening an oligonucleotide library for aptamer ligands of ErbB2. Finally, this manuscript describes the identification of conditions suitable for screening an oligonucleotide library for aptamer ligands of ErbB2. A copy of the manuscript draft is included in the appendix of this report (Riese, *et al*).
- We were awarded an NIH grant (R21CA89274; Dr. David J. Riese II, PI) to isolate aptamer ligands for ErbB2 and to begin assessing the utility of radiolabeled analogs of these molecules as tumor imaging agents.

Conclusions

We have made significant progress on all five of our goals. We have screened and hopefully will continue to screen novel quinazolines and lavendustin A analogs to identify EGFR tyrosine kinase inhibitors that may be suitable for the development of novel tumor imaging agents. We have generated three constitutively-active ErbB4 mutants that are enabling us to elucidate ErbB4 functions. We have characterized the patterns of ErbB family receptor signaling stimulated by four novel NRGs. We have identified an amino acid residue critical for activation of ErbB4 signaling by NRG2. We have developed a reagent and methodologies suitable for screening an oligonucleotide library for aptamer ligands for ErbB2.

References

None

Appendices: List of Documents (144 pages total)

1. Mu F., Coffing S., Riese D.J. II, Geahlen R.L., Verdier-Pinard P., Hamel E., Johnson J., and Cushman M. (2001) "Design, Synthesis, and Biological Evaluation of a Series of Lavendustin A Analogues That Inhibit EGFR and Syk Tyrosine Kinases as Well as Tubulin Polymerization." *J. Med. Chem.* **44**: 441-452 (12 pages).
2. Penington D.J., Bryant I., and Riese D.J. II. "Constitutively-Active ErbB4 and ErbB2 Mutants Exhibit Distinct Biological Activities." For submission to *Cell Growth and Differentiation* (35 pages).
3. "Construction and Analysis of Constitutively-Active Mutants of the ErbB4 Receptor Tyrosine Kinase", M.S. Thesis, Mr. Desi Penington, July 2001 (65 pages).
4. Unpublished Figure 1. "Neuregulin2α and Neuregulin2β stimulate ErbB3 signaling, but Neuregulin3 and Neuregulin4 do not." (1 page)
5. Unpublished Figure 2. "Neuregulin2β is a potent ErbB4 agonist, whereas Neuregulin3 and Neuregulin4 are weaker agonists and Neuregulin2α does not stimulate ErbB4 signaling." (1 page)
6. Unpublished Figure 3. "Phenylalanine45 of NRG2β is required for activation of ErbB4 tyrosine phosphorylation by NRG2β." (1 page)
7. Unpublished Figure 4. "Phenylalanine45 of NRG2β is sufficient for activation of ErbB4 tyrosine phosphorylation by NRG2α." (1 page)
8. Riese D.J. II, Denson C., Sajan S., Vanderpoel J., Vortherms T., Morris A., Slavik S., Coffing S., Hammer R.P., and Beussman D. "Generation and Validation of a Reagent Suitable for the Isolation of Aptamer Ligands for the ErbB2/HER2/Neu Receptor Tyrosine Kinase." For submission to *Biochemical and Biophysical Research Communications* (28 pages).

Design, Synthesis, and Biological Evaluation of a Series of Lavendustin A Analogues That Inhibit EGFR and Syk Tyrosine Kinases, as Well as Tubulin Polymerization

Fanrong Mu,[†] Stephanie L. Coffing,[†] David J. Riese II,[†] Robert L. Geahlen,[†] Pascal Verdier-Pinard,[‡] Ernest Hamel,[‡] Jill Johnson,[§] and Mark Cushman*,[†]

Department of Medicinal Chemistry and Molecular Pharmacology, School of Pharmacy and Pharmacal Sciences, Purdue University, West Lafayette, Indiana 47907, Screening Technologies Branch, Developmental Therapeutics Program, Division of Cancer Treatment and Diagnosis, National Cancer Institute, Frederick Cancer Research and Development Center, Frederick, Maryland 21702, and Developmental Therapeutics Program, Division of Cancer Treatment and Diagnosis, National Cancer Institute, National Institutes of Health, Rockville, Maryland 20852

Received September 5, 2000

A series of *N*-alkylamide analogues of the lavendustin A pharmacophore were synthesized and tested for inhibition of the epidermal growth factor receptor (EGFR) protein tyrosine kinase and the nonreceptor protein tyrosine kinase Syk. Although several compounds in the series were effective inhibitors of both kinases, it seemed questionable whether their inhibitory effects on these kinases were responsible for the cytotoxic properties observed in a variety of human cancer cell cultures. Accordingly, a COMPARE analysis of the cytotoxicity profile of the most cytotoxic member of the series was performed, and the results indicated that its cytotoxicity profile was similar to that of antitubulin agents. This mechanism of action was supported by demonstrating that most compounds in the series were moderately effective as inhibitors of tubulin polymerization. This suggests that the lavendustin A analogues reported here, as well as some of the previously reported lavendustin A analogues, may be acting as cytotoxic agents by a mechanism involving the inhibition of tubulin polymerization.

Introduction

The protein tyrosine kinases (PTKs) play critical roles in many of the signal transduction processes that control cell growth, differentiation, mitosis, and death. They are therefore important targets for the development of therapeutic agents for the treatment of diseases that are characterized by uncontrolled cell proliferation, such as cancer and psoriasis.[1−3] Fractionation of a butyl acetate culture extract from *Streptomyces griseolavendus* led to the isolation of the novel PTK inhibitor lavendustin A.[4] Structure **1** was proposed for lavendustin A on the basis of ^{1}H and ^{13}C NMR data, and this tentative assignment was confirmed by total synthesis.[4] Lineweaver−Burke analysis carried out in the presence of varying concentrations of ATP and the substrate indicated that the inhibition was competitive with respect to ATP and noncompetitive with respect to the substrate when tested on the epidermal growth factor receptor (EGFR) tyrosine kinase,[4] although subsequent studies showed that lavendustin A can function as a hyperbolic mixed-type inhibitor with respect to both ATP and substrate.[5] It was also determined that the lavendustin A fragment **2** was as potent as the parent compound **1**, suggesting that **2** is the biologically active "pharmacophore" of lavendustin A.

These initial reports have stimulated work on the synthesis of lavendustin A itself and the synthesis and biological investigation of a variety of lavendustin

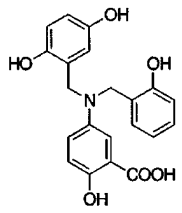

1

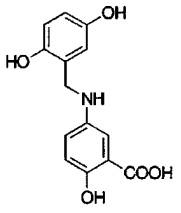

2

analogues.[6−15] The ester derivative **3** and the amide **4** were both found to compare favorably with the lavendustin A pharmacophore **2**. In particular, the ester **3** was as potent as **2** versus the EGFR tyrosine kinase in a cell-free assay, but **3** was more potent than **2** as an inhibitor of EGF-stimulated DNA synthesis in ER 22 cells.[10] Furthermore, the amide **4** was reported to be more potent than **2** as an inhibitor of EGFR tyrosine kinase in a cell-free system.[13] In view of these results, and as an extension of our earlier work on the solid-phase synthesis of lavendustin A and derivatives,[15] we decided to synthesize and evaluate a series of amide derivatives of lavendustin A having the general structure **5**. These compounds have been tested versus both the receptor PTK EGFR in BaF3 mouse lymphoid cells as well as the nonreceptor PTK Syk in a cell-free system. In addition, the new compounds in this series were evaluated as cytotoxic agents using a variety of cultured human cancer cell lines, and the cytotoxicity profile of at least one agent, **13b**, was found to be similar to that of antitubulin drugs when analyzed using the COMPARE algorithm.[16−18] Since the COMPARE program was developed as a predictor of mechanism of action, these results led to the hypothesis that the lavendustin

* To whom correspondence should be addressed. Tel: 765-494-1465. Fax: 765-494-1414. E-mail: cushman@pharmacy.purdue.edu.
[†] Purdue University.
[‡] Frederick Cancer Research and Development Center.
[§] National Institutes of Health.

10.1021/jm000387g CCC: $20.00
Published on Web 01/03/2001

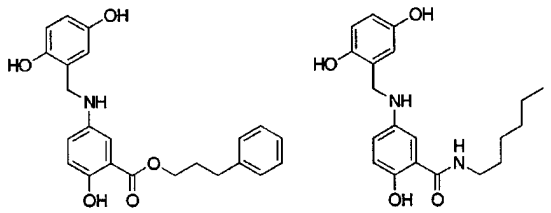

3

4

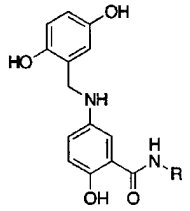

5

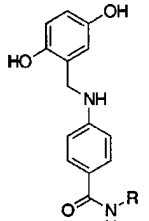

6

A analogues in our series were functioning as inhibitors of tubulin polymerization, and the appropriate assays were performed to test this hypothesis.

The COMPARE Algorithm

The COMPARE program was developed at the Developmental Therapeutics Program, National Cancer Institute (NCI), to interpret the emerging data from the 60-cell line in vitro human cancer cell cytotoxicity screen and display it in way that would facilitate comparison of the different patterns of dose–response curves produced by different cytotoxic agents. Paull and colleagues developed the "mean graph" representation of the screening data in which the mean concentration affecting all 60 cell lines at three levels of effect (GI_{50} = concentration causing 50% inhibition of growth; TGI = concentration causing total inhibition of growth; LC_{50} = concentration causing 50% cell kill) is plotted in the midline of the graph and the behavior of each individual cell line is represented as a deflection to the left for cells more resistant than the mean and to the right for cells more sensitive than the mean.[17] An important application of this manner of presentation is provided by the richly informative patterns of activity that emerge. Correlations of activity patterns can be quantified using a pattern recognition algorithm named COMPARE.[16] Use of the COMPARE program led to the realization that compounds with the same or similar mechanisms of action often result in cytotoxicity patterns that are similar.[16] This approach has resulted in identification of new tubulin polymerization inhibitors,[19] topoisomerase I and II inhibitors,[20,21] and dihydroorotate dehydrogenase inhibitors.[22] In another example, the use of COMPARE linked the effects of cucurbitacin[23] and jasplakinolide[24] to the actin cytoskeleton. Compounds with unique cytotoxicity profiles, suggesting modes of action not shared with the known clinically active classes of chemotherapeutic agents, have also been identified.[25]

A COMPARE analysis for a test agent can be run against the entire database of more than 77 000 compounds that have been tested in the NCI cell line cytotoxicity assay or against a database of standard agents whose mechanism of cytotoxicity is well-documented or against a single compound. The result of the analysis is a list of compounds in rank order and Pearson correlation coefficients, which provide an indication of the similarity of the patterns of cell line responses. Correlation coefficients of ≥ 0.60 are generally considered to be meaningful. For example, when a COMPARE is performed using paclitaxel as the seed, the correlation coefficient for vinblastine sulfate (another tubulin-interactive agent) is 0.88, whereas the correlation coefficient for phyllanthoside (a topoisomerase II inhibitor) is 0.422. The hypothetical mechanism of action suggested by COMPARE analysis can then be confirmed by laboratory testing. The reason that COMPARE analysis is a predictor of mechanism of action is that biological targets are expressed to a different extent in different cell lines, so that compounds which interact with a single biological target will have similar cytotoxicity patterns when tested in these cell lines.[26]

A COMPARE analysis was performed using **13b** as a seed. The top 20 compounds in the COMPARE analysis included 9 taxanes, 3 colchicine analogues, 2 combretastatins, and vinblastine, all of which interact with tubulin. Representative correlation coefficients between **13b** and various tubulin-interactive drugs were docetaxel, 0.790; vinblastine sulfate, 0.761; paclitaxel, 0.703; and maytansine, 0.701.

Synthesis

The synthesis of the series of lavendustin A analogues **13a–m** is a modification of a previously published route used to prepare a series of lavendustin A hydroxamic acid derivatives (Scheme 1).[10] Treatment of commercially available 5-aminosalicylic acid (**7**) with di-*tert*-butyl dicarbonate and triethylamine in aqueous dioxane afforded the Boc-protected intermediate **8**. Reaction of **8** with the appropriate primary amines **9a–m** in the presence of 1-(3-dimethylaminopropyl)-3-ethylcarbodiimide hydrochloride (EDCI), 1-hydroxybenzyltriazole hydrate (HOBt), and triethylamine in dry DMF yielded the series of amides **10a–m**. Deprotection of the intermediates **10a–m** with a mixture of dichloromethane and trifluoroacetic acid resulted in the formation of the primary amines **11a–m**. Reaction of **11a–m** with 2,5-dihydroxybenzaldehyde (**12**) afforded the corresponding Schiff bases, which were reduced with sodium cyanoborohydride to provide the desired lavendustin A analogues **13a–m**.

As outlined in Scheme 2, a variation of this route was executed in order to obtain the congeners **18a–c**, in which the aniline part of the molecule is substituted in the para position with various amides. Similarly, the lavendustin A analogue **23**, having a β-phenethylamide substituent in the meta position relative to the aniline nitrogen but lacking an adjacent phenolic hydroxyl group, was prepared as shown in Scheme 3.

Biological Results and Discussion

The lavendustin A analogues were examined for antiproliferative activity against the human cancer cell lines in the NCI cytotoxicity screen, in which the activity of each compound was evaluated using approximately 55 different cancer cell lines of diverse tumor origins. The mean-graph midpoint values (MGMs) listed in

Scheme 1

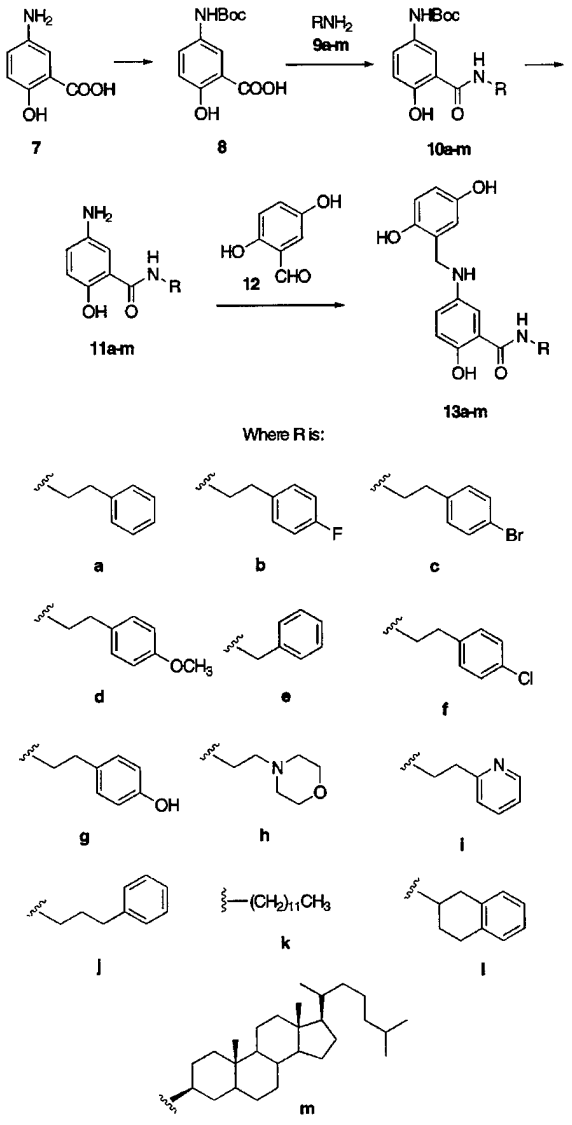

Table 1 are based on a calculation of the average GI_{50} values for all of the cancer cell lines tested (approximately 55) in which GI_{50} values below and above the test range (10^{-4}–10^{-8} M) are taken as the minimum (10^{-8} M) and maximum (10^{-4} M) drug concentrations used in the screening test.[18] A more detailed listing of the cytotoxicities of each compound in eight representative human cancer cell lines is presented in Table 2. With the exception of the cholestane derivative **13m**, all of the compounds in the series were found to be cytotoxic in human cancer cell cultures, with MGM values ranging from 0.35 to 20.4 μM. Starting with the basic β-phenylethylamine **13a**, which had an MGM of 14.8 μM, various substituents were introduced into the para position in order to determine how they affected cytotoxicity. The substituent that resulted in the greatest cytotoxicity was fluorine (**13b**, MGM 0.35 μM), followed by bromine (**13c**, MGM 7.6 μM), chlorine (**13f**, MGM 10.0 μM), methoxy (**13d**, MGM 15.4 μM), and hydroxy (**13g**, MGM 20.4 μM). Lengthening the chain of **13a** by one methylene unit had no appreciable effect

Scheme 2

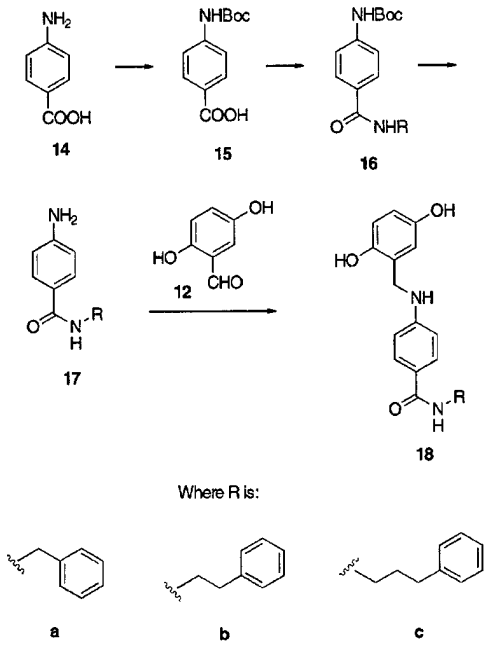

Scheme 3

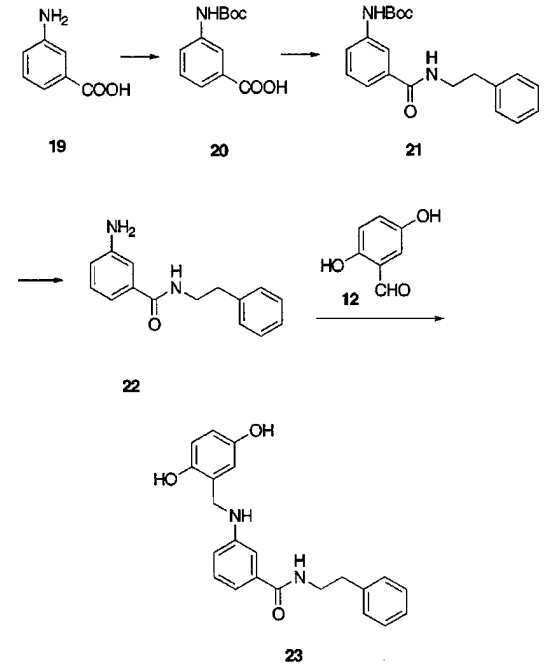

on cytotoxicity (**13j**, MGM 13.2 μM), and shortening it by one methylene group also had little effect on cytotoxicity (**13e**, MGM 15.5 μM). The replacement of the benzene ring by a 2-pyridyl substituent (**13i**, MGM 16.0 μM) or a 2-tetralinyl substituent (**13l**, MGM 11.2 μM) did not result in any appreciable change in activity, while replacement of the benzene ring by a morpholine ring caused a slight decrease in cytotoxicity (**13h**, MGM 19.5 μM). The appendage of a long hydrocarbon chain to the amide in **13k** resulted in one of the more cytotoxic compounds (MGM 2.7 μM), but it was not an inhibitor of tubulin polymerization or Syk PTK (see below).

Table 1. Inhibitory Activities of Lavendustin A Analogues

	IC_{50} (μM)					
compd	MGM[a]	tubulin[b]	Syk[c]	EGFR[d]	MCF-7 DNA[e]	MCF-10A DNA[f]
4	8.7 ± 0.4	3.6 ± 0.7	NT[g]	14 ± 10	11 ± 4	14 ± 3
13a	14.8 ± 1.4	3.6 ± 1	5	10 ± 4	9 ± 3	11 ± 3
13b	0.35 ± 0.05	4.0 ± 0.4	5	4 ± 2	12 ± 4	10 ± 1
13c	7.6 ± 2.4	4.2 ± 0.5	45	35 ± 11	7 ± 0	6 ± 1
13d	15.4	4.2 ± 0.8	50	>100	14 ± 0	11 ± 2
13e	15.5	3.2 ± 0.6	25	8 ± 4	17 ± 4	17 ± 4
13f	10.0 ± 0.95	3.2 ± 0.7	25	46 ± 13	13 ± 2	9 ± 1
13g	20.4	4.5 ± 1	5	~300	16 ± 3	15 ± 2
13h	19.5	2.1 ± 0.4	1.5	>50	14 ± 3	16 ± 5
13i	16.0 ± 0.55	3.6 ± 0.3	NT[g]	15 ± 6	11 ± 5	7 ± 0.0
13j	13.2 ± 0.3	5.0 ± 1	28	1 ± 0.4	2 ± 0.2	2 ± 0.0
13k	2.7 ± 0.1	>40	50	35 ± 7	1 ± 0.3	3 ± 0.5
13l	11.2 ± 1.4	5.3 ± 0.9	8	4 ± 1	10 ± 3	6 ± 0.7
13m	>100	>40	NT[g]	*	>50	NT[g]
18a	8.8 ± 1.7	6.2 ± 1	18	>100	16 ± 3	34 ± 9
18b	6.4 ± 1.2	4.9 ± 0.9	5	>200	3 ± 1	7 ± 2
18c	5.3 ± 1.3	5.7 ± 1	35	33 ± 5	0.4 ± 0.1	3 ± 1
23	12.1 ± 0.8	6.9 ± 1	>100	~500	5 ± 1	6 ± 1

[a] Mean graph midpoint for growth inhibition of all human cancer cell lines (approximately 55) successfully tested. [b] IC_{50} values for inhibition of tubulin polymerization. [c] IC_{50} values for in vitro inhibition of Syk PTK. [d] IC_{50} values for inhibition of EGFR phosphorylation in BaF3 mouse lymphoid cells. [e] IC_{50} values for inhibition of DNA synthesis in MCF-7 cells. [f] IC_{50} values for inhibition of DNA synthesis in MCF-10A cells. [g] NT, not tested. * Stimulates EGFR tyrosine phosphorylation.

Table 2. Cytotoxicities of Lavendustin A Analogues in Human Cancer Cell Cultures

	GI_{50} (μM)[a]									
compd	leukemia CCRF-CEM	lung HOP-62	colon HCT-116	CNS SF-539	melanoma UACC-62	ovarian OVCAR-3	renal SN12C	prostate DU-145	breast MDA-MB-435	MGM[b]
4	0.56	19	17	2.3	12	4.0	6.1	15	15	8.7
13a	2.7	20	18	17	14	7.7	18	16	19	14.8
13b	0.29	12	9.2	9.2	7.8	11	7.7	18	13	0.35
13c	NT[c]	18	7.6	15.8	8.6	4.2	6.3	16	10	7.6
13d	3.2	12	23	16	14	5.5	72	21	16	15.4
13e	3.2	23	17	21	15	21	12	16	30	15.5
13f	1.6	17	15	8.4	13	5.9	9.8	16	20	10.0
13g	NT[c]	2.5	16	2.5	18	62	19	17	23	20.4
13h	1.8	NT[c]	20	19	17	87	22	17	13	19.5
13i	1.0	20	17	29	17	17	19	17	13	16.0
13j	2.4	22	24	16	14	6.5	15	8.4	18	13.2
13k	0.34	3.8	2.1	20	3.2	1.9	2.6	11	3.2	2.7
13l	1.4	17	16	2.7	14	7.9	18	17	9.2	11.2
18a	2.7	20	10	9.7	12	6.8	9.7	15	12	8.8
18b	0.59	13	7.4	8.5	9.4	2.7	7.4	14	5.1	6.4
18c	0.83	16	6.4	3.4	7.9	3.0	3.2	13	5.8	5.3
23	4.4	3.8	16	15	13	2.8	13	17	15	12.1

[a] The cytotoxicity GI_{50} values are the concentrations (μM) corresponding to 50% growth inhibition. [b] Mean graph midpoint for growth inhibition of all human cancer cell lines successfully tested. [c] NT, not tested.

Because the hydrocarbon chain in **13k** might be expected to be membrane-interactive, it was replaced by the cholestanyl moiety in **13m**, since that would be expected to bind strongly to biological membranes. However, the resulting compound **13m** proved to be inactive.

A series of analogues **18a**–**c** was designed by moving the amide to the para position and eliminating the phenolic hydroxyl group. The extension of the amide substituent by consecutive addition of methylene groups led to small increases in cytotoxicity (**18a**, MGM 8.8 μM; **18b**, MGM 6.4 μM; **18c**, MGM 5.3 μM). However, these small differences in cytotoxicity may not be significant based on the standard deviations reported. A final modification in this series involved the elimination of the phenolic hydroxyl group from **13a** (MGM 14.8 μM), resulting in **23** (MGM 12.1). Comparison of **13a** and **23** indicates that the phenolic hydroxyl group of **13a** is not a requirement for cytotoxicity.

Inhibition of EGF-stimulated EGFR phosphorylation by a number of the lavendustin A analogues was tested in BaF3 cells. After addition of inhibitor to the cells, they were stimulated by EGF under conditions which induce abundant receptor phosphorylation but not receptor downregulation or internalization.[27] Immunoprecipitates from the lysed cells were resolved by polyacrylamide gel electrophoresis and electrotransferred onto nitrocellulose. The resulting Western blots were probed with a mouse monoclonal antiphosphotyrosine antibody, and the bound antibody was detected by probing the blot with a horseradish peroxidase-coupled goat anti-mouse antibody. The antibody complexes were visualized by enhanced chemiluminescence. The resulting IC_{50} values for inhibition of EGFR phosphorylation are listed in Table 1. A total of 18 compounds were tested, of which 5 showed appreciable activity (IC_{50} 10 μM or less). The three most potent compounds were **13j** (IC_{50} 1 μM), having a γ-phenyl-

propyl substituent on the amide nitrogen, **13b** (IC_{50} 4 μM), having a *p*-fluoro-β-phenylethyl substituent, and **13l** (IC_{50} 4 μM), having a β-tetralinyl substituent. These three compounds were followed by the benzyl analogue **13e** (IC_{50} 8 μM) and the β-phenylethyl congener **13a** (IC_{50} 10 μM). Each of these values was relatively close to the IC_{50} values for inhibition of DNA synthesis in MCF-7 cells and MCF-10A cells (Table 1). Since MCF-10A cells are EGF-dependent, while MCF-7 cells are not, the fact that the two cell types exhibit similar responses to the lavendustin A analogues is evidence that inhibition of EGFR tyrosine kinase activity is not relevant to the cytotoxic activities of the lavendustin A analogues.[28-31] Compounds **13c,d,f,g**, **18c**, and **23** did not show appreciable activity versus EGFR tyrosine kinase at the concentrations tested.

To assay the new lavendustin A congeners versus a representative nonreceptor PTK, Syk was obtained from lysates of Sf9 cells infected with a baculovirus directing the expression of the full-length enzyme as a fusion protein with glutathione S-transferase. GST-Syk was isolated by affinity chromatography on glutathione-agarose. The activities of the inhibitors were assayed by monitoring the transfer of ^{32}P from [γ-^{32}P]ATP to tyrosyl residues on the immobilized kinase. Reactions were terminated by the addition of EDTA. The immobilized kinase was separated from unreacted [γ-^{32}P]-ATP by centrifugation. The extent of kinase autophosphorylation was determined by liquid scintillation spectrometry. The resulting IC_{50} values are listed in Table 1. In general, IC_{50} values for the inhibition of Syk were comparable to those obtained for the inhibition of EGFR. Four compounds (**13g,h** and **18a,b**), however, did display considerable selectivity for Syk as compared to the EGFR. These IC_{50} values are comparable to that of the Syk-selective inhibitor, piceatannol (**24**), which had an IC_{50} value of 5 μg/mL in this assay.

Whether or not the cytotoxicities of the lavendustin A analogues reported here are due to PTK inhibition is questionable. Since almost all of the EGFR tyrosine kinase activity must be inhibited before effects are seen on cell growth,[27] it is unlikely that the potencies of EGFR inhibitors seen here could possibly be responsible for the effects seen on inhibition of cancer cell growth, since the IC_{50} values for EGFR inhibition are close to the MGMs observed for growth inhibition. The fact that lavendustin A did not inhibit the PTK activity of the mutant protein pp60src^{F527}, but nevertheless did exhibit antiproliferative activity, previously led other investigators to the conclusion that the antiproliferative effects of lavendustin A could be due to actions on cellular targets downstream of pp60src^{F527} or receptors unrelated to the kinase.[11] We therefore also considered other possible targets for the new lavendustin analogues that might be responsible for their inhibitory effects on cancer cell growth.

As stated previously, the COMPARE analysis of **13b** suggested that the lavendustin A analogues in this series might be interacting with tubulin. As shown in Table 1, this turned out to be the case. All of the compounds except **13k,m** inhibited tubulin polymerization with IC_{50} values ranging from 2.1 to 6.9 μM. Under the reaction conditions used here, these values indicate the compounds are moderately active as inhibitors of the polymerization reaction. In previous studies under the same reaction conditions, known potent antimitotic agents such as combretastatin A-4 and dolastatin 10 reproducibly yield IC_{50} values in the 0.5–1.0 μM range. Compounds **4** and **13b,h** were also shown to be weak inhibitors of the binding of [^{3}H]colchicine to tubulin. In an assay with tubulin at 1 μM, [^{3}H]colchicine at 5 μM, and the three agents at 50 μM, the percent inhibitions for these compounds were **13b**, 38 ± 10%; **13h**, 34 ± 20%; and **4**, 45 ± 20%; as compared to 98 ± 2% with 5 μM combretastatin A-4 (**25**) (data not presented).

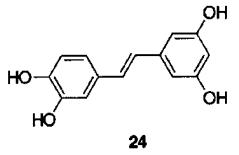

24

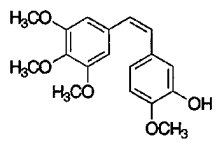

25

The activity of these compounds as inhibitors of tubulin polymerization was unexpected on the basis of prior literature reports, which have indicated that polyhydroxylated *trans*-stilbenes, benzylanilines, and related compounds are inhibitors of the PTKs, while their polymethoxylated *cis*-stilbene analogues and related compounds are inhibitors of tubulin polymerization. For example, in addition to lavendustin A and its analogues, other polyhydroxylated stilbene PTK inhibitors include piceatannol (**24**) and related polyhydroxylated *trans*-stilbenes,[7,32,33] while the polymethoxylated *cis*-stilbene inhibitors of tubulin polymerization include combretastatin A-4 (**25**) and its analogues.[34-37] Polymethoxylated *trans*-stilbenes are much less active as inhibitors of tubulin polymerization and as cytotoxic agents than their cis counterparts.[33] Neussbaumer et al. previously reported that the methylated lavendustin A analogues **26** and **27** have antiproliferative effects and that **27** acts "by blocking the cell cycle at mitosis by perturbing the microtubules of the mitotic spindle apparatus".[12,38] This would basically be in agreement with our prior study which had indicated that the benzylamine **28** and analogous compounds are antimitotic agents that act by inhibition of tubulin polymerization.[37] Furthermore, the methylated lavendustin A analogue **27** did not inhibit EGFR tyrosine kinase in a cell-free system.[38]

However, when we examined human Burkitt lymphoma cells treated with several members (**4**, **13b,c,e,f,k**, and **18a–c**) of this series of compounds for evidence of mitotic arrest (increase in G2/M cells), only **13b** caused such an effect. We thus have evidence for an antitubulin effect at the cellular level only with the most cytotoxic member of the series.

The abilities of the present polyhydroxylated benzylaniline derivatives of lavendustin A to inhibit both receptor and nonreceptor PTKs, as well as tubulin polymerization, is a novel observation which raises the possibility that the antiproliferative effects observed both in this series and in the other series of lavendustin A analogues reported in the literature may actually be due in part to inhibition of tubulin polymerization, rather than any effect on PTK inhibition. The lavendustin A derivatives reported are also unusual tubulin

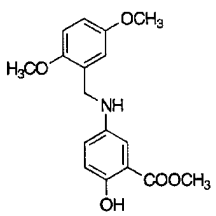

26

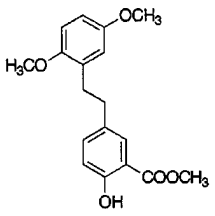

27

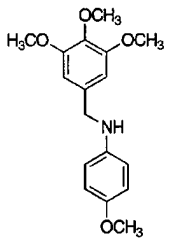

28

polymerization inhibitors, since they are not polymethoxylated *cis*-stilbene or benzylaniline analogues.

Experimental Section

General. Melting points are uncorrected. Nuclear magnetic resonance spectra for proton (^{1}H NMR) were recorded on a 300-MHz spectrometer. The chemical shift values are expressed in ppm (parts per million) relative to tetramethylsilane as internal standard; s = singlet, d = doublet, m = multiplet, bs = broad singlet. Microanalyses were performed at the Purdue Microanalysis Laboratory, and all values were within ±0.4% of the calculated compositions. Column chromatography was carried out using Merck silica gel (230−400 mesh). Analytical thin-layer chromatography (TLC) was performed on silica gel GF (Analtech) glass-coated plates (2.5 × 10 cm with 250 μm layer and prescored), and spots were visualized with UV light at 254 nm. Most chemicals and solvents were analytical grade and used without further purification. Commercial reagents were purchased from Aldrich Chemical Co. (Milwaukee, WI).

Tubulin Assays. Electrophoretically homogeneous tubulin was purified from bovine brain as described previously.[39] The tubulin polymerization and colchicine binding assays were performed as described previously,[40] except that Beckman DU7400/7500 spectrophotometers equipped with "high-performance" temperature controllers were used in the former assay. Unlike the manual control possible with the previously used Gilford spectrophotometers, the polymerization assays required use of programs provided by MDB Analytical Associates, South Plainfield, NJ, since the Beckman instruments are microprocessor-controlled. The Beckman instruments were unable to maintain 0 °C, and the lower temperature in the assays fluctuated between 2 and 4 °C. Temperature changes were, however, more rapid than in the Gilford instruments with the jump from the lower temperature to 30 °C taking about 20 s and the reverse jump about 100 s.

Syk Assays. Preparation of GST-Syk was as described previously.[41] Autophosphorylation reactions contained 50 mM Tris/HCl, pH 7.4, 5 mM $MnCl_2$, 5 μM ATP, 5 μCi [γ-^{32}P]ATP, 1 mM sodium orthovanadate, 5 mM *p*-nitrophenyl phosphate and 1.5% DMSO, which was used as a carrier for the inhibitors. Reactions were terminated by the addition of EDTA to a final concentration of 10 mM. Beads were washed 2 times in 50 mM Tris/HCl, pH 7.4, 1 mM sodium orthovanadate and 10 mM EDTA and counted by liquid scintillation spectrometry. IC_{50} values were determined graphically and represent the concentration of inhibitor that gives half-maximal inhibition as compared to control assays carried out in the absence of inhibitor but in the presence of DMSO carrier.

Cell Lines and Cell Culture. The CEM human T lymphocyte cell line engineered to express ErbB4 (CEM/4) and its culture conditions have been described previously.[42,43] Briefly, these cells were propagated in RPMI supplemented with 10% heat-inactivated fetal bovine serum and 300 μg/mL G418. The BaF3 mouse lymphoid cell lines engineered to express either EGFR (BaF3/EGFR) or ErbB2 and ErbB3 together (BaF3/2+3) and the culture conditions for these cell lines have been described earlier.[27] These cells were propagated in RPMI supplemented with 10% fetal bovine serum, 300 μg/mL G418, and 10% medium conditioned by WeHI cells. This conditioned medium serves as a source for interleukin 3.

MCF-10A human mammary epithelial cells and MCF-7, MDA-MB-231, and MDA-MB-453 human mammary tumor cell lines were obtained from the American Type Culture Collection (ATCC). These lines were propagated according to ATCC recommendations.

Inhibition of Receptor Tyrosine Phosphorylation Assay. The assay for inhibition of ErbB family receptor tyrosine phosphorylation was adapted from a previously described protocol.[27,43] Briefly, 200-mL cultures of CEM/4, BaF3/EGFR, or BaF3/2+3 cells were grown to saturation density (~10^6 cells/mL) and were incubated for 24 h at 37 °C in serum-free medium to reduce basal levels of receptor tyrosine phosphorylation. The cells were collected by centrifugation and resuspended in serum-free medium at a final concentration of ~10^7 cells/mL (~20 mL of cells). Cells were transferred to microcentrifuge tubes in 1-mL aliquots and putative kinase inhibitors were added to the cells. Each tyrosine kinase inhibitor was tested at 3−5 different concentrations. The inhibitors were dissolved in 5 μL of DMSO; hence, cells treated with 5 μL of DMSO were used as a solvent control. Cells were incubated in the presence of inhibitor for 2 h at 37 °C, then were incubated on ice for 20 min. Chilling the cells reduces the amount of ligand-induced receptor downregulation.[27]

Ligand was then added to the appropriate samples at a final concentration of 100 ng/mL and the samples were mixed and incubated on ice for 7 min. Recombinant human EGF (Sigma) was used as the ligand for EGFR, while neuregulin1β (NRG1β; R&D Systems) was used as the ligand for ErbB3 and ErbB4. Note that because ErbB3 lacks kinase activity, ligand-induced ErbB2 and ErbB3 phosphorylation in the BaF3/2+3 cells is the result of ErbB2 kinase activity.[27] Following incubation with ligand, the cells were collected by centrifugation, the supernatant was removed by aspiration, and the cells were resuspended in an isotonic lysis buffer containing 0.5% NP40/Igepal CA-630 (nonionic detergent; Sigma).

The cells were incubated for 20 min on ice to permit lysis. The samples were centrifuged for 10 min at 4 °C to collect the nuclei and cellular debris. The supernatants (cell lysates) were transferred to fresh tubes. Concanavalin A Sepharose (Amersham/Pharmacia) beads were added to each sample (35 μL of a 50% v/v slurry) and the samples were incubated at 4 °C for 30 min. Concanavalin A Sepharose precipitates the cellular glycoproteins, which include ErbB family receptors. The precipitated glycoproteins were washed 3 times with 500 μL of ice-cold lysis buffer, then were eluted by boiling the beads for 5 min in 80 μL of reducing SDS protein sample buffer. The beads were collected by centrifugation and one-half of the eluted glycoproteins (40 μL) were recovered and resolved by SDS/PAGE on a 7.5% acrylamide gel.

The resolved glycoproteins were electroblotted onto nitrocellulose (BiotraceNT; Gelman Sciences). The resulting blot was blocked by incubation for 45 min at room temperature in a solution consisting of 5% bovine serum albumin (Sigma) dissolved in Tris-buffered normal saline (TBS) supplemented with 0.05% Tween-20 (TBS-T). The blot was then probed with a mouse monoclonal antiphosphotyrosine antibody (4G10; Upstate Biotechnology). The blot was washed with TBS-T 5 times for 6 min each, and primary antibody binding was detected by probing the blot with a goat anti-mouse antibody conjugated to horseradish perioxidase (HRP; Pierce). The blot was washed with TBS-T 12 times for 10 min each, after which HRP activity was visualized by enhanced chemiluminescence (ECL; Amersham Pharmacia Biotech). The resulting chemilumigrams were digitized using a Linotype-Hell Jade flatbed

scanner and the amount of receptor tyrosine phosphorylation was quantified using NIH Image software. The amount of receptor tyrosine phosphorylation in samples from cells treated with a putative receptor tyrosine kinase inhibitor were compared to a standard curve generated using samples from cells treated with DMSO solvent control. This enabled us to determine the concentration of a given tyrosine kinase inhibitor that was necessary to cause a 50% reduction in receptor tyrosine phosphorylation. This value is reported as the receptor tyrosine phosphorylation IC_{50} value.

Inhibition of Cellular DNA Synthesis Assay. The assay for inhibition of cellular DNA synthesis was adapted from a previously described protocol.[44] Briefly, human mammary (tumor) cells were seeded in 1-mL aliquots into 24-well culture dishes at a density of 10^5 cells/well. Cells were incubated for 24 h at 37 °C, and a tyrosine kinase inhibitor dissolved in DMSO was added to each well in a volume of 10 μL. Each tyrosine kinase inhibitor was assayed at 3–5 different concentrations and each concentration was assayed using 3–4 wells of cells. Cells treated with 10 μL of DMSO served as the solvent control. Cells were then incubated for 48 h at 37 °C. [^{3}H]Thymidine (1.5 μCi; Amersham Pharmacia Biotech) dissolved in a 1.5 μL of an aqueous solution was added to each well and the cells were incubated for an additional 2 h at 37 °C. The culture medium was aspirated from the wells, and the cells were rinsed once with 1 mL of ice-cold phosphate-buffered saline (PBS) and once with 1 mL of ice-cold 10% trichloroacetic acid (TCA). Incorporated [^{3}H]thymidine was precipitated by incubating the cells for at least 30 min at 4 °C in 1 mL of 10% TCA. Following incubation, the TCA solution was aspirated from each well and the precipitated (incorporated) [^{3}H]thymidine was solubilized by incubating the cells for 30 min at 95 °C in 500 μL of 3% perchloric acid. The perchloric acid samples were transferred to scintillation vials containing 10 mL of Cytoscint scintillation cocktail (ICN). The incorporated [^{3}H]-thymidine was assayed by scintillation counting on a Packard Tricarb scintillation counter. The amount of [^{3}H]thymidine incorporation observed in the cells treated with the solvent control was divided by 2 (two) to determine the amount of half-maximal [^{3}H]thymidine incorporation. Dose–response curves for each combination of putative tyrosine kinase inhibitor and cell line were then constructed using the [^{3}H]thymidine incorporation data. The dose–response curves and the half-maximal [^{3}H]thymidine values were used to calculate the concentration of each inhibitor required to inhibit [^{3}H]thymidine incorporation by 50% in a given cell line. This value is reported as the DNA synthesis IC_{50} value.

5-[*N*-(*tert*-Butoxycarbonyl)amino]salicylic Acid (8). To a mixture of 5-aminosalicylic acid (**7**) (3.0 g, 19.6 mmol) in dioxane (50 mL) and water (25 mL) were added triethylamine (4.0 mL, 29.3 mmol) followed by di-*tert*-butyl dicarbonate (6.4 g, 29.3 mmol). The reaction mixture was stirred at room temperature for 24 h. Solvent was removed by rotary evaporation, and 3 N aqueous hydrochloric acid (30 mL) was added dropwise to the residue. A precipitate was obtained, collected, washed with water, and dried to provide **8** (4.76 g, 96%) as a solid: mp 279–280 °C; ^{1}H NMR (300 MHz, DMSO-d_6) δ 9.29 (s, 1 H), 7.96 (d, J = 1.81 Hz, 1 H), 7.47 (dd, J = 8.93, 2.69 Hz, 1 H), 6.85 (d, J = 8.88 Hz, 1 H), 1.44 (s, 9 H).

5-[*N*-(*tert*-Butoxycarbonyl)amino]-*N*-(β-phenethyl)salicylamide (10a). To a solution of **8** (1.5 g, 5.93 mmol) in dry DMF (15 mL) were added EDCI (1.71 g, 8.92 mmol), HOBt (1.2 g, 8.92 mmol) and triethylamine (1.65 mL, 11.86 mmol). After stirring at room temperature for 24 h, β-phenethylamine **(9a)** (3.7 mL, 29.5 mmol) was added dropwise and the reaction continued for 48 h at room temperature under argon. Water (300 mL) was then added and the mixture stirred for 5 min. The product was then extracted with ethyl acetate (5 × 50 mL). The combined organic extracts were washed with brine (1 × 40 mL), dried over sodium sulfate, filtered, and the solvent removed. Purification was achieved by flash chromatography (silica gel 75 g, ethyl acetate/hexane 1:4 by volume) to yield pure **10a** (1.09 g, 52%) as a white crystalline solid: ^{1}H NMR (300 MHz, $CDCl_3$) δ 12.13 (s, 1 H), 7.74 (s, 1 H), 7.36–7.24 (m, 6 H), 7.00 (dd, J = 8.82, 2.14 Hz, 1 H), 6.90 (d, J = 8.8 Hz, 1 H), 6.60 (bs, 1 H), 6.34 (s, 1 H), 3.68 (q, J = 6.859 Hz, 2 H), 2.93 (t, J = 7.1 Hz, 2 H), 1.51 (s, 9 H).

5-[*N*-(*tert*-Butoxycarbonyl)amino]-*N*-(4-fluoro-β-phenethyl)salicylamide (10b). From compound **8** (0.75 g, 2.9 mmol), EDCI (0.85 g, 4.5 mmol), HOBt (0.6 g, 4.5 mmol), triethylamine (1.65 mL, 11.8 mmol) and 4-fluorophenethylamine (**9b**) (1.2 g, 9.0 mmol), a similar procedure as that described for **10a** gave pure **10b** (0.58 g, 53%) as a white crystalline solid: mp 173–174 °C; ^{1}H NMR (300 MHz, DMSO-d_6) δ 11.68 (s, 1 H), 9.12 (bs, 1 H), 8.70 (t, J = 5.75 Hz, 1 H), 7.87 (s, 1 H), 7.28 (m, 3 H), 7.12 (t, J = 8.79 Hz, 2 H), 6.81 (d, J = 8.83 Hz, 1 H), 3.49 (q, J = 6.92 Hz, 2 H), 2.84 (t, J = 7.35 Hz, 2 H), 1.46 (s, 9 H).

5-[*N*-(*tert*-Butoxycarbonyl)amino]-*N*-(4-bromo-β-phenethyl)salicylamide (10c). From compound **8** (0.66 g, 2.6 mmol), EDCI (0.75 g, 3.9 mmol), HOBt (0.53 g, 3.9 mmol), triethylamine (1.45 mL, 10.4 mmol) and 4-bromophenethylamine (**9c**) (1.0 g, 5.0 mmol), a similar procedure as that described for **10a** gave pure **10c** (0.55 g, 49%) as a white crystalline solid: mp 196–197 °C; ^{1}H NMR (300 MHz, DMSO-d_6) δ 11.66 (s, 1 H), 9.13 (bs, 1 H), 8.71 (t, J = 4.99 Hz, 1 H), 7.81 (s, 1 H), 7.49 (dd, J = 8.20, 1.81 Hz, 1 H), 7.30 (d, J = 8.20 Hz, 2 H), 7.22 (d, J = 8.11 Hz, 2 H), 6.81 (d, J = 9.11 Hz, 1 H), 3.51 (q, J = 6.84 Hz, 2 H), 2.83 (t, J = 7.29 Hz, 2 H), 1.47 (s, 9 H).

5-[*N*-(*tert*-Butoxycarbonyl)amino]-*N*-(4-methoxy-β-phenethyl)salicylamide (10d). From compound **8** (0.74 g, 2.9 mmol), EDCI (0.85 g, 4.5 mmol), HOBt (0.6 g, 4.5 mmol), triethylamine (1.65 mL, 11.8 mmol) and 4-methoxyphenethylamine (**9d**) (1.32 g, 9.0 mmol), a similar procedure as that described for **10a** gave pure **10d** (0.64 g, 55%) as a white crystalline solid: mp 159–160 °C; ^{1}H NMR (300 MHz, DMSO-d_6) δ 11.72 (s, 1 H), 9.12 (bs, 1 H), 8.70 (t, J = 5.01 Hz, 1 H), 7.88 (s, 1 H), 7.29 (dd, J = 8.65, 1.50 Hz, 1 H), 7.16 (d, J = 7.74 Hz, 2 H), 6.86 (d, J = 7.29 Hz, 2 H), 6.81 (d, J = 8.65 Hz, 1 H), 3.72 (s, 3 H), 3.47 (q, J = 6.38 Hz, 2 H), 2.77 (t, J = 8.20 Hz, 2 H), 1.46 (s, 9 H).

5-[*N*-(*tert*-Butoxycarbonyl)amino]-*N*-(benzyl)salicylamide (10e). From compound **8** (0.77 g, 3.0 mmol), EDCI (0.85 g, 4.5 mmol), HOBt (0.6 g, 4.5 mmol), triethylamine (1.65 mL, 11.8 mmol) and benzylamine (**9e**) (0.65 mL, 6.0 mmol), a similar procedure as that described for **10a** gave pure **10e** (0.54 g, 53%) as a white crystalline solid: mp 184–185 °C; ^{1}H NMR (300 MHz, DMSO-d_6) δ 11.74 (s, 1 H), 9.15 (bs, 2 H), 7.94 (s, 1 H), 7.41–7.21 (m, 6 H), 6.84 (d, J = 9.11 Hz, 1 H), 4.51 (d, J = 4.10 Hz, 2 H), 1.46 (s, 9 H).

5-[*N*-(*tert*-Butoxycarbonyl)amino]-*N*-(4-chloro-β-phenethyl)salicylamide (10f). From compound **8** (0.61 g, 2.4 mmol), EDCI (0.69 g, 3.6 mmol), HOBt (0.49 g, 3.6 mmol), triethylamine (1.3 mL, 9.2 mmol) and 4-chlorophenethylamine (**9f**) (1.12 g, 7.2 mmol), a similar procedure as that described for **10a** gave pure **10f** (0.55 g, 58%) as a white crystalline solid: mp 192–193 °C; ^{1}H NMR (300 MHz, $CDCl_3$) δ 11.66 (s, 1 H), 9.13 (bs, 1 H), 8.71 (t, J = 5.42 Hz, 1 H), 7.87 (s, 1 H), 7.31 (d, J = 8.39 Hz, 2 H), 7.29 (d, J = 8.21 Hz, 2 H), 7.27 (dd, J = 8.39, 2.04 Hz, 1 H), 6.80 (d, J = 8.77 Hz, 1 H), 3.52 (q, J = 6.17 Hz, 2 H), 2.84 (t, J = 7.06 Hz, 2 H), 1.47 (s, 9 H).

5-[*N*-(*tert*-Butoxycarbonyl)amino]-*N*-(4-hydroxy-β-phenethyl)salicylamide (10g). From compound **8** (0.61 g, 2.4 mmol), EDCI (0.69 g, 3.6 mmol), HOBt (0.49 g, 3.6 mmol), triethylamine (1.3 mL, 9.3 mmol) and 4-hydroxyphenethylamine (**9g**) (1.2 g, 8.7 mmol), a similar procedure as that described for **10a** gave pure **10g** (0.37 g, 42%) as a white crystalline solid: mp 194–195 °C; ^{1}H NMR (300 MHz, DMSO-d_6) δ 11.73 (s, 1 H), 9.19 (s, 1 H), 9.12 (s, 1 H), 8.69 (t, J = 4.51 Hz, 1 H), 7.88 (s, 1 H), 7.31 (d, J = 9.3 Hz, 1 H), 7.05 (d, J = 8.22 Hz, 2 H), 6.82 (d, J = 8.68 Hz, 1 H), 6.68 (d, J = 7.67 Hz, 2 H), 3.43 (q, J = 8.03 Hz, 2 H), 2.72 (t, J = 7.20 Hz, 2 H), 1.46 (s, 9 H).

5-[*N*-(*tert*-Butoxycarbonyl)amino]-*N*-(2-morpholinoethyl)salicylamide (10h). From compound **8** (0.38 g, 1.5 mmol), EDCI (0.43 g, 2.2 mmol), HOBt (0.30 g, 2.2 mmol), triethylamine (0.87 mL, 6.0 mmol) and 4-(2-aminoethyl)-

morpholine (**9h**) (0.39 mL, 3.0 mmol), a similar procedure as that described for **10a** gave pure **10h** (0.33 g, 56%) as a white crystalline solid: mp 154−155 °C; ^{1}H NMR (300 MHz, $CDCl_3$) δ 11.02 (s, 1 H, OH), 7.83 (bs, 1 H, NH), 7.01 (dd, J = 9.82, 2.14 Hz, 1 H), 6.91 (d, J = 9.9 Hz, 1 H), 6.68 (bs, 1 H), 6.50 (d, J = 2.01 Hz, 1 H), 3.56 (t, J = 4.40 Hz, 4 H), 3.47 (m, 4 H), 2.39 (m, 4 H), 1.43 (s, 9 H).

5-[*N*-(*tert*-Butoxycarbonyl)amino]-*N*-(2-pyridin-2-yl-ethyl)salicylamide (10i). From compound **8** (0.25 g, 0.99 mmol), EDCI (0.28 g, 1.5 mmol), HOBt (0.26 g, 1.5 mmol), triethylamine (0.3 mL, 2.1 mmol) and 2-(2-aminoethyl)pyridine (**9i**) (0.20 mL, 1.7 mmol), a similar procedure as that described for **10a** gave pure **10i** (0.30 g, 85%) as a white crystalline solid: mp 182−184 °C dec; ^{1}H NMR (300 MHz, DMSO-d_6) δ 11.68 (s, 1 H), 9.13 (s, 1 H), 8.53 (d, J = 4.57 Hz, 1 H), 7.88 (s, 1 H), 7.72 (td, J = 7.67, 1.80 Hz, 1 H), 7.30 (d, J = 7.76 Hz, 1 H), 7.23 (m, 2 H), 6.80 (d, J = 8.78 Hz, 1 H), 3.65 (t, J = 7.17 Hz, 2 H), 3.00 (t, J = 7.10 Hz, 2 H), 1.46 (s, 9 H).

5-[*N*-(*tert*-Butoxycarbonyl)amino]-*N*-(3-phenyl-1-propyl)salicylamide (10j). From compound **8** (0.38 g, 1.5 mmol), EDCI (0.43 g, 2.2 mmol), HOBt (0.30 g, 2.2 mmol), triethylamine (0.87 mL, 6 mmol) and 3-phenyl-1-propylamine (**9j**) (0.43 mL, 3.0 mmol), a similar procedure as that described for **10a** gave pure **10j** (0.45 g, 41%) as a white crystalline solid: mp 111−112 °C; ^{1}H NMR (300 MHz, DMSO-d_6) δ 11.85 (s, 1 H), 9.11 (s, 1 H), 8.72 (s, 1 H), 7.75 (s, 1 H), 7.34−7.14 (m, 6 H), 6.82 (d, J = 8.8 Hz, 1 H), 3.27 (t, J = 6.98 Hz, 2 H), 2.59 (t, J = 7.65 Hz, 2 H), 1.80 (quintet, J = 7.15 Hz, 2 H), 1.43 (s, 9 H).

5-[*N*-(*tert*-Butoxycarbonyl)amino]-*N*-(dodecyl)salicylamide (10k). From compound **8** (0.38 g, 1.5 mmol), EDCI (0.43 g, 2.2 mmol), HOBt (0.30 g, 2.2 mmol), triethylamine (0.87 mL, 6 mmol) and dodecylamine (**9k**) (0.55 g, 3.0 mmol), a similar procedure as that described for **10a** gave pure **10k** (0.35 g, 56%) as a white crystalline solid: mp 104−105 °C; ^{1}H NMR (300 MHz, DMSO-d_6) δ 11.89 (s, 1 H), 9.09 (s, 1 H), 7.86 (s, 1 H), 7.28 (d, J = 7.36 Hz, 1 H), 6.81 (d, J = 8.8 Hz, 1 H), 3.25 (t, J = 6.81 Hz, 2 H), 1.46 (s, 9 H), 1.22 (m, 20 H), 0.84 (t, J = 6.73 Hz, 3 H).

5-[*N*-[(*tert*-Butoxycarbonyl)methyl]amino]-*N*-(1,2,3,4-tetrahydronaphthalen-2-yl)salicylamide (10l). From compound **8** (0.40 g, 1.6 mmol), EDCI (0.46 g, 2.4 mmol), HOBt (0.32 g, 2.4 mmol), triethylamine (0.90 mL, 6.3 mmol) and 1,2,3,4-tetrahydronaphthalen-2-amine hydrochloride (**9l**) (0.43 g, 2.3 mmol), a similar procedure as that described for **10a** gave pure **10l** (0.36 g, 59%) as a white crystalline solid: mp 211−212 °C; ^{1}H NMR (300 MHz, DMSO-d_6) δ 11.62 (s, 1 H, OH), 9.11 (s, 1 H, NH), 8.64 (t, J = 7.14 Hz, 1 H), 7.91 (s, 1 H), 7.34 (d, J = 8.71 Hz, 1 H), 7.10 (m, 4 H), 6.82 (d, J = 8.75 Hz, 1 H), 4.23 (m, 1 H), 3.06 (dd, J = 16.19, 4.99 Hz, 1 H), 2.89−2.77 (m, 3 H), 2.06−1.98 (m, 1 H), 1.88−1.75 (m, 1 H), 1.46 (s, 9 H).

4-[*N*-(*tert*-Butoxycarbonyl)amino]-*N*-(3β-cholestanyl)-salicylamide (10m). From compound **8** (0.20 g, 0.8 mmol), EDCI (0.23 g, 1.2 mmol), HOBt (0.16 g, 1.2 mmol), triethylamine (0.44 mL, 3.2 mmol) and 3β-aminocholestane hydrochloride (**9m**) (0.35 g, 0.82 mmol), a similar procedure as that described for **10a** gave pure **10m** (0.31 g, 62%) as a white crystalline solid: mp 230−231 °C dec; ^{1}H NMR (300 MHz, $CDCl_3$) δ 12.36 (s, 1 H, OH), 7.77 (bs, 1 H, NH), 7.26 (s, 1 H), 7.01 (dd, J = 8.88, 2.92 Hz, 1 H), 6.90 (d, J = 8.75 Hz, 1 H), 6.36 (bs, 1 H, NH), 3.95 (m, 1 H), 1.99−1.67 (m, 3 H), 1.63 (d, J = 2.78 Hz, 4 H), 1.52 (s, 9 H), 1.47−0.99 (m, 9 H), 0.91 (d, J = 6.47 Hz, 3 H), 0.87 (dd, J = 6.59, 1.26 Hz, 6 H), 0.81 (s, 3 H), 0.65 (s, 3 H).

5-Amino-*N*-(β-phenethyl)salicylamide (11a). A solution of **10a** (1.0 g, 2.8 mmol) in 6:1 dichloromethane:trifluoroacetic acid (9 mL) was stirred at room temperature for 2 h. The solvent was evaporated in vacuo, and diethyl ether (20 mL) was added. The precipitate was collected, washed with ether and dried to provide white solid **11a** (0.72 g, 100%): mp 190−191 °C; ^{1}H NMR (300 MHz, DMSO-d_6) δ 8.73 (t, J = 1.8 Hz, 1 H), 7.67 (d, J = 2.74 Hz, 1 H), 7.35−7.20 (m, 6 H), 7.03 (d, J = 8.77 Hz, 1 H), 3.54 (q, J = 6.47 Hz, 2 H), 2.86 (t, J = 7.12 Hz, 2 H).

5-Amino-*N*-(4-fluoro-β-phenethyl)salicylamide (11b). From compound **10b** (0.56 g, 1.5 mmol), a similar procedure as that described for **11a** provided white solid **11b** (0.43 g, 104%): mp 200−202 °C dec; ^{1}H NMR (300 MHz, DMSO-d_6) δ 11.9 (bs, 1 H), 9.83 (bs, 1 H), 8.73 (t, J = 5.50 Hz, 1 H), 7.71 (d, J = 2.54 Hz, 1 H), 7.31−7.26 (m, 2 H), 7.23 (d, J = 2.67 Hz, 1 H), 7.12 (t, J = 8.93 Hz, 1 H), 7.02 (d, J = 8.77 Hz, 1 H), 3.54 (q, J = 6.90 Hz, 2 H), 2.84 (t, J = 7.15 Hz, 2 H).

5-Amino-*N*-(4-bromo-β-phenethyl)salicylamide (11c). From compound **10c** (0.54 g, 1.2 mmol), a similar procedure as that described for **11a** provided white solid **11c** (0.41 g, 101%): mp 201−202 °C dec; ^{1}H NMR (300 MHz, DMSO-d_6) δ 12.48 (bs, 1 H), 9.27 (bs, 2 H), 8.73 (t, J = 5.78 Hz, 1 H), 7.77 (d, J = 2.90 Hz, 1 H), 7.49 (d, J = 8.35 Hz, 2 H), 7.27 (dd, J = 9.08, 2.54 Hz, 1 H), 7.23 (d, J = 8.36 Hz, 2 H), 7.00 (d, J = 8.72 Hz, 1 H), 3.55 (q, J = 6.18 Hz, 2 H), 2.84 (t, J = 7.26 Hz, 2 H).

5-Amino-*N*-(4-methoxyphenethyl)salicylamide (11d). From compound **10d** (0.64 g, 1.65 mmol), a similar procedure as that described for **11a** provided white solid **11d** (0.48 g, 100%): mp 196−198 °C dec; ^{1}H NMR (300 MHz, DMSO-d_6) δ 12.03 (bs, 1 H), 9.40 (bs, 2 H), 8.74 (t, J = 5.73 Hz, 1 H), 7.74 (d, J = 2.86 Hz, 1 H), 7.28 (dd, J = 9.06, 2.87 Hz, 1 H), 7.18 (d, J = 8.58 Hz, 2 H), 7.00 (d, J = 8.59 Hz, 1 H), 6.87 (d, J = 8.58 Hz, 2 H), 3.73 (s, 3 H), 3.52 (q, J = 6.19 Hz, 2 H), 2.79 (t, J = 7.63 Hz, 2 H).

5-Amino-*N*-(benzyl)salicylamide (11e). From compound **10e** (0.53 g, 1.55 mmol), a similar procedure as that described for **11a** provided white solid **11e** (0.38 g, 101%): mp 202−204 °C dec; ^{1}H NMR (300 MHz, DMSO-d_6) δ 12.27 (bs, 1 H), 9.40 (m, 2 H), 9.18 (t, J = 5.80 Hz, 1 H), 7.73 (s, 1 H), 7.35 (d, J = 1.78 Hz, 1 H), 7.37−7.20 (m, 5 H), 7.00 (d, J = 8.46 Hz, 1 H), 4.54 (d, J = 5.79 Hz, 2 H).

5-Amino-*N*-(4-chloro-β-phenethyl)salicylamide (11f). From compound **10f** (0.46 g, 1.18 mmol), a similar procedure as that described for **11a** provided white solid **11f** (0.34 g, 100%): mp 199−200 °C dec; ^{1}H NMR (300 MHz, DMSO-d_6) δ 12.48 (bs, 1 H), 9.33 (bs, 2 H), 8.73 (t, J = 5.01 Hz, 1 H), 7.70 (d, J = 2.80 Hz, 1 H), 7.36 (d, J = 8.19 Hz, 2 H), 7.28 (d, J = 8.09 Hz, 2 H), 7.26 (dd, J = 9.21, 2.51 Hz, 1 H), 6.98 (d, J = 8.68 Hz, 1 H), 3.54 (q, J = 6.10 Hz, 2 H), 2.85 (t, J = 7.00 Hz, 2 H).

5-Amino-*N*-(4-hydroxy-β-phenethyl)salicylamide (11g). From compound **10g** (0.35 g, 0.94 mmol), a similar procedure as that described for **11a** provided white solid **11g** (0.25 g, 100%): mp 139−140 °C dec; ^{1}H NMR (300 MHz, CD_3OD) δ 7.82 (d, J = 2.65 Hz, 1 H), 7.34 (dd, J = 8.71, 2.69 Hz, 1 H), 7.08 (d, J = 8.02 Hz, 2 H), 7.02 (d, J = 8.76 Hz, 1 H), 3.60 (t, J = 7.13 Hz, 2 H), 2.81 (t, J = 7.02 Hz, 2 H).

5-Amino-*N*-(2-morpholinoethyl)salicylamide (11h). From compound **10h** (0.30 g, 0.82 mmol), a similar procedure as that described for **11a** provided white solid **11h** (0.21 g, 100%): ^{1}H NMR (300 MHz, $CDCl_3$) δ 10.82 (s, 1 H, OH), 7.83 (bs, 1 H, NH), 7.01 (dd, J = 8.90, 2.14 Hz, 1 H), 6.98 (d, J = 9.01 Hz, 1 H), 6.50 (d, J = 2.01 Hz, 1 H), 3.56 (t, J = 4.20 Hz, 4 H), 3.47 (m, 4 H), 2.39 (m, 4 H).

5-Amino-*N*-(2-pyridin-2-ylethyl)salicylamide (11i). From compound **10i** (0.29 g, 0.81 mmol), a similar procedure as that described for **11a** provided white solid **11i** (0.21 g, 100%): mp 163−165 °C; ^{1}H NMR (300 MHz, DMSO-d_6) δ 12.08 (s, 1 H), 8.85 (t, J = 5.57 Hz, 1 H), 8.69 (d, J = 5.13 Hz, 1 H), 8.11 (td, J = 7.66, 1.67 Hz, 1 H), 7.75 (d, J = 2.67 Hz, 1 H), 7.63 (d, J = 7.92, 1 H), 7.58 (t, J = 6.41 Hz, 1 H), 7.33 (dd, J = 8.71, 2.76 Hz, 1 H), 7.03 (d, J = 8.72 Hz, 1 H), 3.73 (q, J = 5.82 Hz, 2 H), 3.15 (t, J = 6.66 Hz, 2 H).

5-Amino-*N*-(3-phenyl-1-propyl)salicylamide (11j). From compound **10j** (0.35 g, 0.95 mmol), a similar procedure as that described for **11a** provided white solid **11j** (0.23 g, 90%): mp 162−164 °C; ^{1}H NMR (300 MHz, DMSO-d_6) δ 12.10 (bs, 1 H), 8.76 (t, J = 5.52 Hz, 1 H), 7.74 (d, J = 2.69 Hz, 1 H), 7.31−7.02 (m, 6 H), 7.00 (d, J = 8.71 Hz, 1 H), 3.70 (bs, 1 H), 3.32

(q, J = 5.71 Hz, 2 H), 2.63 (t, J = 7.35 Hz, 2 H), 1.84 (quintet, J = 7.37 Hz, 2 H).

5-Amino-*N*-(dodecyl)salicylamide (11k). From compound **10k** (0.35 g, 0.83 mmol), a similar procedure as that described for **11a** provided white solid **11k** (0.27 g, 101%): mp 158–160 °C; ^{1}H NMR (300 MHz, DMSO-d_6) δ 8.70 (s, 1 H), 7.76 (d, J = 2.43 Hz, 1 H), 7.35 (dd, J = 8.72, 2.65 Hz, 1 H), 7.06 (d, J = 8.74 Hz, 1 H), 3.30 (t, J = 6.8 Hz, 2 H), 1.25 (m, 20 H), 0.85 (t, J = 6.64 Hz, 3 H).

5-Amino-*N*-(1,2,3,4-tetrahydronaphthalen-2-yl)salicylamide (11l). From compound **10l** (0.35 g, 0.91 mmol), a similar procedure as that described for **11a** provided white solid **11l** (0.25 g, 98%): mp 208–209 °C dec; ^{1}H NMR (300 MHz, DMSO-d_6) δ 8.67 (d, J = 7.54 Hz, 1 H), 7.75 (d, J = 2.51 Hz, 1 H), 7.25 (dd, J = 8.69, 2.56 Hz, 1 H), 7.10 (m, 4 H), 6.98 (d, J = 8.72 Hz, 1 H), 4.25 (m, 1 H), 3.09 (dd, J = 16.46, 5.29 Hz, 1 H), 2.89–2.76 (m, 3 H), 2.03 (m, 1 H), 1.89–1.79 (m, 1 H).

5-Amino-*N*-(3β-cholestanyl)salicylamide (11m). From compound **10m** (0.29 g, 0.46 mmol), a similar procedure as that described for **11a** provided white solid **11m** (0.21 g, 87%): mp 200–202 °C dec; ^{1}H NMR (300 MHz, DMSO-d_6) δ 12.18 (bs, 1 H, OH), 8.51 (d, J = 7.73 Hz, 1 H), 7.73 (d, J = 2.46 Hz, 1 H), 7.26 (dd, J = 8.72, 2.56 Hz, 1 H), 6.98 (d, J = 8.74 Hz, 1 H), 1.94–0.98 (m, 20 H), 0.88 (d, J = 6.35 Hz, 3 H), 0.83 (d, J = 6.65 Hz, 6 H), 0.80 (s, 3 H), 0.62 (s, 3 H).

5-[*N*-[(2,5-Dihydroxyphenyl)methyl]amino]-*N*-(phenethyl)salicylamide (13a). 2,5-Dihydroxybenzaldehyde **(12)** (0.21 g, 1.40 mmol) was added to **11a** (0.35 g, 1.40 mmol) in benzene (40 mL), and the mixture was heated to reflux under argon for 24 h, using a Dean–Stark trap. The reaction mixture was then concentrated to remove the benzene completely, and the residue was redissolved in methanol (15 mL). While stirring, sodium cyanoborohydride $NaBH_3CN$ (0.18 g, 2.81 mmol) was added in three portions during 30 min, and the reaction mixture was stirred at room temperature for an additional 1 h. To the reaction mixture was then added a saturated solution of NaCl (100 mL) containing 37% HCl (0.28 g, 2.8 mmol). The reaction mixture was extracted with ethyl acetate (3 × 50 mL). The combined organic layers were washed with brine (10 mL), dried over sodium sulfate and concentrated to furnish the crude product, which was further purified by flash chromatography (silica gel 40 g, ethyl acetate:hexane 1:1). The product **13a** (0.37 g, 71.4%) was isolated as a light yellow solid: mp 175–177 °C; ^{1}H NMR (300 MHz, DMSO-d_6) δ 11.43 (s, 1 H, OH), 8.76 (m, 2 H, OH, NH), 8.58 (s, 1 H, OH), 7.35–7.20 (m, 5 H), 7.05 (d, J = 2.51, 1 H), 6.74 (dd, J = 2.28, 8.79 Hz, 1 H), 6.68 (d, J = 8.97 Hz, 1 H), 6.66 (d, J = 3.53 Hz, 1 H), 6.63 (d, J = 8.56 Hz, 1 H), 6.46 (dd, J = 2.75, 8.58 Hz, 1 H), 5.43 (bs, 1 H, NH), 4.11 (s, 2 H), 3.52 (q, J = 6.52 Hz, 2 H), 2.86 (t, J = 7.19 Hz, 2 H); FABMS (Gly) m/z 379 (MH^+). Anal. ($C_{22}H_{22}N_2O_4$) C, H, N.

5-[*N*-[(2,5-Dihydroxyphenyl)methyl]amino]-*N*-(4-fluorophenethyl)salicylamide (13b). From compounds **11b** (0.56 g, 2.0 mmol), **12** (0.35 g, 2.5 mmol), and $NaBH_3CN$ (0.26 g, 4.1 mmol), a similar procedure as that described for **13a** gave pure **13b** (0.34 g, 42%) as a slightly yellow crystalline solid: mp 154–156 °C; ^{1}H NMR (300 MHz, $CDCl_3$) δ 11.37 (s, 1 H), 8.77 (s, 1 H), 8.72 (t, J = 5.33 Hz, 1 H), 8.56 (s, 1 H), 7.27 (t, J = 7.07 Hz, 2 H), 7.10 (t, J = 8.92 Hz, 2 H), 7.00 (d, J = 2.78 Hz, 1 H), 6.74 (dd, J = 8.68, 2.61 Hz, 1 H), 6.67 (d, J = 9.09 Hz, 1 H), 6.62 (s, 1 H), 6.59 (d, J = 8.62 Hz, 1 H), 6.42 (dd, J = 8.44, 2.85 Hz, 1 H), 5.42 (bs, 1 H, NH), 4.09 (d, J = 3.88 Hz. 2 H), 3.47 (q, J = 5.92 Hz, 2 H), 2.82 (t, J = 7.08 Hz, 2 H); ESMS m/z 419 (MNa^+), 397 (MH^+). Anal. ($C_{22}H_{21}FN_2O_4$) C, H, N, F.

5-[*N*-[(2,5-Dihydroxyphenyl)methyl]amino]-*N*-(4-bromo-β-phenethyl)salicylamide (13c). From compounds **11c** (0.48 g, 1.4 mmol), **12** (0.24 g, 1.4 mmol) and $NaBH_3CN$ (0.20 g, 2.9 mmol), a similar procedure as that described for **13a** gave pure **13c** (0.42 g, 64%) as a white crystalline solid: mp 179–180 °C; ^{1}H NMR (300 MHz, $CDCl_3$) δ 11.35 (s, 1 H), 8.77 (s, 1 H), 8.71 (t, J = 2.44 Hz, 1 H), 8.56 (s, 1 H), 7.48 (d, J = 8.20 Hz, 2 H), 7.21 (d, J = 8.28 Hz, 2 H), 7.00 (d, J = 2.87, 1 H), 6.72 (dd, J = 8.55, 2.40 Hz, 1 H), 6.67 (d, J = 9.37 Hz, 1 H), 6.60 (s, 1 H), 6.61 (d, J = 9.76 Hz, 1 H), 6.44 (dd, J = 8.40, 2.65 Hz, 1 H), 5.43 (bs, 1 H, NH), 4.09 (d, J = 4.68 Hz, 2 H), 3.49 (q, J = 7.22 Hz, 2 H), 2.81 (t, J = 7.15 Hz, 2 H); ESMS m/z 458 (M^+ + 2), 457 (M^+ + 1), 456 (M^+). Anal. ($C_{22}H_{21}BrN_2O_4$) C, H, N, Br.

5-[*N*-[(2,5-Dihydroxyphenyl)methyl]amino]-*N*-(4-methoxy-β-phenethyl)salicylamide (13d). From compounds **11d** (0.60 g, 2.0 mmol), **12** (0.35 g, 2.5 mmol) and $NaBH_3CN$ (0.25 g, 4.0 mmol), a similar procedure as that described for **13a** gave pure **13d** (0.50 g, 61%) as a white crystalline solid: mp 173–174 °C dec; ^{1}H NMR (300 MHz, DMSO-d_6) δ 11.42 (s, 1 H, OH), 8.78 (s, 1 H, OH), 8.71 (t, J = 5.42 Hz, 1 H, NH), 8.57 (s, 1 H, OH), 7.15 (d, J = 8.60, 2 H), 7.02 (d, J = 2.41 Hz, 1 H), 6.85 (d, J = 8.64 Hz, 2 H), 6.72 (dd, J = 8.76, 2.57 Hz, 1 H), 6.65 (d, J = 8.88 Hz, 1 H), 6.63 (d, J = 3.03 Hz, 1 H), 6.60 (d, J = 8.53 Hz, 1 H), 6.44 (dd, J = 8.48, 2.88 Hz, 1 H), 5.42 (t, J = 5.68 Hz, 1 H, NH), 4.10 (d, J = 4.82 Hz, 2 H), 3.72 (s, 3 H), 3.46 (q, J = 6.91 Hz, 2 H), 2.76 (t, J = 7.02 Hz, 2 H); ESMS m/z 431 (MNa^+), 409 (MH^+). Anal. ($C_{23}H_{24}N_2O_5$) C, H, N.

5-[*N*-[(2,5-Dihydroxyphenyl)methyl]amino]-*N*-(benzyl)salicylamide (13e). From compounds **12** (0.38 g, 2.6 mmol), **11e** (0.54 g, 2.2 mmol) and $NaBH_3CN$ (0.14 g, 2.2 mmol), a similar procedure as that described for **13a** gave pure **13e** (0.55 g, 69%) as a white crystalline solid: mp 195–196 °C; ^{1}H NMR (300 MHz, DMSO-d_6) δ 11.43 (s, 1 H), 9.18 (t, J = 6.24 Hz, 1 H), 8.75 (s, 1 H), 8.56 (s, 1 H), 7.38–7.20 (m, 5 H), 7.09 (d, J = 2.69 Hz, 1 H), 6.76 (dd, J = 8.46, 2.66 Hz, 1 H), 6.68 (d, J = 8.91 Hz, 1 H), 6.65 (d, J = 3.11 Hz, 1 H), 6.60 (d, J = 8.46 Hz, 1 H), 6.43 (dd, J = 8.46, 3.12 Hz, 1 H), 5.41 (t, J = 5.41 Hz, 1 H), 4.49 (d, J = 5.79, 2 H), 4.09 (d, J = 5.35 Hz, 2 H); CIMS m/z 379 (MH^+). Anal. ($C_{21}H_{20}N_2O_4$) C, H, N.

5-[*N*-[(2,5-Dihydroxyphenyl)methyl]amino]-*N*-(4-chloro-β-phenethyl)salicylamide (13f). From compounds **11f** (0.34 g, 1.2 mmol), **12** (0.16 g, 1.2 mmol) and $NaBH_3CN$ (0.15 g, 2.4 mmol), a similar procedure as that described for **13a** gave pure **13f** (0.34 g, 69%) as a light yellow crystalline solid: mp 158–160 °C; ^{1}H NMR (300 MHz, DMSO-d_6) δ 11.35 (s, 1 H, OH), 8.77 (s, 1 H, OH), 8.71 (t, J = 5.31 Hz, 1 H, NH), 8.56 (s, 1 H, OH), 7.48 (d, J = 8.20 Hz, 2 H), 7.21 (d, J = 8.28 Hz, 2 H), 7.00 (d, J = 2.87, 1 H), 6.72 (dd, J = 8.55, 2.40 Hz, 1 H), 6.67 (d, J = 9.37 Hz, 1 H), 6.60 (s, 1 H), 6.61 (d, J = 9.76 Hz, 1 H), 6.44 (dd, J = 8.40, 2.65 Hz, 1 H), 5.44 (t, J = 5.29 Hz, 1 H, NH), 4.09 (d, J = 4.68 Hz, 2 H), 3.49 (q, J = 7.22 Hz, 2 H), 2.81 (t, J = 7.15 Hz, 2 H); ESMS m/z 414 (M^+ + 2), 412 (M^+). Anal. ($C_{22}H_{21}ClN_2O_4$) C, H, N, Cl.

5-[*N*-[(2,5-Dihydroxyphenyl)methyl]amino]-*N*-(4-hydroxyphenethyl)salicylamide (13g). From compounds **11g** (0.22 g, 0.81 mmol), **12** (0.14 g, 0.97 mmol) and $NaBH_3CN$ (0.15 g, 2.3 mmol), a similar procedure as that described for **13a** gave pure **13g** (0.18 g, 55%) as a slightly yellow crystalline solid: mp 175–176 °C; ^{1}H NMR (300 MHz, DMSO-d_6) δ 11.38 (s, 1 H, OH), 9.87 (s, 1 H, OH), 8.76 (s, 1 H, OH), 8.68 (t, J = 5.33 Hz, 1 H, NH), 8.56 (s, 1 H, OH), 7.30 (t, J = 7.07 Hz, 2 H), 7.10 (t, J = 8.92 Hz, 1 H), 7.00 (d, J = 2.78 Hz, 1 H), 6.73 (dd, J = 8.68, 2.61 Hz, 1 H), 6.67 (d, J = 9.09 Hz, 2 H), 6.62 (d, J = 2.50 Hz, 1 H), 6.59 (d, J = 8.62 Hz, 1 H), 6.42 (dd, J = 8.44, 2.85 Hz, 1 H), 5.40 (bs, 1 H, NH), 4.11 (d, J = 3.88 Hz, 2 H), 3.47 (q, J = 5.92 Hz, 2 H), 2.82 (t, J = 7.08 Hz, 2 H); ESMS m/z 417 (MNa^+), 395 (MH^+). Anal. ($C_{22}H_{22}N_2O_5$) C, H, N.

5-[*N*-[(2,5-Dihydroxyphenyl)methyl]amino]-*N*-(2-morpholinoethyl)salicylamide (13h). From compounds **12** (0.12 g, 0.80 mmol), **11h** (0.20 g, 0.75 mmol) and $NaBH_3CN$ (0.19 g, 3.0 mmol), a similar procedure as that described for **13a** gave pure **13h** (0.18 g, 55%) as a yellow crystalline solid: mp 184–186 °C dec; ^{1}H NMR (300 MHz, DMSO-d_6) δ 11.25 (s, 1 H, OH), 8.77 (s, 1 H, OH), 8.66 (t, J = 4.39 Hz, 1 H, NH), 8.55 (s, 1 H, OH), 7.02 (d, J = 2.21 Hz, 1 H), 6.74 (dd, J = 8.80, 2.55 Hz, 1 H), 6.67 (d, J = 8.00 Hz, 1 H), 6.63 (d, J = 2.87 Hz, 1 H), 6.60 (d, J = 8.66 Hz,1 H), 6.43 (dd, J = 8.42, 2.85 Hz, 1 H), 5.45 (s, 1 H, NH), 4.08 (s, 2 H), 3.56 (t, J = 4.42 Hz, 4 H), 3.38 (m, 4 H), 2.43 (m, 4 H); ESMS m/z 388 (MH^+). Anal. ($C_{20}H_{25}N_3O_5$) C, H, N.

5-[*N*-[(2,5-Dihydroxyphenyl)methyl]amino]-*N*-(2-pyridin-2-ylethyl)salicylamide (13i). From compounds **11i** (0.24 g, 0.93 mmol), **12** (0.17 g, 1.2 mmol) and $NaBH_3CN$ (0.25 g, 4.0 mmol), a similar procedure as that described for **13a** gave pure **13i** (0.18 g, 51%) as a white solid: mp 114−116 °C dec; ^{1}H NMR (300 MHz, DMSO-d_6) δ 11.68 (s, 1 H, OH), 9.13 (s, 1 H, OH), 8.79 (m, 2 H), 8.62 (t, J = 2.12 Hz, 1 H, NH), 8.59 (s, 1 H, OH), 8.53 (d, J = 4.67 Hz, 1 H), 7.72 (td, J = 7.67, 1.80 Hz, 1 H), 7.01 (d, J = 2.51 Hz, 1 H), 6.74 (dd, J = 8.87, 2.31 Hz, 1 H), 6.69 (d, J = 8.83 Hz, 1 H), 6.65 (d, J = 2.53 Hz, 1 H), 6.61 (d, J = 8.94 Hz, 1 H), 6.46 (dd, J = 8.61, 2.77 Hz, 1 H), 5.39 (t, J = 1.98 Hz, 1 H, NH), 4.08 (s, 2 H), 3.65 (t, J = 7.20 Hz, 2 H), 3.05 (t, J = 7.31 Hz, 2 H); ESMS m/z 380 (MH^+). Anal. ($C_{21}H_{21}N_3O_4$) C, H, N.

5-[*N*-[(2,5-Dihydroxyphenyl)methyl]amino]-*N*-(3-phenyl-1-propyl)salicylamide (13j). From compounds **12** (0.13 g, 0.98 mmol) **11j** (0.22 g, 0.81 mmol) and $NaBH_3CN$ (0.2 g, 3.1 mmol), a similar procedure as that described for **13a** gave pure **13j** (0.19 g, 60%) as a white crystalline solid: mp 152−154 °C; ^{1}H NMR (300 MHz, DMSO-d_6) δ 11.56 (s, 1 H, OH), 8.77 (s, 1 H, OH), 8.69 (t, J = 4.58 Hz, 1 H, NH), 8.56 (s, 1 H, OH), 7.32−7.16 (m, 5 H), 7.03 (d, J = 2.42 Hz, 1 H), 6.75 (dd, J = 8.82, 2.53 Hz, 1 H), 6.68 (d, J = 8.80 Hz, 1 H), 6.64 (d, J = 2.90 Hz, 1 H), 6.62 (d, J = 8.59 Hz, 1 H), 6.45 (dd, J = 8.53, 2.94 Hz, 1 H), 5.40 (t, J = 5.78 Hz, 1 H, NH), 4.10 (d, J = 4.51 Hz, 2 H), 3.29 (q, J = 4.87 Hz, 2 H), 2.62 (t, J = 7.53 Hz, 2 H), 1.83 (quintet, J = 7.26 Hz, 2 H); CIMS m/z 393 (MH^+). Anal. ($C_{23}H_{24}N_2O_4$) C, H, N.

5-[*N*-[(2,5-Dihydroxyphenyl)methyl]amino]-*N*-(dodecyl)-salicylamide (13k). From compounds **11k** (0.30 g, 0.93 mmol), **12** (0.14 g, 1.0 mmol) and $NaBH_3CN$ (0.13 g, 2.0 mmol), a similar procedure as that described for **13a** gave pure **13k** (0.23 g, 56%) as a slightly yellow crystalline solid: mp 126−128 °C; ^{1}H NMR (300 MHz, DMSO-d_6) δ 11.59 (s, 1 H, OH), 8.77 (s, 1 H, OH), 8.62 (t, J = 2.12 Hz, 1 H, NH), 8.56 (s, 1 H, OH), 7.01 (d, J = 2.51 Hz, 1 H), 6.74 (dd, J = 8.87, 2.31 Hz, 1 H), 6.69 (d, J = 8.83 Hz, 1 H), 6.65 (d, J = 2.53 Hz, 1 H), 6.61 (d, J = 8.94 Hz, 1 H), 6.46 (dd, J = 8.61, 2.77 Hz, 1 H), 5.39 (t, J = 1.98 Hz, 1 H, NH), 4.09 (s, 2 H), 3.25 (t, J = 7.90 Hz, 2 H), 1.50 (m, 2 H), 1.20 (s, 18 H), 0.88 (t, J = 6.87 Hz, 3 H); CIMS m/z 443 (MH^+). Anal. ($C_{26}H_{38}N_2O_4$) C, H, N.

5-[*N*-[(2,5-Dihydroxyphenyl)methyl]amino]-*N*-(1,2,3,4-tetrahydronaphthalen-2-yl)salicylamide (13l). From compounds **11l** (0.32 g, 1.13 mmol), **12** (0.19 g, 1.36 mmol) and $NaBH_3CN$ (0.3 g, 4.7 mmol), a similar procedure as that described for **13a** gave pure **13l** (0.28 g, 61%) as a yellow crystalline solid: mp 159−161 °C; ^{1}H NMR (300 MHz, DMSO-d_6) δ 11.30 (s, 1 H, OH), 8.79 (s, 1 H, OH), 8.62 (t, J = 4.58, 1 H, NH), 8.58 (s, 1 H, OH), 7.11 (m, 5 H), 6.74 (dd, J = 8.83, 2.41 Hz, 1 H), 6.67 (d, J = 8.87 Hz, 1 H), 6.65 (d, J = 2.82 Hz, 1 H), 6.60 (d, J = 8.49 Hz, 1 H), 6.45 (dd, J = 8.44, 2.84 Hz, 1 H), 5.45 (t, J = 5.30 Hz, 1 H, NH), 4.22 (m, 1 H), 4.11 (d, J = 4.51 Hz, 2 H), 3.07 (dd, J = 16.34, 5.10 Hz, 1 H), 2.89−2.76 (m, 3 H), 2.03 (m, 1 H), 1.80 (m, 1 H); CIMS m/z 405 (MH^+). Anal. ($C_{24}H_{24}N_2O_4$) C, H, N.

5-[*N*-[(2,5-Dihydroxyphenyl)methyl]amino]-*N*-(3β-cholestanyl)salicylamide (13m). From compounds **11m** (0.15 g, 0.28 mmol), **12** (0.05 g, 0.35 mmol) and $NaBH_3CN$ (0.14 g, 2.2 mmol), a similar procedure as that described for **13a** gave pure **13m** (0.08 g, 44%) as a yellow solid: mp 202−204 °C dec; ^{1}H NMR (300 MHz, DMSO-d_6) δ 11.65 (s, 1 H, OH), 8.79 (s, 1 H, OH), 8.58 (s, 1 H, OH), 8.38 (d, 1 H, NH), 7.04 (d, J = 2.16 Hz, 1 H), 6.72 (dd, J = 8.81, 2.18 Hz, 1 H), 6.66−6.64 (m, 2 H), 6.59 (d, J = 8.56 Hz, 1 H), 6.45 (dd, J = 8.50, 2.70 Hz, 1 H), 5.35 (bs, 1 H, NH), 4.09 (s, 2 H), 3.81 (m, 1 H), 1.95−1.00 (m, 21 H), 0.90 (d, J = 6.34 Hz, 3 H), 0.86 (dd, J = 6.66, 1.17 Hz, 6 H), 0.82 (s, 3 H), 0.63 (s, 3 H); CIMS m/z 646 (MH^+). Anal. ($C_{41}H_{60}N_2O_4$) C, H, N.

4-[(*tert*-Butoxycarbonyl)amino]benzoic Acid (15). From 4-aminobenzoic acid (**14**) (0.5 g, 3.65 mmol), triethylamine (1.02 mL, 7.30 mmol) and di-*tert*-butyl dicarbonate (1.59 g, 7.30 mmol), a similar procedure as that described for **8** provided pure **15** (0.86 g, 100%) as a white solid: mp 191−192 °C; ^{1}H NMR (300 MHz, DMSO-d_6) δ 9.71 (s, 1 H), 7.82 (d, J = 8.64 Hz, 2 H), 7.54 (d, J = 8.68 Hz, 2 H), 1.47 (s, 9 H).

4-[*N*-(*tert*-Butoxycarbonyl)amino]-*N*-(benzyl)benzamide (16a). From compound **15** (0.38 g, 1.5 mmol), EDCI (0.43 g, 2.2 mmol), HOBt (0.30 g, 2.2 mmol), triethylamine (0.87 mL, 6.0 mmol) and benzylamine (**9e**) (0.33 mL, 3.0 mmol), a similar procedure as that described for **10a** gave pure **16a** (0.34 g, 69%) as a white crystalline solid: mp 198−199 °C; ^{1}H NMR (300 MHz, $CDCl_3$) δ 7.74 (d, J = 8.58 Hz, 2 H), 7.43 (d, J = 8.55 Hz, 2 H), 7.37−7.26 (m, 5 H), 4.64 (d, J = 5.63 Hz, 2 H), 1.52 (s, 9 H).

4-[*N*-(*tert*-Butoxycarbonyl)amino]-*N*-(β-phenethyl)benzamide (16b). From compound **15** (0.278 g, 1.16 mmol), EDCI (0.45 g, 2.34 mmol), HOBt (0.32 g, 2.34 mmol), triethylamine (0.36 mL, 4.68 mmol) and β-phenethylamine (**9a**) (1.0 mL, 11.7 mmol), a similar procedure as that described for **10a** gave pure **16b** (0.23 g, 58%) as a white crystalline solid: mp 210−211 °C; ^{1}H NMR (300 MHz, $CDCl_3$) δ 7.64 (d, J = 8.69 Hz, 2 H), 7.40 (d, J = 8.65 Hz, 2 H), 7.36−7.22 (m, 5 H), 6.62 (s, 1 H), 6.05 (t, J = 6.5 Hz, 1 H), 3.71 (q, J = 6.8 Hz, 2 H), 2.93 (t, J = 6.9 Hz, 2 H), 1.52 (s, 9 H).

4-[*N*-(*tert*-Butoxycarbonyl)amino]-*N*-(3-phenyl-1-propyl)benzamide (16c). From compound **15** (0.38 g, 1.5 mmol), EDCI (0.43 g, 2.2 mmol), HOBt (0.30 g, 2.2 mmol), triethylamine (0.87 mL, 6.0 mmol) and 3-phenyl-1-propylamine (**9j**) (0.43 mL, 3.0 mmol), a similar procedure as that described for **10a** gave pure **16c** (0.43 g, 81%) as a white crystalline solid: mp 178−180 °C; ^{1}H NMR (300 MHz, $CDCl_3$) δ 7.61 (d, J = 8.69 Hz, 2 H), 7.42 (d, J = 8.70 Hz, 2 H), 7.33−7.19 (m, 5 H), 4.69 (q, J = 6.19 Hz, 2 H), 2.73 (t, J = 7.28 Hz, 2 H), 1.97 (quint, J = 7.47 Hz, 2 H), 1.53 (s, 9 H).

4-Amino-*N*-(benzyl)benzamide (17a). From compound **16a** (0.30 g, 0.92 mmol), a similar procedure as that described for **11a** provided white solid **17a** (0.20 g, 100%): mp 199−200 °C dec; ^{1}H NMR (300 MHz, DMSO-d_6) δ 8.67 (t, J = 5.66 Hz, 1 H, NH), 7.70 (d, J = 8.57 Hz, 2 H), 7.34−7.20 (m, 5 H), 6.71 (d, J = 8.52 Hz, 2 H), 5.11 (bs, 2 H, NH_2), 4.44 (d, J = 4.22 Hz, 2 H).

4-Amino-*N*-(β-phenethyl)benzamide (17b). From compound **16b** (0.066 g, 0.19 mmol), a similar procedure as that described for **11a** provided **17b** (0.045 g, 98.6%) as a white solid: ^{1}H NMR (300 MHz, $CDCl_3$) δ 7.54 (d, J = 8.51 Hz, 2 H), 7.35−7.24 (m, 5 H), 6.65 (d, J = 8.44 Hz, 2 H), 6.15 (bs, 1 H), 4.46 (bs, 2 H), 3.68 (q, J = 6.32 Hz, 2 H), 2.92 (t, J = 6.80 Hz, 2 H).

4-Amino-*N*-(3-phenyl-1-propyl)benzamide (17c). From compound **16c** (0.43 g, 0.92 mmol), a similar procedure as that described for **11a** provided **17c** (0.23 g, 100%) as a white solid: mp 126−128 °C; ^{1}H NMR (300 MHz, DMSO-d_6) δ 8.11 (t, J = 5.25 Hz, 1 H, NH), 7.64 (d, J = 8.59 Hz, 2 H), 7.30−7.17 (m, 5 H), 6.71 (d, J = 8.55 Hz, 2 H), 5.51 (bs, 2 H, NH_2), 3.23 (q, J = 7.04 Hz, 2 H), 2.60 (t, J = 7.39 Hz, 2 H), 1.81 (quint, J = 7.21 Hz, 2 H).

4-[*N*-[(2,5-Dihydroxyphenyl)methyl]amino]-*N*-(benzyl)benzamide (18a). From compounds **12** (0.17 g, 1.25 mmol), **17a** (0.34 g, 1.04 mmol) and $NaBH_3CN$ (0.26 g, 4.2 mmol), a similar procedure as that described for **13a** gave pure **18a** (0.28 g, 77%) as a slightly yellow crystalline solid: mp 204−205 °C; ^{1}H NMR (300 MHz, DMSO-d_6) δ 8.81 (s, 1 H, OH), 8.57 (t, J = 3.79 Hz, 1 H, NH), 8.57 (s, 1 H, OH), 7.65 (d, J = 8.72 Hz, 2 H), 7.32−7.18 (m, 6 H), 6.63 (d, J = 8.37 Hz, 1 H), 6.58 (d, J = 2.76 Hz, 1 H), 6.55 (d, J = 8.72 Hz, 2 H), 6.44 (dd, J = 8.46, 2.81 Hz, 1 H), 4.43 (d, J = 5.88 Hz, 2 H), 4.16 (s, 2 H); CIMS m/z 349 (MH^+). Anal. ($C_{21}H_{20}ClN_2O_3$) C, H, N.

4-[*N*-[(2,5-Dihydroxyphenyl)methyl]amino]-*N*-(β-phenethyl)benzamide (18b). From compounds **12** (0.031 g, 0.22 mmol), **17b** (0.045 g, 0.22 mmol) and $NaBH_3CN$ (0.03 g, 0.47 mmol), a similar procedure as that described for **13a** gave pure **18b** (0.040 g, 59%) as a yellow solid: mp 154−156 °C; ^{1}H NMR (300 MHz, DMSO-d_6) δ 8.81 (s, 1 H, OH), 8.57 (s, 1 H, OH), 8.10 (t, J = 5.38 Hz, 1 H, NH), 7.58 (d, J = 8.41 Hz, 2 H), 7.33−7.17 (m, 6 H), 6.63 (d, J = 8.47 Hz, 1 H), 6.58 (d, J = 2.74 Hz, 1 H), 6.54 (d, J = 8.48 Hz, 2 H), 6.45 (dd, J = 8.47, 2.83 Hz, 1 H), 4.17 (d, J = 4.56 Hz, 2 H), 3.41 (q, J = 8.15 Hz,

2 H), 2.80 (t, J = 7.89 Hz, 2 H); CIMS m/z 363 (MH^+). Anal. ($C_{22}H_{22}N_2O_3$) C, H, N.

4-[*N*-[(2,5-Dihydroxyphenyl)methyl]amino]-*N*-(3-phenyl-1-propyl)benzamide (18c). From compounds **12** (0.17 g, 0.85 mmol), **17c** (0.20 g, 0.8 mmol) and $NaBH_3CN$ (0.21 g, 3.2 mmol), a similar procedure as that described for **13a** gave pure **18c** (0.22 g, 73%) as a slightly yellow crystalline solid: mp 133−134 °C; ^1H NMR (300 MHz, DMSO-d_6) δ 8.80 (s, 1 H, OH), 8.57 (s, 1 H, OH), 8.00 (t, J = 5.49 Hz, 1 H, NH), 7.58 (d, J = 8.69 Hz, 2 H), 7.30−7.14 (m, 6 H), 6.62 (d, J = 8.54 Hz, 1 H), 6.57 (d, J = 2.76 Hz, 1 H), 6.53 (d, J = 8.70 Hz, 2 H), 6.42 (dd, J = 8.50, 2.90 Hz, 1 H), 4.15 (s, 2 H), 3.21 (q, J = 6.60 Hz, 2 H), 2.59 (t, J = 7.84 Hz, 2 H), 1.79 (quint, J = 7.55 Hz, 2 H); CIMS m/z 377 (MH^+). Anal. ($C_{23}H_{24}N_2O_3$) C, H, N.

3-[*N*-(*tert*-Butoxycarbonyl)amino]benzoic Acid (20). From 3-aminobenzoic acid (**14**) (0.75 g, 5.47 mmol), triethylamine (1.5 mL, 8.20 mmol) and di-*tert*-butyl dicarbonate (1.78 g, 8.20 mmol), a similar procedure as that described for **8** provided pure **20** (1.3 g, 100%) as a white solid: mp 189−190 °C; ^1H NMR (DMSO-d_6) δ 9.53 (s, 1 H), 8.13 (s, 1 H), 7.61 (d, J = 7.66 Hz, 1 H), 7.53 (d, J = 7.52 Hz, 1 H), 7.35 (t, J = 7.91 Hz, 1 H), 1.47 (s, 9 H).

3-[*N*-(*tert*-Butoxycarbonyl)amino]-*N*-(β-phenethyl)benzoylamide (21). From compound **20** (0.48 g, 2.03 mmol), EDCI (0.45 g, 2.34 mmol), HOBt (0.33 g, 2.34 mmol), triethylamine (0.37 mL, 4.68 mmol) and β-phenethylamine (**9a**), a similar procedure as that described for **10a** gave pure **21** (0.35 g, 51%) as a white solid: mp 186−188 °C; ^1H NMR (300 MHz, $CDCl_3$) δ 7.51 (t, J = 4.86 Hz, 1 H), 7.36−7.31 (m, 4 H), 7.24 (d, J = 4.08 Hz, 1 H), 7.22 (d, J = 2.3 Hz, 1 H), 6.61 (s, 1 H), 6.22 (bs, 1 H), 3.71 (q, J = 6.9 Hz, 2 H), 2.93 (t, J = 7.0 Hz, 2 H), 1.53 (s, 9 H).

3-Amino-*N*-(β-phenethyl)benzamide (22). From compound **21** (0.23 g, 0.66 mmol), a similar procedure as that described for **11a** provided white solid **22** (0.16 g, 100%): mp 137−139 °C; ^1H NMR (300 MHz, DMSO-d_6) δ 8.47 (t, 1 H), 7.35−7.18 (m, 7 H), 6.99 (s, 2 H), 3.46 (q, J = 7.00 Hz, 2 H), 2.83 (t, J = 7.06 Hz, 2 H).

3-[*N*-[(2,5-Dihydroxyphenyl)methyl]amino]-*N*-(β-phenethyl)benzamide (23). From compounds **12** (0.25 g, 1.77 mmol), **22** (0.38 g, 1.58 mmol) and $NaBH_3CN$ (0.2 g, 3.16 mmol), a similar procedure as that described for **13a** gave pure **23** (0.42 g, 73%) as a light yellow solid: mp 124−126 °C; ^1H NMR (300 MHz, DMSO-d_6) δ 8.81 (s, 1 H, OH), 8.58 (s, 1 H, OH), 8.35 (t, J = 4.93 Hz, 1 H, NH), 7.33−7.19 (m, 5 H), 7.11 (t, J = 7.74 Hz, 1 H), 7.03 (d, J = 2.11 Hz, 1 H), 6.95 (d, J = 7.61 Hz, 1 H), 6.69 (dd, J = 2.24, 8.24 Hz, 1 H), 6.64 (d, J = 8.40 Hz, 1 H), 6.24 (s, 1 H), 6.45 (dd, J = 2.91, 8.28 Hz, 1 H), 6.20 (t, J = 4.56 Hz, 1 H, NH), 4.17 (d, J = 5.46 Hz, 2 H), 3.48 (q, J = 6.55 Hz, 2 H), 2.83 (t, J = 7.67 Hz, 2 H); CIMS m/z 363 (MH^+). Anal. ($C_{22}H_{22}N_2O_3$) C, H, N.

Acknowledgment. This research was made possible by grants from the Showalter Trust, Purdue Research Foundation, National Institutes of Health (CA37372 and CA80770), and American Chemical Society (IRG 58-006-40).

Supporting Information Available: Elemental analyses for compounds **13a−m**, **18a−c**, and **23**. This material is available free of charge via the Internet at http://pubs.acs.org.

References

(1) Levitzki, A. Protein Tyrosine Kinase Inhibitors as Novel Therapeutic Agents. *Pharmacol. Ther.* **1999**, *82*, 231−239.
(2) Traxler, P.; Furet, R. Strategies Toward the Design of Novel and Selective Protein Tyrosine Kinase Inhibitors. *Pharmacol. Ther.* **1999**, *82*, 195−206.
(3) Hamby, J. M.; Showalter, H. D. Small Molecule Inhibitors of Tumor-Promoted Angiogenesis, Including Protein Tyrosine Kinase Inhibitors. *Pharmacol. Ther.* **1999**, *82*, 169−193.
(4) Onoda, T.; Iinuma, H.; Sasaki, Y.; Hamada, M.; Isshiki, K.; Naganawa, H.; Takeuchi, T. Isolation of a Novel Tyrosine Kinase Inhibitor, Lavendustin A, from *Streptomyces griseolavendus*. *J. Nat. Prod.* **1989**, *52*, 1252−1257.
(5) Hsu, C.-Y. J.; Persons, P. E.; Spada, A. P.; Bednar, R. A.; Levitzki, A.; Zilberstein, A. Kinetic Analysis of the Inhibition of the Epidermal Growth Factor Receptor Tyrosine Kinase by Lavendustin A and Its Analogue. *J. Biol. Chem.* **1991**, *266*, 21105−21112.
(6) Imoto, M.; Sujikai, I.; Ui, H.; Umezawa, K. Involvement of Tyrosine Kinase in Growth Factor-Induced Phospholipase C Activation in NIH3T3 Cells. *Biochim. Biophys. Acta* **1993**, *1166*, 188−192.
(7) Smyth, M. S.; Stefanova, I.; Hartman, F.; Horad, I. D.; Osherov, N.; Levitzki, A. Non-Amine Based Analogues of Lavendustin A as Protein-Tyrosine Kinase Inhibitors. *J. Med. Chem.* **1993**, *36*, 3010−3014.
(8) Smyth, M. S.; Stefanova, I.; Horak, I. D.; Burke, T. R. J. Hydroxylated 2-(5′-Salicyl)naphthalenes as Protein-Tyrosine Kinase Inhibitors. *J. Med. Chem.* **1993**, *36*, 3015−3020.
(9) Chen, H.; Boiziau, J.; Parker, F.; Maroun, R.; Tocque, B.; Roques, B. P.; Garbay-Jaureguiberry, C. Synthesis and Structure−Activity Studies of a Series of [(Hydroxybenzyl)amino]salicylates as Inhibitors of EGF Receptor-Associated Tyrosine Kinase Activity. *J. Med. Chem.* **1993**, *36*, 4094−4098.
(10) Chen, H.; Boiziau, J.; Parker, F.; Mailliet, P.; Commerçon, A.; Tocque, B.; Le Pecq, J.-B.; Roques, B.-P.; Garbay, C. Structure−Activity Relationships in a Series of 5-[(2,5-Dihydroxybenzyl)-amino]salicylate Inhibitors of EGF−Receptor-Associated Tyrosine Kinase: Importance of Additional Hydrophobic Aromatic Interactions. *J. Med. Chem.* **1994**, *37*, 845−859.
(11) Agbotounou, W. K.; Umezawa, K.; Jacuemin-Sablon, A.; Pierre, J. Inhibition by Two Lavendustins of the Tyrosine Kinase Activity of $pp60^{F527}$ In Vitro and in Intact Cells. *Eur. J. Pharmacol.* **1994**, *269*, 1−8.
(12) Nussbaumer, P.; Winiski, A. P.; Cammisuli, S.; Hiestand, P.; Weckbecker, G.; Stütz, A. Novel Antiproliferative Agents Derived from Lavendustin A. *J. Med. Chem.* **1994**, *37*, 4079−4084.
(13) Liu, T.; Shirai, R.; Matsui, T.; Umezawa, K.; Iwasaki, S. Synthesis and Biological Activity of 5-[2,5-Dihydroxybenzyl)-amino]salicylic Acid Analogues as Inhibitors of EGF Receptor-Associated Protein Tyrosine Kinase. *Bioorg. Med. Chem. Lett.* **1997**, *7*, 365−368.
(14) Green, J. Solid-Phase Synthesis of Lavendustin A and Analogues. *J. Org. Chem.* **1995**, *60*, 4287−4290.
(15) Devraj, R.; Cushman, M. A Versatile Solid Phase Synthesis of Lavendustin A and Certain Biologically Active Analogues. *J. Org. Chem.* **1996**, *61*, 9368−9373.
(16) Paull, K. D.; Hamel, E.; Malspeis, L. *Prediction of Biochemical Mechanism of Action from the In Vitro Antitumor Screen of the National Cancer Institute*; American Chemical Society: Washington, DC, 1995.
(17) Paull, K. D.; Shoemaker, R. H.; Hodes, L.; Monks, A.; Scudiero, D. A.; Rubinstein, L.; Plowman, J.; Boyd, M. R. Display and Analysis of Patterns of Differential Activity of Drugs Against Human Tumor Cell Lines: Development of Mean Graph and COMPARE Algorithm. *J. Natl. Cancer Inst.* **1989**, *81*, 1088−1092.
(18) Boyd, M. R.; Paull, K. D. Some Practical Considerations and Applications of the National Cancer Institute In Vitro Anticancer Drug Discovery Screen. *Drug Dev. Res.* **1995**, *34*, 91−109.
(19) Paull, K. D.; Lin, C. M.; Malspeis, L.; Hamel, E. Identification of Novel Antimitotic Agents Acting at the Tubulin Level by Computer-assisted Evaluation of Differential Cytotoxicity Data. *Cancer Res.* **1992**, *52*, 3892−3900.
(20) Kohlhagen, G.; Paull, K.; Cushman, M.; Nagafuji, P.; Pommier, Y. Protein-Linked DNA Strand Breaks Induced by NSC 314622, a Novel Noncamptothecin Topoisomerase I Poison. *Mol. Pharmacol.* **1998**, *54*, 50−58.
(21) Leteurtre, F.; Kohlhagen, G.; Paull, K. D.; Pommier, Y. Topoisomerase II Inhibition and Cytotoxicity of the Anthrapyrazoles DuP 937 and DuP 941 (Losaxantrone) in the National Cancer Institute Preclinical Antitumor Drug Discovery Screen. *J. Natl. Cancer Inst.* **1994**, *86*, 1239−1244.
(22) Cleaveland, E. S.; Monks, A.; Vaigro-Wolff, A.; Zaharevitz, D. W.; Paull, K.; Ardalan, K.; Cooney, D. A.; Ford, H. J. Site of Action of Two Pyrimidine Biosynthesis Inhibitors Accurately Predicted by the COMPARE Program. *Biochem. Pharmacol.* **1995**, *49*, 947−954.
(23) Duncan, K. K.; Duncan, M. D.; Alley, M. C.; Sausville, E. A. Cucurbitacin E-Induced Disruption of the Actin and Vimentin Cytoskeleton in Prostate Carcinoma Cells. *Biochem. Pharmacol.* **1996**, *52*, 1553−1560.
(24) Bubb, M. R.; Senderowicz, A. M.; Sauville, E. A.; Duncan, K. K.; Korn, E. D. Jasplakinolide, a Cytotoxic Natural Product, Induces Actin Polymerization and Competitively Inhibits the Binding of Phalloidin to F-Actin. *J. Biol. Chem.* **1994**, *269*, 14869−14871.
(25) Bradshaw, T. D.; Wrigley, S.; Shi, D.-F.; Schultz, R. J.; Paull, K. D.; Stevens, M. F. G. 2-(4-Aminophenyl)benzothiazoles: Novel Agents with Selective Profiles of In Vitro Antitumor Activity. *Br. J. Cancer* **1998**, *77*, 745−752.

(26) Wosikowski, K.; Schuurhuis, D.; Johnson, K.; Paull, K. D.; Myers, T. G.; Weinstein, J. N.; Bates, S. E. Identification of Epidermal Growth Factor Receptor and C-erb-B2 Pathway Inhibitors by Correlation with Gene Expression Patterns. *J. Natl. Cancer Inst.* **1997**, *89*, 1505−1515.
(27) Riese, D. J. I.; van Raaij, T. M.; Plowman, G. D.; Andrews, G. C.; Stern, D. F. The Cellular Response to Neuregulins is Governed by Complex Interactions of the ErbB Receptor Family. *Mol. Cell. Biol.* **1995**, *15*, 5770−5776.
(28) Normanno, N.; Selvam, M. P.; Qi, C.-F.; Saeki, T.; Johnson, G.; Kim, N.; Ciardiello, F.; Shoyab, M.; Plowman, G.; Brandt, R.; Todaro, G.; Salomon, D. S. Amphiregulin as an Autocrine Growth Factor for C-Ha-*ras*- and c-*erbB-2*-Transformed Human Mammary Epithelial Cells. *Proc. Natl. Acad. Sci. U.S.A.* **1994**, *91*, 2790−2794.
(29) Soule, H. D.; Maloney, T. M.; Wolman, S. R.; Peterson, W. D. J.; Brenz, R.; McGrath, C. M.; Russo, J.; Pauley, R. J.; Jones, R. F.; Brooks, S. C. Isolation and Characterization of a Spontaneously Immortalized Human Breast Epithelial Cell Line, MCF-10. *Cancer Res.* **1990**, *50*, 6075−6086.
(30) Dickstein, B.; Valverius, E. M.; Wosikowski, K.; Saceda, M.; Pearson, J. W.; Martin, M. B.; Bates, S. E. Increased Epidermal Growth Factor Receptor in an Estrogen-responsive, Adriamycin-resistant MCF-7 Cell Line. *J. Cell. Physiol.* **1993**, *157*, 110−118.
(31) Dong, X. F.; Berthois, Y.; Colomb, E.; Martin, P. M. Cell Cycle Phase Dependence of Estrogen and Epidermal Growth Factor (EGF) Receptor Expression in MCF-7 Cells. *Endocrinology* **1991**, *129*, 2719−2728.
(32) Geahlen, R. L.; McLaughlin, J. L. Piceatannol (3,4,3′,5′-Tetrahydroxy-*trans*-stilbene) is a Naturally Occurring Protein Tyrosine Kinase Inhibitor. *Biochem. Biophys. Res. Commun.* **1989**, *165*, 241−245.
(33) Thakkar, K.; Geahlen, R. L.; Cushman, M. Synthesis and Protein-Tyrosine Kinase Inhibitory Activity of Polyhydroxylated Stilbene Analogues of Piceatannol. *J. Med. Chem.* **1993**, *36*, 2950−2955.
(34) Lin, C. M.; Singh, S. B.; Chu, P. S.; Dempcy, R. O.; Schmidt, J. M.; Pettit, G. R.; Hamel, E. Interactions of Tubulin with Potent Natural and Synthetic Analogues of the Antimitotic Agent Combretastatin: a Structure−Activity Study. *Mol. Pharmacol.* **1988**, *34*, 200−208.
(35) Cushman, M.; Nagarathnam, D.; Gopal, D.; Chakraborti, A. K.; Lin, C. M.; Hamel, E. Synthesis and Evaluation of Stilbene and Dihydrostilbene Derivatives as Potential Anticancer Agents that Inhibit Tubulin Polymerization. *J. Med. Chem.* **1991**, *34*, 2579−2588.
(36) Cushman, M.; Nagarathnam, D.; Gopal, D.; He, H.-M.; Lin, C. M.; Hamel, E. Synthesis and Evaluation of Analogues of (Z)-1-(4-Methoxyphenyl)-2-(3,4,5-trimethoxyphenyl)ethene as Potential Cytotoxic and Antimitotic Agents. *J. Med. Chem.* **1992**, *35*, 2293−2306.
(37) Cushman, M.; He, H.-M.; Lin, C. M.; Hamel, E. Synthesis and Evaluation of a Series of Benzylaniline Hydrochlorides as Potential Cytotoxic and Antimitotic Agents Acting by Inhibition of Tubulin Polymerization. *J. Med. Chem.* **1993**, *36*, 2817−2821.
(38) Cammisuli, S.; Winiski, A.; Nussbaumer, P.; Hiestand, P.; Stutz, A.; Weckbecker, G. SDZ 281-977: a Modified Partial Structure of Lavendustin A that Exerts Potent and Selective Antiproliferative Activities In Vitro and In Vivo. *Int. J. Cancer* **1996**, *65*, 351−359.
(39) Hamel, E.; Lin, C. M. Separation of Active Tubulin and Microtubule-Associated Proteins by Ultracentrifugation and Isolation of a Component Causing the Formation of Microtubule Bundles. *Biochemistry* **1984**, *23*, 4173−4184.
(40) Verdier-Pinard, P.; Lai, J. Y.; Yoo, H.-D.; Yu, J.; Marquez, B.; Nagle, D. G.; Nambu, M.; White, J. D.; Falck, J. R.; Gerwick, W. H.; Day, B. W.; Hamel, E. Structure−Activity Analysis of the Interaction of Curacin A, the Potent Colchicine Site Antimitotic Agent, with Tubulin and Effects of Analogues of the Growth of MCF-7 Breast Cancer Cells. *Mol. Pharmacol.* **1998**, *53*, 62−76.
(41) Peters, J. D.; Furlong, M. T.; Asai, D. J.; Harrison, M. L.; Geahlen, R. L. Syk, Activated by Cross-linking the B-cell Antigen Receptor Localizes to the Cytosol Where It Interacts with and Phosphorylates α-Tubulin on Tyrosine. *J. Biol. Chem.* **1996**, *271*, 4755−4762.
(42) Plowman, G. D.; Green, J. M.; Culouscou, J.-M.; Carlton, G. W.; Rothwell, V. M.; Buckley, S. Heregulin Induces Tyrosine Phosphorylation of HER4/p180erbB4. *Nature* **1993**, *366*, 473−475.
(43) Riese, D. J. I.; Komurasaki, T.; Plowman, G. D.; Stern, D. F. Activation of ErbB4 by the Bifunctional EGF Family Hormone Epiregulin is Regulated by ErbB2. *J. Biol. Chem.* **1998**, *273*, 11288−11294.
(44) Hwang, E.-S.; Riese, D. J. I.; Settleman, J.; Nilson, L. A.; Honig, J.; Flynn, S.; DiMaio, D. Inhibition of Cervival Carcinoma Cell Line Proliferation by the Introduction of a Bovine Papillomavirus Regulatory Gene. *J. Virol.* **1993**, *67*, 3720−3729.

JM000387G

Constitutively-active ErbB4 and ErbB2 Mutants Exhibit Distinct Biological Activities

Desi J. Penington, Ianthe Bryant, and David J. Riese II*

Department of Medicinal Chemistry and Molecular Pharmacology
Purdue University, West Lafayette, Indiana 47907-1333

* Corresponding Author:
Department of Medicinal Chemistry and Molecular Pharmacology
Purdue University
1333 RHPH, Room 224D,
West Lafayette, IN 47907-1333.
Phone: (765) 494-6091; Fax: (765) 494-1414
E-mail: driese@purdue.edu

Running title: Constitutively-active ErbB4 mutants

Draft Date: 7/25/01
For Submission to *Cell Growth and Differentiation*

Abstract

ErbB4 is a member of the epidermal growth factor receptor (EGFR) family of tyrosine kinases, which includes EGFR/ErbB1, ErbB2/HER2/Neu, and ErbB3/HER3. These receptors play important roles both in normal development and in neoplasia. For example, deregulated signaling by ErbB1 and ErbB2 is observed in many human malignancies. In contrast, the roles that ErbB4 plays in tumorigenesis and normal biological processes have not been clearly defined. To identify the biological responses that are coupled to ErbB4, we have constructed three constitutively-active ErbB4 mutants. Unlike a constitutively-active ErbB2 mutant, the ErbB4 mutants are not coupled to increased cell proliferation, loss of contact inhibition, or anchorage independence in a rodent fibroblast cell line. This suggests that ErbB2 and ErbB4 may play distinct roles in tumorigenesis *in vivo*.

Introduction

ErbB4 (HER4/p180^{erbB4}) is a member of the epidermal growth factor receptor (EGFR/ErbB) family of receptor tyrosine kinases. These receptors play important roles in the embryonic development of heart, lung, and nervous tissues (1-4), and they have been implicated in the progression of metastatic disease. For example, EGFR/ErbB1 is overexpressed, amplified, or mutated in a number of human malignancies including breast, ovary, prostate, and lung cancers (5-7). ErbB2 overexpression correlates with tumor aggressiveness and poor prognosis for survival in node positive breast cancer patients (Reviewed in 8). Furthermore, ErbB3 overexpression is observed in a subset of human mammary and gastric cancers (9, 10).

Some reports indicate that increased ErbB4 expression or signaling is associated with tumorigenesis. ErbB4 overexpression has been observed in a variety of cancers, including tumors of the thyroid, breast, and gastrointestinal tract (11-13). However, the prognostic significance of ErbB4 expression in tumors may also depend on which ErbB family members are co-expressed with ErbB4. In the case of childhood meduloblastoma (one of the most common solid tumors of childhood), patients with tumors overexpressing both ErbB2 and ErbB4 have a significantly worse prognosis for survival than patients with tumors that overexpress either receptor alone (14).

Increased ErbB4 expression or signaling also correlates with tumor cell differentiation and reduced aggressiveness. ErbB4 overexpression in breast tumors is associated with progesterone receptor (PR) and estrogen receptor (ER) expression and a more favorable prognosis (15-17). In contrast, ErbB2 overexpression varies inversely with PR and ER levels and indicates tumors that are more likely to be metastatic and fatal (18). In one survey of common solid human cancers, the loss of ErbB4 expression is seen in a significant percentage of

breast, prostate, and head and neck malignancies (19). These findings raise the intriguing possibility that ErbB4 is unique to the ErbB family of receptors in that ErbB4 expression and signaling may couple to reduced tumorigenesis or tumor cell proliferation. However, in the face of the conflicting evidence we have summarized here it remains unclear what general or specific roles ErbB4 plays in differentiation, tumor suppression, or proliferation.

Efforts to elucidate ErbB4 function have been hampered by many factors. First, there are no known agonists or antagonists specific to the ErbB4 receptor. All of the peptide hormones of the Epidermal Growth Factor (EGF) family that are capable of binding ErbB4 also bind at least one other ErbB family member. For example, epiregulin (EPR) and betacellulin (BTC) bind and activate both ErbB1 and ErbB4 (20, 21). Furthermore, ligands that do not bind an ErbB family receptor can still activate signaling by that receptor in *trans* through ligand-induced receptor heterodimerization (reviewed in 22, 23). For example, EGF stimulates ErbB2 tyrosine phosphorylation when ErbB2 is coexpressed with ErbB1, whereas EGF will not stimulate ErbB2 tyrosine phosphorylation in the absence of ErbB1 (24). Consequently, ligands that bind and directly activate ErbB4 receptor (neuregulin, betacellulin, amphiregulin, and epiregulin) also stimulate ErbB1, ErbB2, and ErbB3 signaling (20, 21, 25, 26, reviewed in 22, 23). Therefore, in most contexts it is virtually impossible to use an EGF family hormone to study the functional consequences of ErbB4 signaling.

To study ErbB4 function we have opted to generate ErbB4 mutants that contain a cysteine substitution in the extracellular domain. This is predicted to result in constitutively-dimerized and constitutively-active ErbB4 mutants. Introducing cysteine residues to form covalently-linked, dimeric, constitutively-active receptor tyrosine kinases is not novel. This strategy has been used to generate dimeric, constitutively-active mutants of EGFR/ErbB1 and

ErbB2 (27,28). Cysteine substitutions also lead to constitutively active mutants of the Fibroblast Growth Factor Receptor 2 (FGFR2) and FGFR3 (29, 30).

Here we report the generation and characterization of three constitutively-active ErbB4 mutants. These mutants were generated through the introduction of a cysteine residue in the extracellular region of ErbB4. These mutants exhibit increased ligand-independent ErbB4 tyrosine phosphorylation, dimerization, and kinase activity. However, these constitutively-active ErbB4 mutants do not induce increased proliferation, loss of contact inhibition, or anchorage-independent growth in Fischer Rat 3T3 fibroblasts. In contrast, a constitutively-active ErbB2 mutant does induce increased proliferation, loss of contact inhibition, and anchorage-independent growth in Fischer Rat 3T3 fibroblasts. These results suggest that ErbB4 and ErbB2 couple to different signaling pathways and biological responses. These results also suggest that ErbB4 and ErbB2 may play distinct roles in tumorigenesis *in vivo*.

Results

ErbB4 mutants are constitutively tyrosine phosphorylated We substituted a single cysteine for amino acids Pro645, Gln646, His647, Ala648 and Arg649 in the juxtamembrane region of the ErbB4 extracellular domain. These ErbB4 mutants (P645C, Q646C, H647C, A648C, and R649C) were generated in the context of the pLXSN-ErbB4 recombinant retroviral expression vector (26). Because these cysteine substitutions might cause inappropriate protein folding and decreased protein stability, we assayed the ErbB4 mutants for stable expression. We transfected the recombinant retroviral vectors containing the ErbB4 mutant constructs into the Ψ2 ecotropic retrovirus packaging cell line, selected for stable transformants, and generated pooled cell lines. We harvested low-titer ecotropic retrovirus stocks from these cell lines and we analyzed the expression and tyrosine phosphorylation of the ErbB4 mutants in these cell lines. Three ErbB4 mutants (Q646C, H647C, and A648C) exhibit abundant expression and ligand-independent tyrosine phosphorylation (data not shown). However, the R649C ErbB4 mutant is not efficiently expressed and the P645C mutant does not display ligand-independent tyrosine phosphorylation (data not shown).

Overexpression of ErbB family receptors causes ligand-independent receptor tyrosine phosphorylation (31-33). Consequently, we were concerned that the ligand-independent phosphorylation of the Q646C, H647C, and A648C ErbB4 mutants in the transfected Ψ2 cells was a consequence of overexpression. Therefore, we infected the PA317 amphotropic retrovirus packaging cell line with the ErbB4 mutant recombinant ecotropic retroviruses at low multiplicities of infection (MOI less than 0.1), selected for infected cells, and generated pooled cell lines. Since these cell lines were generated by infection at low multiplicities of infection, it

is likely that each cell contains only one or two copies of the ErbB4 expression construct. This reduces the likelihood of ErbB4 overexpression in these cell lines.

We analyzed ErbB4 expression and tyrosine phosphorylation in the PA317 cell lines by anti-ErbB4 immunoprecipitation and either anti-ErbB4 (Figure 1, right panel) or anti-phosphotyrosine (Figure 1, left panel) immunoblotting. As expected, cells infected with the LXSN vector control retrovirus do not exhibit ErbB4 expression (Figure 1, right panel) or tyrosine phosphorylation (Figure 1, left panel). Cells infected with the wild-type or mutant ErbB4 retroviruses exhibit ErbB4 expression (Figure 1, right panel). However, cells infected with the mutant ErbB4 retroviruses exhibit abundant ErbB4 tyrosine phosphorylation, whereas cells infected with the wild-type ErbB4 retrovirus exhibit minimal ErbB4 tyrosine phosphorylation (Figure 1, left panel).

Quantification of the chemilumigrams shown in Figure 1 suggests that the expression levels of the three ErbB4 mutants is less than three times greater than the amount of wild-type ErbB4 expression (Table 1). In contrast, the amounts of tyrosine phosphorylation of the three ErbB4 mutants appear to be much greater than the amount of wild-type ErbB4 tyrosine phosphorylation. Moreover, the ratios of ErbB4 tyrosine phosphorylation to ErbB4 expression for the three ErbB4 mutants appear to be at least four times greater than the ratio for wild-type ErbB4. These data suggest that the three ErbB4 mutants exhibit greater amounts of tyrosine phosphorylation on a per molecule basis than does wild-type ErbB4. Consequently, these data indicate that the Q646C, H647C, and A648C ErbB4 mutants are constitutively active for signaling.

ErbB4 mutants have increased *in vitro* kinase activity. Next, we assessed whether the increased tyrosine phosphorylation of the three ErbB4 mutants correlates with increased kinase

activity. Lysates were prepared from PA317 cells that express wild-type ErbB4 or the ErbB4 mutants. Equal amounts of lysate were immunoprecipitated with an anti-ErbB4 polyclonal antibody. Kinase reactions were performed on the immunoprecipitates in the presence of [γ-^{32}P] ATP. The reaction products were resolved by SDS/PAGE on a 7.5% acrylamide gel. The gel was dried and the reaction products were visualized by autoradiography.

In Figure 2, we show that PA317 cells infected with the LXSN vector control retrovirus lack detectable ErbB4 kinase activity. Moreover, PA317 cells that express the three constitutively-active ErbB4 mutants exhibit greater ErbB4 tyrosine kinase activity than cells that express wild-type ErbB4. Quantification of the bands on the autoradiogram indicates that the Q646C and H647C ErbB4 mutants exhibit approximately 5-fold more kinase activity than does wild-type ErbB4, whereas the A648C ErbB4 mutant exhibits approximately 9-fold more kinase activity than does wild type ErbB4. Given that the expression of the ErbB4 mutants is somewhat greater than the expression of wild-type ErbB4 (Table 1), it appears that the intrinsic kinase activity of the three ErbB4 mutants is approximately 2-fold greater than the intrinsic kinase activity of wild-type ErbB4.

Constitutively-active ErbB4 mutants do not induce a loss of contact inhibition. Once we determined that the Q646C, H647C, and A648C ErbB4 mutants are constitutively active for signaling, we performed experiments using these mutants to identify the biological events coupled to ErbB4 signaling. A common assay for genes that encode growth control or signaling proteins involves transfecting an established rodent fibroblast cell line with the gene and assaying the transfected cells for foci of piled-up cells. These foci indicate a loss of contact inhibition, a common attribute of malignant cells. Thus, this transfection assay is commonly used to identify genes that encode proteins that are coupled to malignant growth transformation.

Conflicting results have been obtained from assays for growth transformation by ErbB4. Transfection and consequent overexpression of ErbB4 induces foci (loss of contact inhibition) in NIH 3T3 clone 7 cells in the absence of ligand. Moreover, in these cells focus formation was stimulated by the ErbB4 ligand Neuregulin 2β (31). In contrast, NIH 3T3 clone 7d cells (which lack EGFR expression) transfected with wild-type ErbB4 did not form foci in the presence or absence of neuregulin 1β; however, ErbB4 cotransfected with EGFR/ErbB1 or ErbB2 does induce foci in these cells (32,33). One possible explanation is that ErbB4 lacks intrinsic transforming activity, but does permit EGFR/ErbB1 or ErbB2 signaling and coupling to growth transformation in the presence of an ErbB4 ligand.

To test whether ErbB4 signaling is sufficient to transform the growth of cultured rodent fibroblasts, Fischer Rat 3T3 (FR3T3) fibroblasts were infected with 200 Cfu of the ErbB4 mutant recombinant ecotropic retrovirus stocks and assayed for focus formation. Cells infected with the LXSN vector control recombinant ecotropic retrovirus and with the wild-type ErbB4 recombinant ecotropic retrovirus served as negative controls. Cells infected with the constitutively-active mutant ErbB2* retrovirus served as a positive control.

FR3T3 cells infected with the ErbB2* retrovirus formed foci nine days after infection, whereas cells infected with the vector control retrovirus did not (Figure 3). In contrast, cells infected with the wild-type or mutant ErbB4 retroviruses did not form foci. Eighteen days after infection, the foci arising from FR3T3 cells infected with the ErbB2* retrovirus completely covered the surface of the tissue culture plate and had begun to detach from the surface of the plate (data not shown). In contrast, the FR3T3 cells infected with the vector control retrovirus did not form any foci. FR3T3 cells infected with the constitutively-active ErbB4 mutant retroviruses formed a few foci; however, the number of foci was comparable to the number seen

in FR3T3 cells infected with the wild-type ErbB4 retrovirus. Thus, while the constitutively-active ErbB2* mutant readily induces foci in FR3T3 fibroblasts, the constitutively-active ErbB4 mutants do not. This suggests that ErbB2 and ErbB4 are coupled to distinct cellular signaling pathways and biological events.

Constitutively-active ErbB4 mutants do not induce anchorage-independent growth. Next we assayed FR3T3 cells that express the constitutively-active ErbB4 mutants for growth while suspended in semi-solid medium. Because anchorage-independent growth is another characteristic attribute of tumor cells *in vivo*, this assay is another way to determine whether ErbB4 signaling is coupled to malignant growth transformation.

FR3T3 cells were infected with the ErbB4 mutant recombinant ecotropic retroviruses at a low multiplicity of infection and infected cells were selected using G418. Drug-resistant colonies of cells were pooled and expanded into cell lines. Control cell lines were generated through infection of FR3T3 cells with the wild-type ErbB4 retrovirus, the constitutively-active ErbB2 retrovirus, and with the LXSN vector control retrovirus. These cell lines were seeded at a density of $2x10^4$ cells/ml in 60 mm dishes in semi-solid medium containing 0.3% low melting point (LMP) agarose. Fresh medium containing LMP-agarose was added every three days. Photographs were taken of representative fields after ten days.

FR3T3 cells that express the constitutively-active ErbB2* mutant exhibit anchorage-independent growth (Figure 4). In contrast, cells that were infected with the LXSN recombinant retroviral vector control and cells that express wild-type ErbB4 or the ErbB4 mutants do not exhibit anchorage-independent growth. The results of this assay are consistent with the results of the focus formation assay; both assays indicate that ErbB4 signaling is distinct from ErbB2

signaling in that ErbB4 signaling is not coupled to malignant growth transformation in FR3T3 fibroblasts.

Constitutively-active ErbB4 mutants do not increase the growth rate or saturation density. Another characteristic of malignantly-transformed fibroblasts is that their growth rates and saturation densities are higher than those of their nontransformed counterparts. Indeed, constitutive ErbB2 signaling is coupled to increased growth rates (Reviewed in 8). Thus, we assessed whether the constitutively-active ErbB4 mutants affected the growth rate or saturation density of FR3T3 fibroblasts. The FR3T3 cell lines described earlier were seeded in 60 mm dishes at a density of 2×10^4 cells per dish (700 cells/cm^2). Cells were incubated for 10 days to permit proliferation. During this period cells were counted every twenty-four hours.

The growth rate of the cells that express ErbB2* is slightly greater than the growth rates of the other cell lines (Figure 5). Note that the growth rates of the cells that express the constitutively-active ErbB4 mutants are indistinguishable from the growth rates of cell lines that express wild-type ErbB4 or the vector control. The growth curves in Figure 5 were used to determine the saturation densities for the six cell lines (Table 2). Note that the saturation density of the cell line that expresses ErbB2* is higher than the saturation densities of the other cell lines. Moreover, the saturation densities of the cell lines that express the ErbB4 mutants are not markedly higher than the saturation densities of the vector control cell line or the cell line that expresses wild-type ErbB4. Once again, these data suggest that constitutive ErbB4 signaling is not coupled to malignant growth transformation in fibroblasts. Thus, the signaling pathways and biological responses that are coupled to ErbB4 are distinct from those that are coupled to ErbB2.

Discussion

In this report we describe the construction and initial characterization of three constitutively-active ErbB4 mutants. These mutants display increased dimerization (data not shown), ligand-independent tyrosine phosphorylation and kinase activity. In these respects, the ErbB4 mutants resemble constitutively-active mutants of ErbB2 or EGFR. However, unlike constitutively-active ErbB2 mutants, these mutants are not coupled to malignant growth transformation in FR3T3 fibroblasts; they do not induce foci, anchorage-independent growth, or increases in the growth rate or saturation density. These data suggest that ErbB2 and ErbB4 play distinct roles in tumorigenesis *in vivo*.

Clearly, additional work is necessary to define the roles that ErbB4 plays in tumorigenesis and in regulating cellular functions *in vivo*. However, important clues have emerged to guide these future studies. In a significant percentage of breast and prostate tumor samples ErbB4 expression is reduced or lost, and tumor aggressiveness appears to inversely correlate with ErbB4 expression (15-17). Moreover, ligands for ErbB4 can induce terminal differentiation and growth arrest of some mammary tumor cell lines (34, 35). These data indicate that ErbB4 signaling may be coupled to differentiation, growth arrest, and tumor suppression. The ErbB4 mutants described in this study will enable us to evaluate this hypothesis. Indeed, preliminary data from our laboratory indicate that the Q646C ErbB4 mutant causes reduced colony formation in plastic dishes by a number of cultured human breast and prostate tumor cell lines.

We will also perform additional studies to characterize the biochemistry of signaling by the three ErbB4 mutants. Whereas these mutants exhibit greater ligand-independent tyrosine phosphorylation and autokinase activity than the wild-type receptor, it is unclear whether this is

due to increased intrinsic kinase activity or due to increased availability of substrate. Additional experiments are warranted to distinguish between these two possibilities.

Another area of future study will focus on identifying the mechanisms by which ErbB4 is coupled to biological responses. Initial studies will identify the sites of ErbB4 tyrosine phosphorylation for these mutants. If our preliminary studies indicating that the Q646C ErbB4 mutant is coupled to prostate and mammary tumor cell growth arrest hold true, then we will use genetic strategies to identify the sites of ErbB4 tyrosine phosphorylation that are sufficient and necessary to couple the Q646C ErbB4 mutant to this biological response. A similar strategy has been used to identify the sites of ErbB2 and platelet-derived growth factor receptor tyrosine phosphorylation that are critical for coupling these receptors to biological responses (36, 37).

Once we have identified the site(s) of tyrosine phosphorylation that is sufficient for coupling to biological responses, we will identify signaling proteins that bind this phosphorylation site and couple it to biological responses. Using this strategy we will begin to construct the ErbB4 signaling pathway. Our prediction is that the three constitutively-active ErbB4 mutants are phosphorylated on different tyrosine residues and that these mutants differentially couple to biological responses. We have previously shown that different ErbB4 ligands cause phosphorylation on different sites on ErbB4 and differential coupling to biological responses (38). Moreover, one cysteine substitution mutation in the rat ErbB2 extracellular domain (V656C) results in low amounts of constitutive receptor tyrosine phosphorylation and efficient coupling to malignant growth transformation in rodent fibroblasts. In contrast, another rat ErbB2 extracellular domain cysteine substitution mutant (T657C) exhibits very high levels of constitutive receptor tyrosine phosphorylation but a relatively low amount of coupling to malignant growth transformation in rodent fibroblasts (28).

We were somewhat surprised to discover that the three constitutively-active ErbB4 mutants failed to coupled to malignant growth transformation in a rodent fibroblasts cell line. Nonetheless, these mutants will enable us to assess ErbB4 function in a wide variety of cell, tissue, and organismal contexts. Given that ErbB4 appears to regulate diverse functions in a number of distinct contexts, much work remains to complete this story.

Figure 1. ErbB4 mutants are constitutively tyrosine phosphorylated. ErbB4 expression and tyrosine phosphorylation were assayed in PA317 cells infected with retroviruses that direct the expression of wild-type ErbB4 or the ErbB4 mutants. Cells infected with the LXSN recombinant retrovirus vector control served as the negative control. Lysates were prepared from each of the cell lines and ErbB4 was immunoprecipitated from 1000 μg of each lysate. Samples were resolved by SDS-PAGE, electroblotted to nitrocellulose, and immunoblotted with an anti-phosphotyrosine antibody (left panel). The blot was then stripped and probed with an anti-ErbB4 rabbit polyclonal antibody (right panel). ErbB4 is represented by the band at the top of the blots.

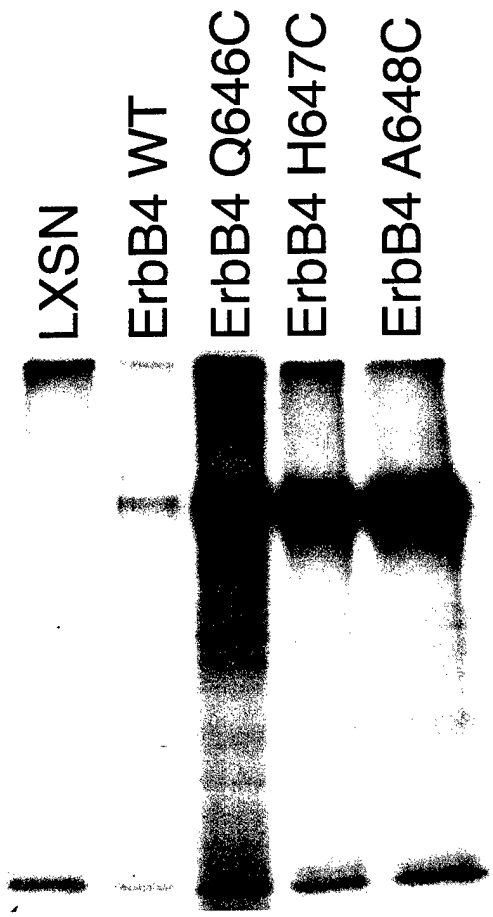

Figure 2. Q646C, H647C, and A648C mutants exhibit increased *in vitro* kinase activity. Equal amounts of protein lysates from PA317 cells that stably express wild-type ErbB4 or the ErbB4 mutants (Q646C, H647C, A648C) were immunoprecipitated with an anti-ErbB4 rabbit polyclonal antibody. Lysates from PA317 cells that express the LXSN vector served as the negative control. Kinase reactions were performed on the immunoprecipitates in the presence of [γ-^{32}P]ATP. The products were resolved by SDS-PAGE. The gel was dried overnight and exposed to X-ray film for approximately 20 hours to visualize the products of the kinase reactions.

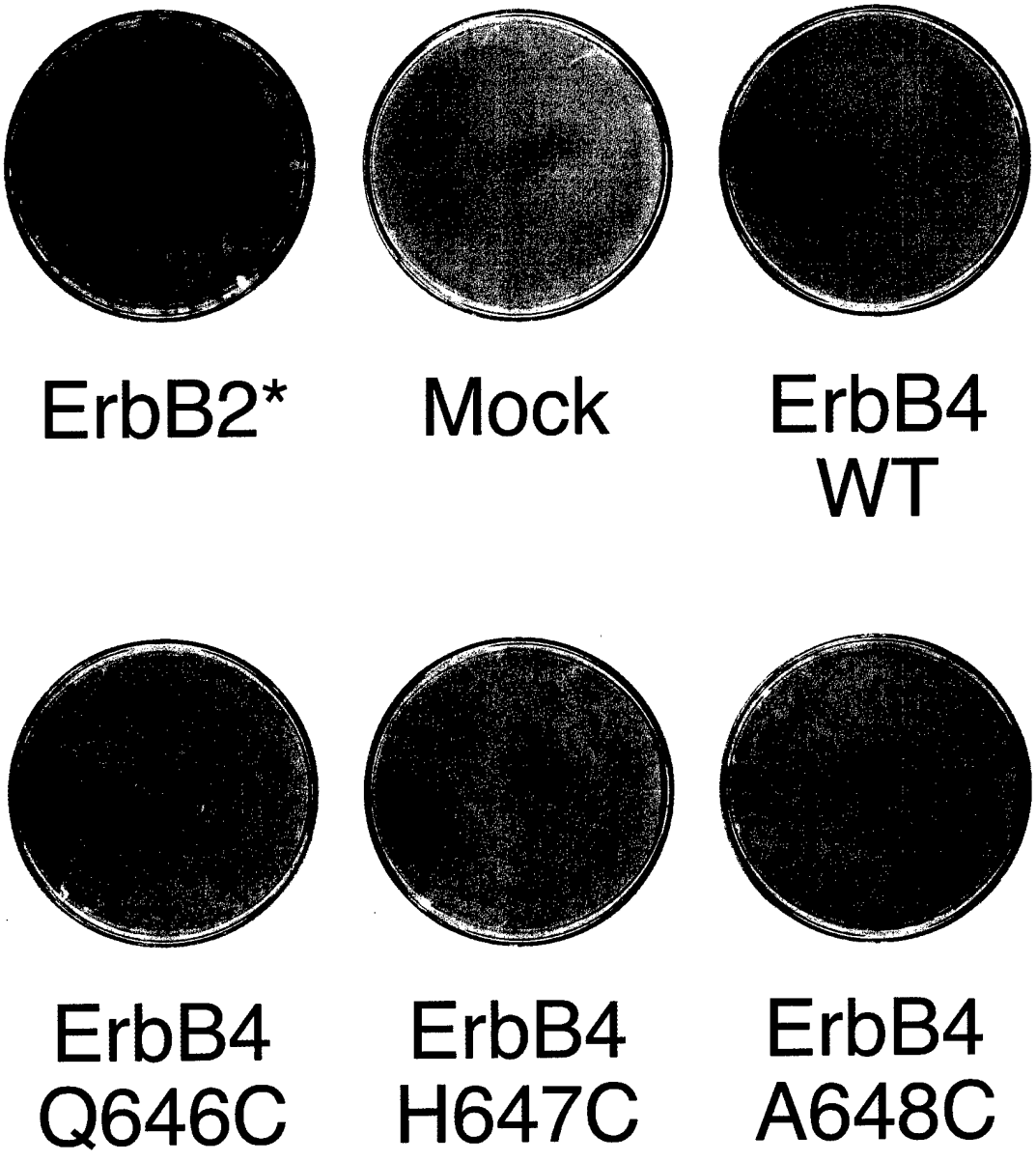

Figure 3. Constitutively-active ErbB4 receptors do not induce a loss of contact inhibition. FR3T3 fibroblasts infected with the LXSN (vector control) retrovirus, the wild-type ErbB4 retrovirus, the constitutively-active ErbB2* retrovirus, or the constitutively-active ErbB4 mutant retroviruses were assayed for loss of contact inhibition (focus formation).

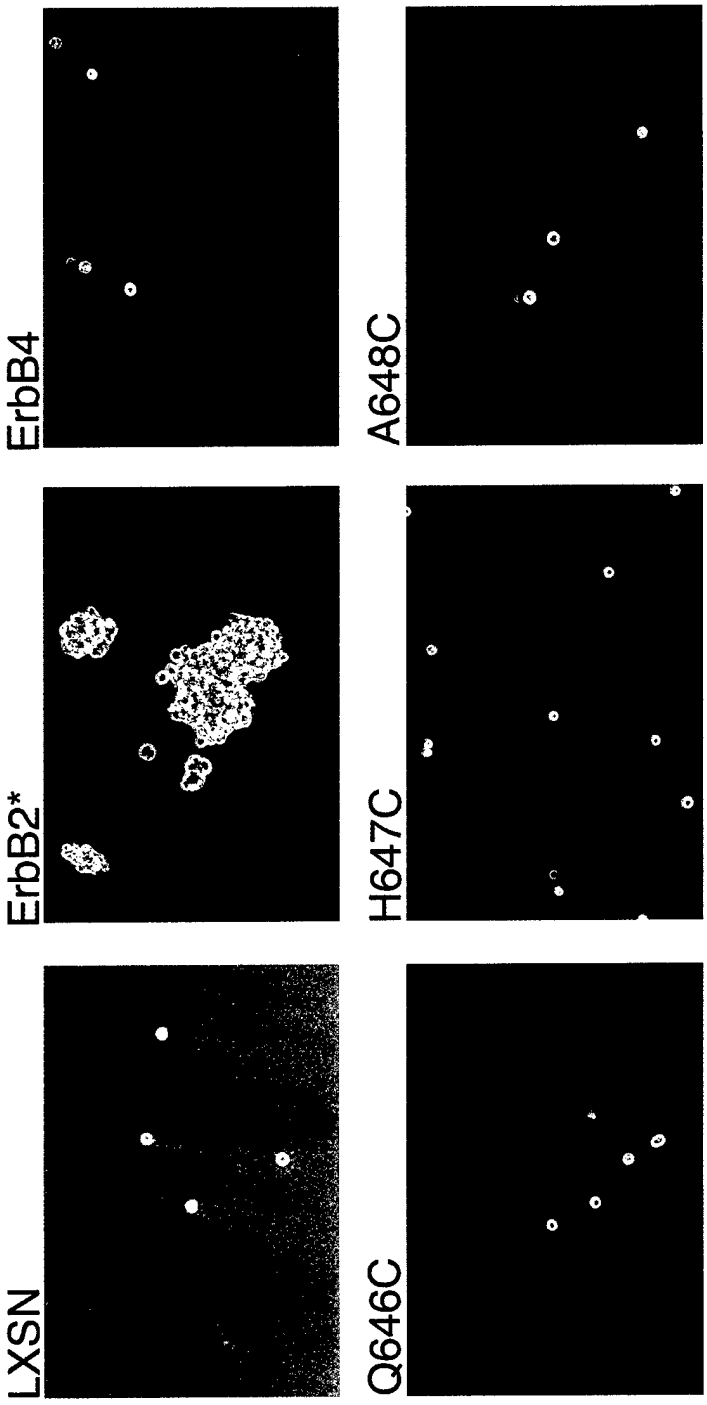

Figure 4. Constitutively-active ErbB4 receptors do not induce growth in semi-solid medium. FR3T3 cells that stably express the LXSN vector control, the constitutively-active ErbB2 mutant (ErbB2*), wild-type ErbB4, or the constitutively-active ErbB4 mutants (Q646C, H647C, A648C) were seeded in semi-solid medium at a density of 2 x 10^4 cells/ml in 60 mm dishes. The cells were incubated for 10 days, after which images were recorded by photomicroscopy. Images shown are representative of those obtained in three independent experiments.

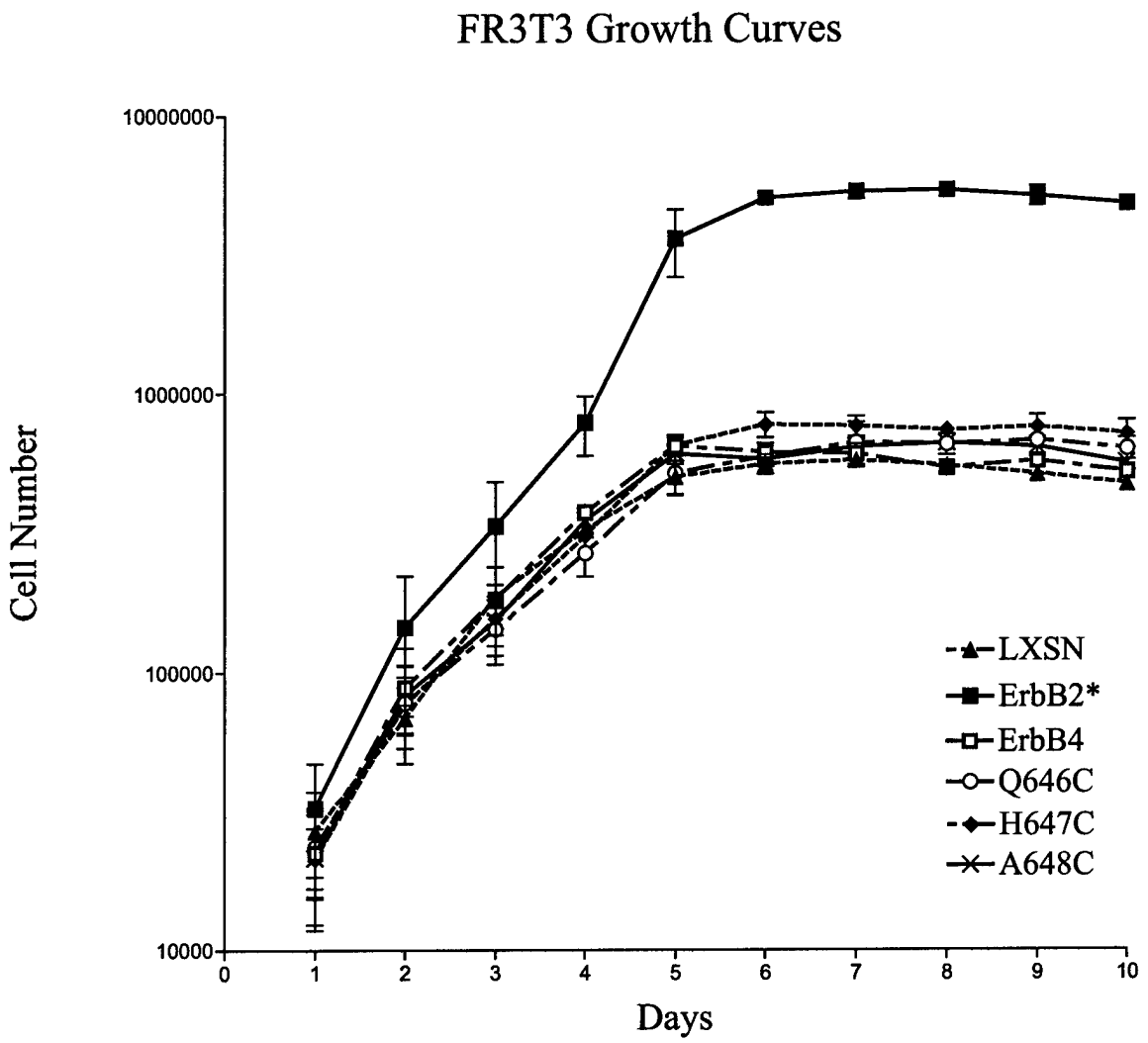

Figure 5. Constitutively-active ErbB4 mutants do not increase the growth rate of FR3T3 fibroblasts. FR3T3 cells that express the LXSN vector control, the constitutively-active ErbB2* mutant, wild-type ErbB4, or the constitutively-active ErbB4 mutants (Q646C, H647C, A648C) were plated at a density of 2 x 10^4 cells in 60 mm dishes (700 cells/cm^2) and were incubated for one to ten days. Cells were counted daily to assess growth rates and saturation densities. The means for three independent experiments are shown with error bars that represent the standard errors of the means.

Table 1. The Q646C, H647C, and A648C ErbB4 mutants exhibit increased normalized tyrosine phosphorylation.

Cell Line	ErbB4 Tyrosine Phosphorylation	ErbB4 Expression	Ratio
Wild-type ErbB4	212867	1831340	0.116
ErbB4 Q646C	1860472	3329432	0.558
ErbB4 H647C	2944443	4659376	0.631
ErbB4 A648C	3981658	4509147	0.883

Table 2. Constitutively-active ErbB4 mutants do not increase the saturation density of FR3T3 fibroblasts.

	Saturation Densities
LXSN	$5.8 \pm 0.3 \times 10^5$
ErbB2*	$5.4 \pm 0.1 \times 10^6$
ErbB4	$6.1 \pm 0.5 \times 10^5$
Q646C	$6.6 \pm 0.6 \times 10^5$
H647C	$7.6 \pm 0.7 \times 10^5$
A648C	$6.6 \pm 0.4 \times 10^5$

Materials and Methods

Cell Lines, Cell Culture, and Antibodies. The Ψ2, PA317, and FR3T3 cell lines were generous gifts from Daniel DiMaio, Yale University. All cell lines were propagated in Dulbecco's modified Eagle's medium (DMEM) supplemented with 10% fetal bovine serum (FBS), 50 IU/ml penicillin, 50 μg/ml streptomycin (Mediatech), and 0.25 μg/ml fungizone (Amphotericin B; Gibco/BRL). Recombinant cell lines generated in the course of the following experiments were propagated in the media described above supplemented with 200 μg/ml G418 (Mediatech).

The anti-ErbB4 mouse monoclonal (SC-8050), anti-ErbB4 rabbit polyclonal (SC-283), and anti-ErbB2 rabbit polyclonal (C-18) antibodies were purchased from Santa Cruz Biotechnology. Goat anti-mouse and goat anti-rabbit horseradish peroxidase conjugated antibodies were purchased from Pierce. Enhanced chemiluminescence (ECL) Western blotting reagents, Redivue™ adenosine 5'-[γ-^{32}P] –triphosphate, and Protein-A Sepharose (CL-4B) were purchased from Amersham Pharmacia Biotech. The 4G10 anti-phosphotyrosine mouse monoclonal antibody was purchased from Upstate Biotechnology.

Plasmids. The recombinant retroviral vector pLXSN (39) was obtained from Daniel DiMaio, Yale University. This construct contains two recombinant LTRs derived from the Maloney Murine Leukemia Virus and the Maloney Murine Sarcoma Virus. These LTRs flank the Ψ packaging signal and the aminoglycoside 3'-phosphotransferase (Neo^R) gene under the transcriptional control of the SV40 early promoter. The Neo^R gene confers resistance to the aminoglycoside antibiotic G418 (geneticin, Gibco/BRL).

The recombinant retroviral construct pLXSN-ErbB4 (26) was generated by subcloning the human ErbB4 cDNA into pLXSN. In this construct the ErbB4 cDNA is under the transcriptional control of the upstream LTR. The recombinant retroviral construct pLXSN-ErbB2* (40) was a gift of Lisa Petti, Albany Medical College. It was generated by subcloning the cDNA encoding the constitutively active rat ErbB2 mutant (ErbB2*) into pLXSN. In this construct the ErbB2* cDNA is under the transcriptional control of the upstream LTR.

ErbB4 Mutagenesis. The plasmid pLXSN-ErbB4 was used as the template for site-directed mutagenesis (QuikChange™ Site Directed Mutagenesis Kit, Stratagene) to construct the putative constitutively-active ErbB4 mutants. The mutants were constructed by introducing mutations that substitute a cysteine residue for Proline645, Glutamine646, Histidine647, Alanine648, or Arginine649 in the ErbB4 extracellular juxtamembrane domain. These mutants are denoted as follows: P645C, Q646C, H647C, A648C, and R649C. A new restriction enzyme site was also engineered in each mutant to facilitate the identification of the mutants. The following primers were used for mutagenesis. "T" denotes the upper primer, while "B" denotes the lower primer. The novel cysteine codons and anticodons are indicated by bold type, the point mutations that create the novel cysteine residues are double underlined, and the novel restriction enzyme sites are singly underlined.

P645CT: 5'-ATTTACTACCCATGGACCGGTCATTCCACTTTA**TGC**CAACATGCTAGAACTCCC-3'

P645CB: 5'-GGGAGTTCTAGCATGTTG**GCA**TAAAGTGGAATGACCGGTCCATGGGTAGTAAAT-3'

Q646CT: 5'-TACTACCCATGGACCGGTCATTCCACTTTACCA**TGC**CATGCTAGAACTCCCCTG-3'

Q646CB: 5'-CAGGGGAGTTCTAGCATG**GCA**TGGTAAAGTGGAATGACCGGTCCATGGGTAGTA-3'

H647CT: 5'-CATTTACTACCCATGGACCGGTCATTCCACTTTACCACAA**TGT**GCTAGAACTCCCCT-3'

H647CB: 5'-AGGGGAGTTCTAGC**ACA**TTGTGGTAAAGTGGAATGACCGGTCCATGGGTAGTAAATG-3'

A648CT: 5'-TCCACTTTACCACAACATTGTAGAACTCCTCTGATTGCAGCTGGA-3'

A648CB: 5'-TCCAGCTGCAATCAGAGGAGTTCTACAATGTTGTGGTAAAGTGGA-3'

R649CT: 5'-ACTTTACCACAACATGCTTGCACTCCTCTGATTGCAGCTGGA-3'

R649CB: 5'-TCCAGCTGCAATCAGAGGAGTGCAAGCATGTTGTGGTAAAGT-3'

The site-directed mutagenesis reactions were performed according to manufacturer's instructions. Standard techniques (41) were used for bacterial transformations, small-scale plasmid DNA preparations, restriction enzyme analysis of the clones, and large-scale plasmid DNA preparations. Positive clones were sequenced by the University of Wisconsin Biotechnology Center to confirm their identity.

Production of Recombinant Retroviruses and Retroviral Infections. The ErbB4 mutant constructs were transfected using standard techniques (42, 43) into the ψ2 ecotropic retrovirus packaging cell line (44) to generate cell lines that express the ErbB4 mutants and to package the constructs into low-titer ecotropic retrovirus particles (42, 43). ψ2 cells were transfected with the pLXSN vector control plasmid, pLXSN-ErbB4, and pLXSN-ErbB2* to generate control cell lines and recombinant ecotropic retroviruses. The PA317 amphotropic packaging cell line (45) and the FR3T3 rat fibroblast cell line were infected with the ecotropic recombinant retroviruses using standard techniques (42, 43) to generate additional cell lines that express the ErbB4 mutants.

Immunoblot Assays for Receptor Tyrosine Phosphorylation and Expression. The analysis of ErbB4 and ErbB2 tyrosine phosphorylation by immunoprecipitation and anti-phosphotyrosine immunoblotting has been described previously (21, 26). Briefly, cell lysates were generated and protein content was quantified using a Coomassie® Protein Assay Reagent

(46; Pierce Chemical). ErbB2 or ErbB4 was immunoprecipitated from equal amounts of protein using specific antibodies. The immunoprecipitates were resolved by SDS/PAGE on a 7.5% acrylamide gel and electrotransferred onto nitrocellulose. The blots were probed with the anti-phosphotyrosine monoclonal antibody 4G10. Antibody binding was detected and visualized using a goat anti-mouse horseradish peroxidase coupled antibody and enhanced chemiluminescence. The blots were then stripped and probed with the anti-ErbB4 polyclonal antibody to assess ErbB4 expression levels. Antibody binding was detected and visualized using a goat anti-mouse horseradish peroxidase coupled antibody and enhanced chemiluminescence.

The amounts of receptor tyrosine phosphorylation and expression were quantified by digitizing the chemilumigrams using a Linotype-Hell Jade 2-dimensional scanning densitometer set at 600 dpi resolution. The bands on the images were quantified using NIH Image for Macintosh v1.6 software. Values are expressed as arbitrary units. Background levels were computed using the vector control lanes and were subtracted from the gross values to produce net receptor expression and tyrosine phosphorylation values. The digitized images were also cropped and annotated using Adobe Photoshop for Macintosh v3.0.5 software.

***In Vitro* Kinase Assay.** ErbB2 and ErbB4 were immunoprecipitated from protein extracts from PA317 cells as previously described (26). Immune complex kinase reactions were performed as previously described (31). Briefly, 35 µl Protein-A Sepharose and 5 µl of anti-ErbB2 or anti-ErbB4 rabbit polyclonal antibodies were used to immunoprecipitate the receptors from lysates containing the same amount of protein. Immunoprecipitates were washed five times in 500 µl kinase buffer (20 mM Tris-HCl, pH 7.4, 5 mM $MgCl_2$, 3 mM $MnCl_2$). After the last wash, the samples were resuspended in 100 µl kinase buffer supplemented with 10 µCi of [γ-^{32}P]ATP and were incubated for 10 minutes at room temperature to permit the kinase reaction to

occur. The beads were then washed two times in NET-N (47) and boiled for 5 minutes in SDS/PAGE protein sample buffer. The samples were resolved by SDS/PAGE on a 7.5% acrylamide gel. The gels were dried overnight and exposed to X-ray film for approximately 20 hours. The autoradiograms were digitized using a Linotype-Hell Jade 2-dimensional scanning densitometer set at 600 dpi resolution. The bands on the images were quantified using NIH Image for Macintosh v1.6 software. Values are expressed as arbitrary units. Background levels were computed using the vector control lanes and were subtracted from the gross values to produce net kinase activity values. The digitized images were also cropped and annotated using Adobe Photoshop for Macintosh v3.0.5 software.

Focus Formation Assay for Loss of Contact Inhibition. FR3T3 cells were infected with recombinant ecotropic retroviruses as described earlier and in previously-published reports (42, 43). Briefly, 60 mm dishes of cells at approximately 70% confluence were infected with ecotropic retrovirus stocks. Approximately 24 hours after infection, cells were passaged into three 60 mm dishes. Cells were maintained in DMEM supplemented with 10% FBS until foci appeared. The medium was changed every three days. Cells were fixed in 100% methanol and stained with Giemsa (Fisher) to visualize the foci. The plates were digitized using a Linotype-Hell Jade 2-dimensional scanning densitometer set at 600 dpi resolution. The digitized images were cropped and annotated using Adobe Photoshop for Macintosh v3.0.5 software.

Assay for Anchorage Independence. FR3T3 cells were seeded at a density of 2×10^4 cells in 60 mm dishes containing 2.5 ml of 0.3% Low Melting Point Agarose (LMP-agarose; Gibco/BRL) as described previously (48). Every three days DMEM supplemented with 10% FBS and 0.3% LMP-agarose was added to each plated. The cells were incubated at 37°C for 10 days and fields were photographed with an Olympus OM-10 camera attached to an Olympus

CK-2 phase-contrast inverted microscope. The images were digitized by the photofinishing firm. These images were cropped and annotated using Adobe Photoshop for Macintosh v3.0.5 software. Images are representative of three independent experiments.

Growth Rate/Saturation Density Assay. Stable FR3T3 cell lines expressing the wild-type ErbB4 receptor, ErbB2*, or the ErbB4 mutants (Q646C, H647C, A648C) were plated in ten 60 mm dishes at a density of 2×10^4 cells per dish. Cells were incubated from one to ten days at 37°C. Cells were counted (Coulter Counter® ZM) each day for a total of ten days. The mean and standard error of the mean (SEM) are representative of three independent experiments.

Acknowledgements

The authors thank Gar Park, Roberto Ricardo, and Fernando Cruz-Guilloty for their preliminary studies that led to these experiments. The authors gratefully acknowledge the support of a Purdue University Graduate Opportunities Minority Student fellowship (D.J.P.), a MARC-AIM minority undergraduate research fellowship (I.B.), an American Society for Microbiology undergraduate research fellowship (I.B.), an American Cancer Society Institutional Grant to the Purdue Cancer Research Center (IRG-58-006), and grants from the Purdue Cancer Research Center (D.J.R.), the Showalter Trust (D.J.R.), the Indiana Elks Foundation (D.J.R.), the US Army Medical Research and Material Command Breast Cancer Research Program (DAMD17-00-1-0415 & DAMD17-00-1-0416), and the National Cancer Institute (CA80770).

References

1. Miettinen, P.J., Berger, J.E., Meneses, J., Werb, Z., and Derynck, R. Epithelial immaturity and multiorgan failure in mice lacking epidermal growth factor receptor. *Nature* 376: 337-344, 1995.

2. Lee, K., Simon, H., Chen, H., Bates, B., Hung, M., and Hauser, C. Requirement for neuregulin receptor ErbB2 in neuronal and cardiac development. *Nature* **378**: 394-398, 1995.

3. Riethmacher, D., Sonnenberg-riethmacher, E., Brinkmann, V., Yamaai, T., Lewin, G.R., and Birchmeier, C. Severe neuropathies in mice with targeted mutations in the ErbB3 receptor. *Nature* **389**: 725-730, 1997.

4. Gassmann, M., Casagranda, F., Orioli, D., Simon, H., Lai, C., Klein, R., and Lemke, G. Aberrant neuronal and cardiac development in mice lacking the ErbB4 neuregulin receptor. *Nature* **378**: 390-394, 1995.

5. Wong, A.J., Ruppert, J.M., Bigner, S.H., Grzeschik, C.H., Humphrey, P.A., Bigner, D.S., and Vogelstein, B. Structural alterations of the epidermal growth factor receptor gene in human gliomas. *Proc. Natl. Acad. Sci. USA* **89**: 2965-2969, 1992.

6. Moscatello, D.K., Holgado-Madruga, M., Godwin, A.K., Ramirez, G., Gunn, G., Zoltick, P.W., Biegel, J.A., Hayes, R.L., Wong, A.J. Frequent expression of a mutant epidermal growth factor receptor in multiple human tumors. *Cancer Res.* **55**: 5536-5539, 1995.

7. Gorgoulis, V., Aninos, D., Mikou, P., Kanavaros, P., Karameris, A., Joardanoglou, J., Rasidakis, A., Veslemes, M., Ozanne, B., Spandidos, D.A. Expression of EGF, TGF-α, and EGFR in squamous cell lung carcinoma. *Anticancer Res.* **12**: 1183-1187, 1992.

8. Hynes, N.E., and Stern, D.F. The biology of ErbB-2/Neu/HER-2 and its role in cancer. *Biochemica et Biophysica Acta.* **1198**: 165-184, 1994.

9. Kraus, M.H., Issing, W., Miki, T., Popescu, N.C., and Aaronson, S.A. Isolation and characterization of ERBB3, a third member of the ERBB/epidermal growth factor receptor family: evidence for overexpression in a subset of human mammary tumors. *Proc. Natl. Acad. Sci. USA* **86**: 9193-9197, 1989.

10. Sanidas, E.E., Filipe, M.I., Linehean, J., Lemoine, N.R., Gullick, W.J., Rajkumar, T., and Levinson, D.A. Expression of the c-ErbB-3 gene product in gastric cancer. *Int. J. Cancer* **54**: 935-940, 1993.

11. Haugen, D.R., Akslen, L.A., Varhaug, J.E., and Lillehaug, J.R. Expression of c-erbB-3 and c-erbB-4 proteins in papillary thyroid carcinomas. *Cancer Res.* **56**: 1184-1188, 1996.

12. Kew, T.Y., Bell, J.A., Pinder, S.E., Denley, H., Srinivasan, R., Gullick, W.J., Nicholson, R.I., Blamey, R.W., and Ellis, I.O. c-ErbB-4 protein expression in human breast cancer. *Br. J. Cancer* **82**: 1163-1170, 2000.

13. Kato, T. Expression of mRNA for heregulin and its receptor, ErbB-3 and ErbB-4, in human upper gastrointestinal mucosa. *Life Sci.* **63**: 553-564, 1998.

14. Bacus, S.S, Zelnick, C.R., Plowman, G., and Yarden, Y. Expression of the ErbB-2 family of growth factor receptors and their ligands in breast cancer: implications for tumor biology and clinical behavior. *Am. J. Clin. Pathol.* **102**: S13-S24, 1994.

15. Knowlden, J.M., Gee, J.W., Seery, L.T., Farrow, L., Gullick, W.J., Ellis, I.O., Blamey, R.W., Robertson, J.R., and Nicholson, R.I. c-ErbB3 and c-ErbB4 expression is a feature of the endocrine responsive phenotype in clinical cancer. *Oncogene* **17**: 1949-1957, 1998.

16. Bacus, S.S., Chin, D., Yarden, Y., Zelnick, C.R., and Stern, D.F. Type 1 receptor tyrosine kinases are differentially phosphorylated in mammary carcinoma and differentially associated with steroid receptors. *Am. J. Pathol.* **148**: 549-558, 1996.

17. Gilbertson, R.J., Perry, R.H., Kelly, P.J., Pearson, A.D.J., and Lunec, J. Prognostic significance of HER2 and HER4 coexpression in childhood medulloblastoma. *Cancer Res.* **57**: 3272-3280, 1997.

18. Borg. A., Tandon, A.K., Sigurdsson, H., Clark, G.M., Ferno, M., Fuqua, S.A.W., Killander, D., McGuire, W.L. HER-2/neu amplification predicts poor survival in node-positive breast cancer. *Cancer Res.* **50**: 4332-4337, 1990.

19. Srinivasan, R., Poulsom, R., Hurst, H.C., and Gullick, W.J. Expression of the c-erbB4 /HER4 protein and mRNA in normal human fetal and adult tissues and in a survey of nine solid tumor types. *J. Pathol.* **185**: 236-245, 1998.

20. Riese, D.J. II, Bermingham, Y., van Raaij, T.M., Buckley, S., Plowman, G.D., and Stern, D.F. Betacellulin activates the epidermal growth factor receptor and erbB-4 and induces cellular response patterns distinct from those stimulated by epidermal growth factor or neuregulin-β. *Oncogene* **12**: 345-353, 1996.

21. Riese, D.J. II, Komurasaki, T., Plowman, G.D., and Stern, D.F. Activation of ErbB4 by the bifunctional epidermal growth factor family hormone epiregulin is regulated by ErbB2*. *J. Biol. Chem.* **273**: 11288-11294, 1998.

22. Alroy, I., and Yarden, Y. The ErbB signaling network in embryogenesis and oncogenesis: signal diversification through combinatorial ligand-receptor interactions. *FEBS Lett.* **410**: 83-86, 1997.

23. Riese, D.J. II and Stern, D.F. Specificity within the EGF family/ErbB receptor family signaling network. *Bioesssays* **20**, 41-48, 1998.

24. Stern, D.F., and Kamps, M. EGF-stimulated tyrosine phosphorylation of p185neu: A potential model for receptor interactions. *EMBO J.* **7**: 995-1001, 1988.

25. Riese, D.J. II, Kim, E.D., Elenius, K., Buckley, S., Klagsbrun, M., Plowman, G.D., and Stern, D.F. The epidermal growth factor receptor couples transforming growth factor-α, heparin-binding epidermal growth factor-like factor, and amphiregulin to Neu, ErbB-3, and ErbB-4. *J. Biol. Chem.* **271**: 20047-20052, 1996.

26. Riese, D.J. II, Van Raaij, T.M., Plowman, G.D., Andrews, G.C., and Stern, D.F. The cellular response to neuregulins is governed by complex interactions of the erbB receptor family. *Mol. Cell. Biol.* **15**: 5770-5776, 1995.

27. Sorkin, A., Lemmon, M.A., Ulrich, A., and Schlessinger, J. Stabilization of an active dimeric form of the epidermal growth factor receptor by introduction of an inter-receptor disulfide bond. *J. Biol. Chem.* **269**: 9752-9759, 1994.

28. Burke, C.L., and Stern, D.F. Activation of Neu (ErbB-2) mediated by disulfide bond-induced dimerization reveals a receptor tyrosine kinase dimer interface. *Mol. Cell. Biol.* **18**: 5371-5379, 1998.

29. d'Avis, P.Y., Robertson, S.C., Meyer, A.N., Bardwell, W.M., Webster, M.K., and Donoghue, D.J. Constitutive activation of fibroblast growth factor receptor 3 by mutations responsible for the lethal skeletal dysplasia thanatophoric dysplasia type I. *Cell Growth Diff.* **9**: 71-78, 1998.

30. Galvin, B.D., Hart, K.C., Meyer, A.N., Webster, M.K., Donoghue, D.J. Constitutive receptor activation by crouzon syndrome mutations in fibroblasts growth factor receptor (FGFR) 2 and FGFR2/Neu chimeras. *Proc. Natl. Acad. Sci. USA* **93**: 7894-7899, 1996.

31. Cohen, B.D., Green, J.M., Foy, L., and Fell, H.P. HER4 mediated biological and biochemical properties in NIH 3T3 cells. *J. Biol. Chem.* **271**: 4813-4818, 1996a.

32. Cohen, B.D., Kiener, P.A., Green, J.M., Foy, L., Perry Fell, H., and Zhang, K. The relationship between human epidermal growth-like factor receptor expression and cellular transformation in NIH3T3 cells. *J. Biol. Chem.* **271**: 30897-30903, 1996b.

33. Zang, K., Sun, J., Liu, N., Wen, D., Chang, D., Thomason, A., and Yoshinaga, S.K. Transformation of NIH3T3 cells by HER3 or HER4 receptors requires the presence of HER1 or HER2*. *J. Biol. Chem.* **271**: 3884-3890, 1996.

34. Peles, E., Bacus, S.S., Koski, R.A., Lu, H.S., Wen, D., Ogden, S.G., Ben Levy, R., and Yarden, Y. Isolation of the Neu/HER-2 stimulatory ligand: a 44 kd glycoprotein that induces differentiation of mammary tumor cells. *Cell* **69**: 205-216, 1992.

35. Jones, F.E., Jerry, D.J., Guarino, B.C., Andrews, G.C., and Stern, D.F. Heregulin induces *in vivo* proliferation and differentiation of mammary epithelium into secretory lobuloalveoli. *Cell Growth Diff.* **7**: 1031-1038, 1996.

36. Dankort, D.L., Wang, Z., Blackmore, V., Moran, M.F., and Muller, W.J. Distinct tyrosine autophosphorylation sites negatively and positively modulate Neu-mediated transformation. *Mol. Cell. Biol.* **17**: 5410-5425, 1997.

37. Drummond-Barbosa, D., Vaillancourt, R.R., Kazlauskas, A., and DiMaio, D. Ligand-independent activation of the platelet-derived growth factor b receptor: requirements for bovine papillomavirus E5-induced mitogenic signaling. *Mol. Cell. Biol.* **15**: 2570-2581, 1995.

38. Sweeney, C., Lai, C., Riese II, D.J., Diamonti, A.J., Cantley, L.C., and Carraway III, K.L. Ligand discrimination in signaling through an ErbB4 receptor homodimer. *J. Biol. Chem.* **275**: 19803-19807, 2000.

39. Miller, D.A., Rosman, G.J. Improved retroviral vectors for gene transfer and expression. *BioTechniques* **7**: 980-990, 1989.

40. Petti, L.M., and Ray, F.A. Transformation of mortal human fibroblasts and activation of a growth inhibitory pathway by the bovine papillomavirus E5 oncoprotein. *Cell Growth Diff.* **11**: 395-408, 2000.

41. Sambrook, J., and Russell, D.W. *Molecular cloning: A laboratory manual.* Cold Spring Harbor, New York: Cold Spring Harbor Laboratory Press, 2001.

42. Leptak, C., Ramon y Cajal, S., Kulke, R., Horwitz, B.H., Riese II, D.J., Dotto, G.P., and DiMaio, D. Tumorigenic transformation of murine keratinocytes by the E5 genes of bovine papillomavirus type I and human papillomavirus type 16. *J. Virol.* **65**: 7078-7083, 1991.

43. Riese, D.J. II and DiMaio, D. An intact PDGF signaling pathway is required for efficient growth transformation of mouse C127 cells by the bovine papillomavirus E5 protein. *Oncogene* **10**, 1431-1439, 1999.

44. Mann, R., Mulligan, R.C., and Baltimore, D. Construction of a retrovirus packaging mutant and its use to produce helper-free defective retrovirus. *Cell* **33**: 153-159, 1983.

45. Miller, D.A., and Buttimore, C. Redesign of retrovirus packaging cell lines to avoid recombination leading to helper virus production. *Mol. Cell. Biol.* **6**: 2895-2902, 1986.

46. Bradford, M. A rapid and sensitive method for the quantification of microgram quantities of protein utilizing the principle of protein dye-binding. *Anal. Biochem.* **72**: 248-254, 1976.

47. Petti, L., Nilson, L.A., and DiMaio, D. Activation of the platelet-derived growth factor receptor by the bovine papillomavirus E5 transforming protein. *EMBO J.* **10**: 845-855, 1991.

48. Hwang, E., Riese, D.J. II, Settleman, J., Nilson, L.A., Honig, J., Flynn, S., Dimaio, D. Inhibition of cervical carcinoma cell line proliferation by the introduction of a bovine papillomavirus regulatory gene. *J. Virol.* **67**: 3720-3729, 1993.

CONSTRUCTION AND ANALYSIS OF CONSTITUTIVELY-ACTIVE MUTANTS OF THE ERBB4 RECEPTOR TYROSINE KINASE

A Thesis

Submitted to the Faculty

Of

Purdue University

By

Desi Jay Penington

In Partial Fulfillment of the

Requirements for the Degree

Of

Master of Science

August 2001

Dedicated to my parents

ACKNOWLEDGEMENTS

This collection of papers presents the outcome of my research that was carried out during the two years I spent as a graduate student at Purdue University. During this period, I had the honor of working with many individuals whom have in some way influenced and supported the direction and content of my work. This period was filled with enriching and meaningful experiences and without the support and guidance from the following individuals would not have been possible.

First and foremost, I would like to express my sincere gratitude to my supervisor, Dr. David J. Riese II. He persuaded me to join this project, and his guidance throughout has been invaluable; this thesis has certainly benefited from his insight and innumerable suggestions.

Many thanks are due to the Department that made all of this research possible, the Department of Medicinal Chemistry and Molecular Pharmacology. In addition, the Department of Biochemistry and Molecular Biology, where I began my graduate career, provided me with opportunities that would have not been possible otherwise. Special thanks goes to Elizabeth Chandler and Sally Bateman for their endless patience and goodwill.

Of course, to my thesis committee, Dr. Robert Geahlen, Dr. Michael Kinch, and Dr. Kevin Hannon, I extend my sincere gratitude to you for your support, guidance and constructive criticism, especially near the end of the journey. Without your continued belief in me, this thesis would not be completed.

Furthermore, I am especially indebted to Ianthe "Cookie" Bryant who has worked along side me since the beginning. Her continued perseverance and constant assistance has greatly benefited this project. To Cookie, " Whether you think you can or think you can't – you are right" –Henry Ford.

I am also grateful to Tim Vortherms, Medhane Cumbay, Dave Roman, Stephanie Coffing, and Dr. Robert Hammer for their invaluable suggestions and for providing an environment that fostered my learning as a graduate student and scientist. I am eternally grateful, thank you all.

Mom and Dad this is for you.

TABLE OF CONTENTS

Page

LIST OF TABLES vii

LIST OF FIGURES viii

LIST OF ABBREVIATIONS ix

ABSTRACT xi

CHAPTER I: INTRODUCTION 1

Structure and Activation of ErbB Receptors 7

ErbB4 9

Strategy For Studying ErbB4 Receptor Function 11

CHAPTER II: MATERIALS AND METHODS 14

Antibodies and Reagents 14

ErbB4 Mutagenesis 14

Cell Lines 18

Retroviral Infections 18

Immunoprecipitations and Immunoblotting 19

Dimerization Assay 20

In Vitro Kinase Assay 20

Focus Forming Assay 21

Anchorage Independency Assay 21

Growth Rate/Saturation Density 22

CHAPTER III: RESULTS 23

ErbB4 mutant receptors have increased signaling 23

ErbB4 mutant receptors are constitutively-dimerized 30

ErbB4 mutant receptors have increased *in vitro* kinase activity 33

Page

Constitutively-active ErbB4 mutant receptors lack transforming activity 35
Constitutive ErbB4 signaling does not induce anchorage-independent growth 37
Constitutive ErbB4 signaling does not increase the growth rate or saturation density of cells 38
CHAPTER IV: DISCUSSION 41
LIST OF REFERENCES 45
APPENDICES
Appendix A
Diagrammatic Representation of Specific Phosphotyrosine Residues and Signaling Molecules For The ErbB Family of Receptor Tyrosine Kinases 52
Appendix B
The ErbB Signaling Network 53
Appendix C
ErbB4 Isoforms 54

LIST OF TABLES

Table Page

3.1 The Q646C, H647C, and A648C ErbB4 mutants exhibit increased normalized tyrosine phosphorylation 27

3.2 Titers of Ψ2 retroviral particles 29

3.3 Saturation densities of FR3T3 cell expressing constitutively-active ErbB4 receptors 40

LIST OF FIGURES

Figure Page

1.1 The ErbB family of growth factor receptors 3

1.2 Schematic diagram of ErbB ligands and their associated receptors 6

1.3 Model for ligand-induced activation of ErbB receptors 8

1.4 The ErbB4 receptor tyrosine kinase 10

1.5 Extracellular region of the ErbB4 receptor 12

1.6 ErbB4 site-directed mutants 13

3.1 Expression and phosphorylation of ErbB4 mutant receptors in Ψ2 cells 25

3.2 ErbB4 mutants are constitutively tyrosine phosphorylated 28

3.3 Constitutively-dimerized ErbB4 mutant receptors 31

3.4 Phosphorylation of constitutively-dimerized ErbB4 mutant receptors 32

3.5 Q646C, H647C, and A648C mutants exhibit increased *in vitro* kinase activity 34

3.6 Constitutively-active ErbB4 receptors do not induce a significant loss of contact inhibition 36

3.7 Constitutively-active ErbB4 receptors do not induce growth in soft agar 37

3.8 Growth curves of constitutively-active ErbB4 mutant receptors parallel the wild-type ErbB4 receptor 39

LIST OF ABBREVIATIONS

AR	Amphiregulin
ATP	Adenosine Triphosphate
BSA	Bovine Serum Albumin
BTC	Betacellulin
Cfu	Colony forming units
DMEM	Dulbecco's Modified Eagle's Medium
ECL	Enhanced Chemiluminescence
EDTA	Ethylene Diamine Tetra Acetic Acid
EGF	Epidermal Growth Factor
EGFR	Epidermal Growth Factor Receptor
EPR	Epiregulin
ER	Estrogen Receptor
FBS	Fetal Bovine Serum
FGFR	Fibroblast Growth Factor Receptor
HB-EGF	Heparin-binding EGF-like Growth Factor
HRP	Horseradish Peroxidase
Ig3	Immumoglobulin-Like Domain 3
LMP	Low Melting Point Agarose
MAPK	Mitogen-Activated Protein Kinase
Neo^R	Neomycin-Resistance Gene
NRG	Neuregulin
PAGE	Polyacrylamide Gel Electrophoresis
PI3K	Phosphatidylinositol 3'-Kinase
PKC	Protein Kinase C

PMA	Phorbol 12-Myristate 13-Acetate
PR	Progesterone Receptor
PTB	Phosphotyrosine Binding Domain
RTK	Receptor Tyrosine Kinase
SDS	Sodium Dodecyl Sulfate
SH2	Src Homology Domain
TBS-T	Tris Buffered Normal Saline supplemented with Tween-20
TDI	Thanatophoric Dysplasia Type I
TGF-α	Transforming Growth Factor-alpha

ABSTRACT

Penington, Desi J., M.S., Purdue University, August 2001. Construction and Analysis of Constitutively-Active Mutants of the ErbB4 Receptor Tyrosine Kinase. Major Professor: Dr. David J. Riese II

ErbB4 is a member of the epidermal growth factor receptor (EGFR) family of tyrosine kinases, which includes ErbB1/EGFR, ErbB2/HER2/Neu, and ErbB3/HER3. These receptors play important roles in both normal development and neoplasia. Previous studies have demonstrated that deregulated signaling by ErbB1 and ErbB2 occurs in many human malignancies. In contrast, the role ErbB4 plays in tumorigenesis has not been clearly defined. Multiple studies have suggested that increased ErbB4 signaling couples to uncontrolled cell proliferation and metastatic disease. Others have suggested that ErbB4 signaling regulates cell differentiation, growth suppression or that the loss of ErbB4 signaling couples to tumorigenesis. To study biological responses coupled to ErbB4, we have constructed three constitutively-active ErbB4 mutants that signal in the absence of ligand. Using a fibroblast cell line, we have assayed these constitutively-active receptors for coupling to a loss of contact inhibition and for coupling to increased proliferation, saturation density, and anchorage independence. We have determined that the proliferation of cells expressing these gain-of-function mutants is still inhibited by contact and is not anchorage independent. Moreover, the ErbB4 mutants do not alter cell growth rates or saturation density. Our data appears to reinforce studies of the mammary gland that suggests ErbB4 couples to terminal differentiation. Indeed, our results suggest that ErbB4 may act as a tumor suppressor or limit coupling to metastatic disease.

CHAPTER I
INTRODUCTION

Cellular environments are continuously changing to influence the activity of cells. Characterizing how cells interpret and respond to these signals is essential for understanding biological systems. Cell surface receptors mediate the physiological responses from the surrounding microenvironment by transducing signals that govern growth, migration, differentiation, and death (Schlessinger *et al.*, 2000). Hormones, neurotransmitters, and growth factors act through these cell surface receptors to stimulate protein kinase cascades that dictate physiological responses. Often, deregulated signaling by these receptors leads to tumor pathogenesis. Undoubtedly, understanding how cell surface receptors function will contribute to better therapeutic strategies to limit human disease.

ErbB4 (HER4/p180^{erbB4}) is a member of the epidermal growth factor receptor (EGFR) family of tyrosine kinases (RTK), which includes EGFR/ErbB1/HER1, ErbB2/HER2/Neu, and ErbB3/HER3 (see Figure 1.1). A number of different tissues of epithelial, mesenchymal, and neuronal origin express these receptors (ErbB receptors). Numerous studies have demonstrated that ErbB receptors play important roles in regulating and specifying fundamental cellular processes including differentiation, proliferation, and development (Jones *et al.*, 1996; Jones *et al.*, 1999; Schroeder and Lee, 1998). The functional roles of ErbB receptors, and ErbB4 in particular, have been well documented in genetically modified mice lacking individual receptors. Mice null for EGFR/ErbB1 have impaired epithelial development in several organs, including skin, lung, and the gastrointestinal tract (Miettinen *et al.*, 1995; Threadgill *et al.*, 1995; Sibilia and Wagner, 1995). ErbB2 null mice die at midgestation (E10.5) due to malformation of myocardial trabeculae (Lee *et al.*, 1995). ErbB3 deficient mice lack Schwann-cell

development in the peripheral nervous system, affecting axons of sensory and motor neurons (Riethmacher *et al.,* 1997). Embryos homozygous for the disruption of the *neuregulin 1* gene (NRG1, an ErbB ligand) or the *erbb4* gene display similar developmental defects as ErbB2 null mice (Meyer and Birchmeier, 1995; Gassmann *et al.,* 1995). Indeed, the absence of cardiac ventricular trabeculation is a prominent feature of ErbB4 null mice. Normal formation of ventricular trabeculae is essential for the homeostasis of blood flow during early stages of heart development. Embryonic lethality results from trabecular malformation, which causes irregular blood flow and defective cardiac function. Overall, homozygous mice defective in NRG1, ErbB2, ErbB3, or ErbB4 die *in utero* between 10 and 14 days following fertilization. Clearly, ErbB receptors play essential roles in modulating the proper development of cardiac muscle and the nervous system.

The physiological roles of ErbB receptors in adult tissues are much less defined. Direct analysis of receptor function has been limited by the embryonic lethality of animals lacking these receptors (Gassmann *et al.,* 1995; Lee *et al.,* 1995; Meyer and Birchmeier, 1995; Riethmacher *et al.,* 1997). In spite of the limitations, ErbB receptor expression patterns in adult tissues reveal that all four ErbB receptors are coordinately expressed during early, mid, and late pregnancy in the mammary glands of mice (Schroeder and Lee, 1998). Interestingly, ErbB1 and ErbB2 are expressed in glands of virgin mice, whereas ErbB4 is not. ErbB1 and ErbB2 display similar levels of expression in puberty and involution (Darcy *et al.,* 2000). Higher expression levels of ErbB4 are seen during late pregnancy and early lactation where epithelial differentiation predominates over proliferation (Jones *et al.,* 1999). ErbB4 is predominantly expressed in mature females, suggesting functional roles in differentiation (Darcy *et al.,* 2000). The coordinate expression of ErbB receptors is not unique to the mammary gland. Pancreatic islet development and ductal growth also appears to depend on multiple ErbB family members (Kritzik *et al.,* 2000).

Ligands for the ErbB family receptors are also coordinately expressed. Epidermal growth factor (EGF), transforming growth factor-α (TGF-α), heparin-binding EGF-like growth factor (HB-EGF) and neuregulin (NRG) are the predominate ligands associated

with mammary morphogenesis (Yang *et al.*, 1995; Jones *et al.*, 1996). In the mammary gland, the expression of NRG correlates with ErbB3 and ErbB4 levels, whereas expression of TGF-α and HB-EGF parallel the expression of ErbB1 and ErbB2. Functionally, all EGF ligands are capable of activating more than one ErbB receptor. For example, neuregulin binds either ErbB3 or ErbB4 to induce receptor heterodimerization with ErbB2 (Riese *et al.*, 1995). Whether the biological activity associated with neuregulin expression occurs through ErbB2:ErbB3 or ErbB2:ErbB4 heterodimers is unclear. Indeed, the complexity of receptor heterodimerization and the ability of ErbB family members to bind multiple ligands have limited the discovery of functional roles played by each receptor in adult tissues.

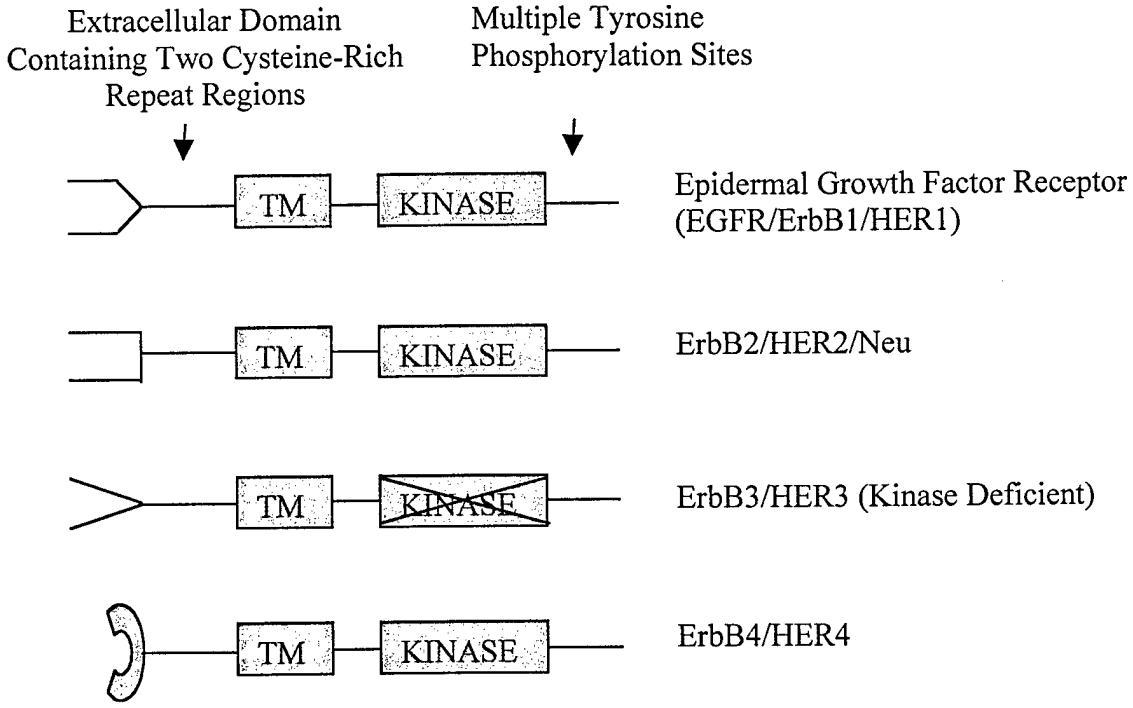

Figure 1.1 **The ErbB family of growth factor receptors.** ErbB1, ErbB2, and ErbB4 all contain a highly conserved intrinsic tyrosine kinase domain (KINASE) and hydrophobic transmembrane (TM) regions. ErbB3 has impaired kinase activity due to substitutions in critical residues in its kinase domain (indicated by the X). ErbB2 is an orphan receptor having no known ligand.

Deregulated expression and/or signaling of ErbB family members occurs in many human malignancies. In particular, ErbB1 or ErbB2 are frequently overexpressed in breast, lung, prostate, ovarian, colon, and pancreatic cancers (Tang and Lippman, 1998; Hynes and Stern, 1994). ErbB1 and ErbB2 overexpression correlates with tumor aggressiveness and poor prognosis for survival (Slamon *et al.,* 1987). There is, however, no detailed analysis of the biological roles played by ErbB4 in metastatic disease.

Although the functional roles ErbB4 plays are unknown, its overexpression has been associated with favorable prognosis in breast cancer (Bacus *et al.,* 1994; Knowlden *et al.,* 1998). A strong positive correlation exists between ErbB4 expression and two favorable prognostic markers for breast cancer, estrogen (ER) and progesterone (PR) receptor expression (Bacus *et al.,* 1996). In contrast, ErbB2 overexpression varies inversely with both PR and ER levels and indicates tumors that are more likely to be metastatic and fatal. The prognostic significance of ErbB4 expression in tumors may also depend on which ErbB family members are co-expressed with ErbB4. In the case of childhood meduloblastoma (one of the most common solid tumors of childhood), patients with tumors overexpressing both ErbB2 and ErbB4 have a significantly worse prognosis for survival than patients with tumors that overexpress either receptor alone (Gilbertson *et al.,* 1997). Finally, loss of ErbB4 expression has been seen in 40-80% in one study of nine solid tumor types of various malignancies, including breast, prostate, and up to 100% in squamous cell carcinomas of the head and neck (Srinivasan *et al.,* 1998). These results raise the intriguing possibility that ErbB4 is unique to this family of receptors. The loss of ErbB4 expression in metastatic disease and the correlation of ErbB4 expression to favorable outcomes in cancer suggest that ErbB4 signaling may limit tumorigenesis. Nonetheless, whether ErbB4 plays roles in differentiation, tumor suppression, or proliferation is still unclear.

Initial efforts to elucidate ErbB4 function have been hampered by many factors. First, there are no known agonists or antagonists specific to the ErbB4 receptor. All of the peptide hormones of the Epidermal Growth Factor (EGF) family that are capable of binding ErbB4 also bind at least one other ErbB family member. For example, epiregulin (EPR) and betacellulin (BTC) activate both ErbB1 and ErbB4 (see Figure 1.2; Riese *et*

al., 1996a; Riese *et al.*, 1998). Receptor signaling by ErbB proteins is triggered by at least 10 different members of the EGF family of polypeptide hormones, including epidermal growth factor (EGF), amphiregulin (AR), transforming growth factor-α (TGF-α), heparin-binding EGF-like growth factor (HB-EGF), and several differentially-spliced variants of neuregulin (NRG). These ligands are capable of activating all ErbB receptors, *in trans* (transmodulation), through ligand-induced receptor heterodimerization (see Figure 1.3; Alroy and Yarden, 1997). For example, EGF stimulates ErbB2 signaling through heterodimerization of ErbB2 with EGFR/ErbB1 (Stern and Kamps, 1988). Yet, EGF will not activate ErbB2 in the absence of EGFR/ErbB1. Consequently, ligands that bind ErbB4 (NRG, BTC, EPR) also stimulate signaling by ErbB1, ErbB2, and ErbB3 (Riese *et al.*, 1996a; Riese *et al.*, 1996b). As a result, a single ErbB ligand stimulates signaling by multiple ErbB receptors. Finally, examination of each ErbB receptor reveals a distinct pattern of carboxyl-terminal phosphorylation sites responsible for coupling to downstream adapter proteins (see Appendix A). As a result, signaling elicited by a receptor heterodimer is not simply the activation of an individual dimerization partner, but rather a unique property acquired by the heterodimer. Thus, the abundance of signaling diversification by ErbB receptors has hampered identifying the biological roles played by each receptor.

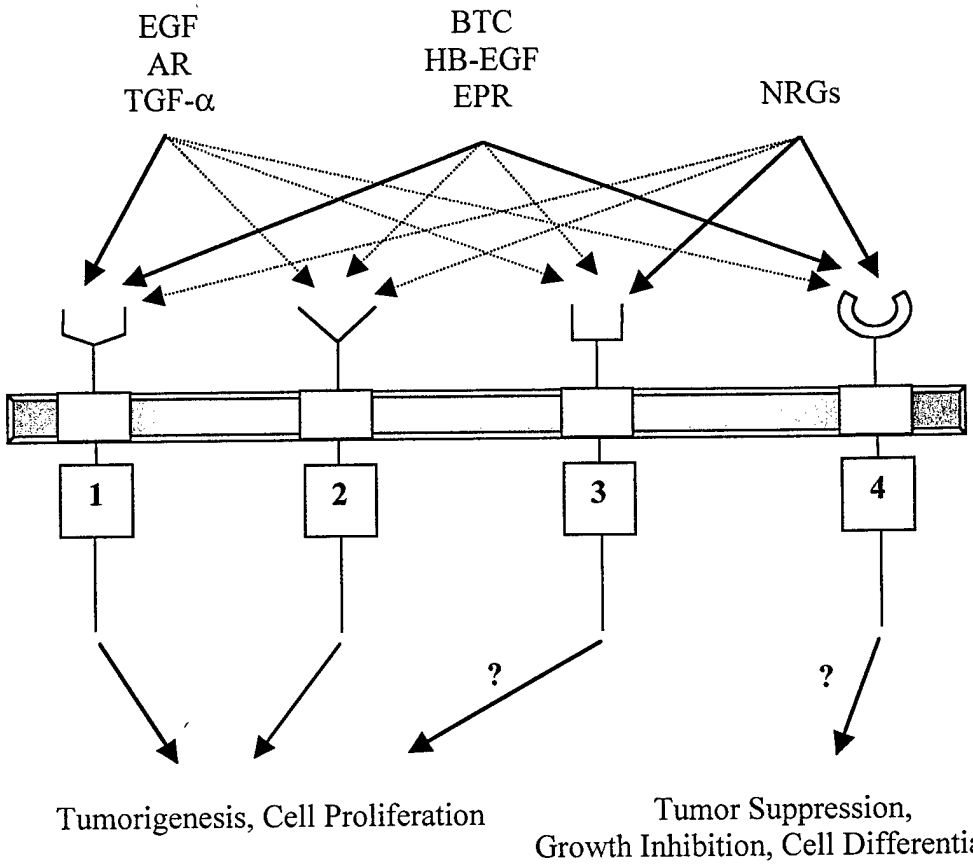

Figure 1.2 **Schematic diagram of ErbB ligands and their associated receptors.** Solid lines represent direct ligand binding, dash lines represent indirect activation of receptors through heterodimerization. EGF, AR, TGF-α bind ErbB1; BTC, HB-EGF, and EPR bind ErbB1 and ErbB4; NRGs bind ErbB3 and ErbB4. ErbB1 and ErbB2 have been demonstrated to couple to tumorigenesis and cell proliferation. The roles for ErbB3 and ErbB4 are less defined and only suggestive.

Structure and Activation of ErbB Receptors

ErbB receptors belong to the type I superfamily of receptor tyrosine kinases on the basis of sequence similarities and structural organization (Ullrich and Schlessinger, 1990). These receptors all possess glycosylated extracellular domains containing two cysteine-rich repeat sequences, a single hydrophobic transmembrane region, a cytoplasmic region containing the catalytic kinase domain, and a carboxyl-terminal cytoplasmic tail with tyrosine phosphorylation sites.

Activation of growth factor receptor signaling is typified by ligand-induced receptor dimerization and subsequent autophosphorylation across receptor dimers on specific carboxyl-terminal tyrosine residues (Schlessinger, 2000). Consequently, phosphorylated tyrosine residues provide docking sites for downstream signaling molecules possessing Src homology (SH2) domains or phosphotyrosine binding (PTB) domains (Cohen *et al.*, 1996a; Sepp-Lorenzino *et al.*, 1996; Crovello *et al.*, 1998). These include adapter proteins like Shc, Gab1, Grb2, Grb7, Crk, and kinases, such as Src and phosphatidylinositol 3'-kinase (PI3K; Prenzel *et al.*, 2001). In addition, ErbB signaling is mediate by protein tyrosine phosphatase SHP1 (Keilhack *et al.*, 1998). The molecules bound to the receptor activate signaling cascades, such as the mitogen-activated protein kinase (MAPK) pathway, protein kinase C (PKC), and the Akt pathway, resulting in coupling to transcription factors that include fos, jun, myc, Sp1, and Egr1 (Yarden and Sliwkowski, 2001). These transcription factors bind specific DNA sequences to affect the expression of multiple target genes (see Appendix B).

Activated receptor complexes have largely been studied in cells engineered to express ErbB receptor family members singly or in pairwise combinations (Riese *et al.*, 1995; Riese *et al.*, 1996a; Riese *et al.*, 1996b; Riese *et al.*, 1998). In cells expressing multiple ErbB family members, extensive receptor-receptor interactions constitute a signaling network whose potential for specification of diverse biological responses is enormous. To limit the complications associated with heterodimeric complexes, we have chosen to study ErbB4 function by expressing receptor mutants that are predicted to form only homodimers and not heterodimers.

A. HOMODIMERIZATION

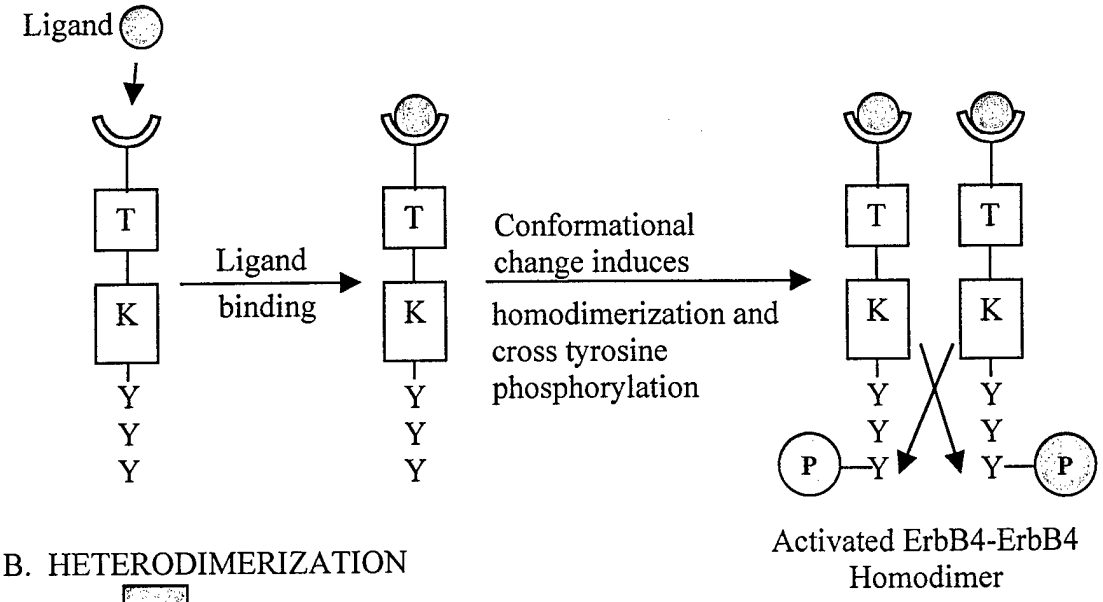

B. HETERODIMERIZATION

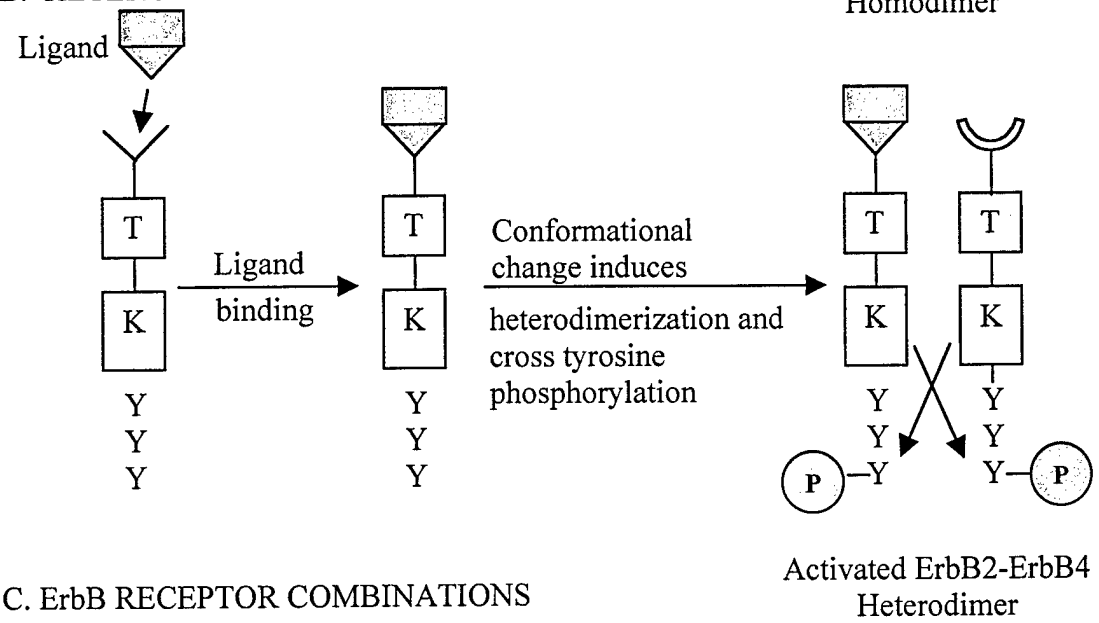

C. ErbB RECEPTOR COMBINATIONS

1:1 1:2 1:3 1:4 2:2 2:3 2:4 3:3 3:4 4:4

Figure 1.3 **Model for ligand-induced activation of ErbB receptors.** Ligand binding causes a conformational change to allow receptor dimerization and tyrosine Phosphorylation across the dimer. A. Homodimerization of two identical ErbB receptors (ErbB4 shown). B. Heterodimerization of two different ErbB receptors (ErbB2-ErbB4 shown). C. ErbB receptor combinations.

ErbB4

ErbB4 encodes a protein of 1,308 amino acids containing the characteristic organization of a receptor tyrosine kinase ((Plowman *et al.,* 1993; see Figure 1.4). ErbB4 shares a high degree of homology with the other members of the ErbB family. The ErbB4 gene is localized on the distal region of the long arm of chromosome 2 (Zimonjic *et al.,* 1995). Recently, multiple ErbB4 isoforms that vary in the extracellular juxtamembrane or cytoplasmic domain regions have been shown to be differentially expressed *in vivo* (Sawyer *et al.,* 1998; Elenius *et al.,* 1997). This may contribute to the conflicting results concerning ErbB4 function.

The presence of multiple ErbB4 isoforms is novel for this family of proteins. The cytoplasmic variants (CYT-1 and CYT-2) have been found in cell lines of normal and malignant breast tissues (Sawyer *et al.,* 1998). Juxtamembrane variants (JM-a and JM-b) are differentially expressed in neuronal, kidney, and heart tissues (Elenius *et al.,* 1997; see Appendix C for ErbB4 isoforms).

The various ErbB4 isoforms differentially couple to cellular responses. For example, the ErbB4 CYT-2 isoform is unable to couple to PI3-K activation, whereas the ErbB4 CYT-1 isoform is capable of binding PI3-K. (Elenius *et al.,* 1999; Kainulainen *et al.,* 2000). Futhermore, the juxtamembrane isoforms differ in their susceptibility to proteolytic cleavage in response to phorbol 12-myristate 13-acetate (PMA). Treatment with PMA prevented the binding of ^{125}I-NRG-β1 to ErbB4 JM-a, but not ErbB4 JM-b (Elenius *et al.,* 1997). Whether these differences in signaling by ErbB4 isoforms are biologically relevant is still unclear and warrants further investigation.

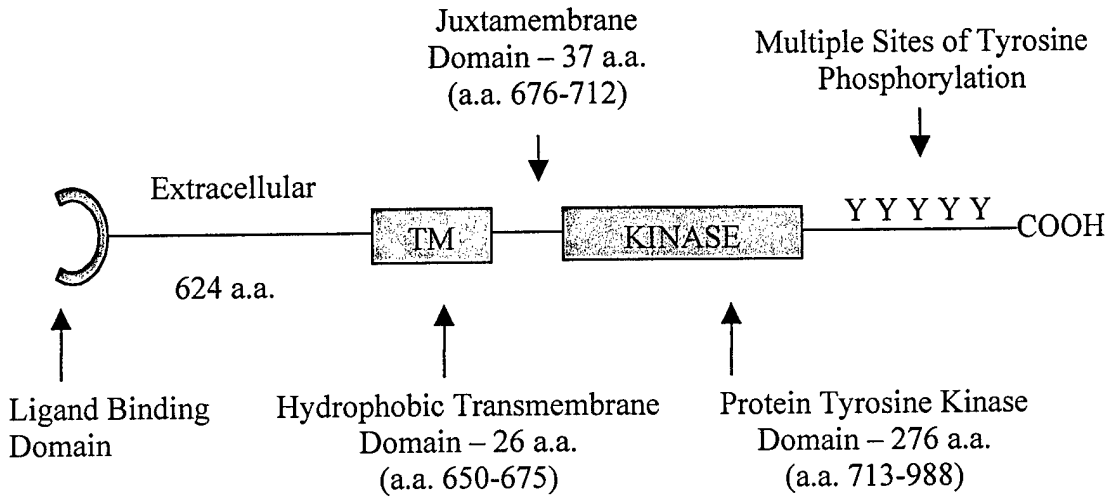

Figure 1.4 **The ErbB4 receptor tyrosine kinase.** The ErbB4 open reading frame encodes 1,308 amino acids with a predicted M_r of 180,000. The ErbB4 receptor contains 18 carboxyl-terminal tyrosine residues with four sites homologous to EGFR autophosphorylation sites (Y1162, Y1188, Y1258, Y1284). ErbB4 contains all 50 cysteine residues conserved in the extracellular domain of ErbB family receptors and contains 11 potential sites for N-linked glycosylation.

Strategy For Studying ErbB4 Receptor Function

As mentioned earlier, it is difficult to use ErbB4 ligands to study ErbB4 function. Consequently, we have opted to generate constitutively-active ErbB4 alleles through the introduction or elimination of extracellular cysteine residues. This is predicted to result in constitutively-dimerized and -active ErbB4 mutants. Introducing cysteine residues to form covalent dimeric receptors is not novel. This technique has been utilized in studying ErbB1 activation. Introducing cysteine residues in the ErbB1 extracellular juxtamembrane region results in the cross-linking of two ErbB1 receptors via disulfide bond formation. These disulfide mediated dimers, in the case of ErbB1, were formed only when EGF was present (Sorkin *et al.,* 1994). Once formed, these constitutive dimers were stable after EGF removal and represented the activated state of the receptor.

Much of our approach to elucidating the biological activities of ErbB4 has come from previous studies on the ErbB2/Neu proto-oncogene. A constitutively-active ErbB2* allele differs from wild-type ErbB2 by only a single substitution in the transmembrane domain (Glu for Val; Bargmann and Weinberg, 1988). The introduction of the valine residue within the transmembrane domain of ErbB2 results in constitutive dimerization, increased kinase activity, and increased oncogenic potential. Although this single mutation is not predicted to form covalent bonds as in the case with our mutants, it is believed that the biological activity of ErbB2* is enhanced by a specific intermolecular interaction that is important in receptor activation (Bargmann and Weinberg, 1988). Furthermore, mutations that eliminate cysteine residues in the extracellular region of the wild-type ErbB2 receptor results in constitutive ErbB2 dimerization and signaling (Siegel and Muller, 1996).

Mutations that either destroy or create cysteine residues in the extracellular region of Fibroblast Growth Factor Receptor 1 (FGFR1), FGFR2, and FGFR3 arise in many craniosynostosis and skeletal syndromes (Webster and Donoghue, 1997). Thanatophoric dysplasia type I (TDI) is a neonatal lethal dwarfism resulting from covalent FGFR homodimers that exhibit increased tyrosine phosphorylation, *in vitro* kinase activity, and biological signaling (d'Avis *et al.,* 1998). Crouzon syndrome is characterized by novel cysteine substitutions within the immunoglobulin-like domain 3 (Ig3), resulting in

constitutive FGFR signaling leading to craniosynostosis, shallow eye orbits, maxillary hypoplasia, and ocular proptosis (Galvin *et al.,* 1996). The constitutive activity of these receptors is a direct result of cysteine residue substitutions in their extracellular domains.

Normally, cysteine residues are predicted to form intramolecular disulfide bonds that are critical for folding, stability, and oligomerization of many glycoproteins (Braakman *et al.*, 1992). The introduction of a cysteine residue is predicted to result in disulfide bonds that align receptor monomers in a dimerized configuration that is productive for signaling (Burke and Stern, 1998). Once aligned, these constitutive complexes mimic the ligand-activated dimeric state of the receptor and provide a powerful functional tool for studying receptor signaling. Furthermore, the elimination of a cysteine residue that might normally participate in intrareceptor disulfide bonds would result in unpaired cysteines that would bond with cysteines on neighboring receptors (interreceptor bonds) to form dimeric complexes.

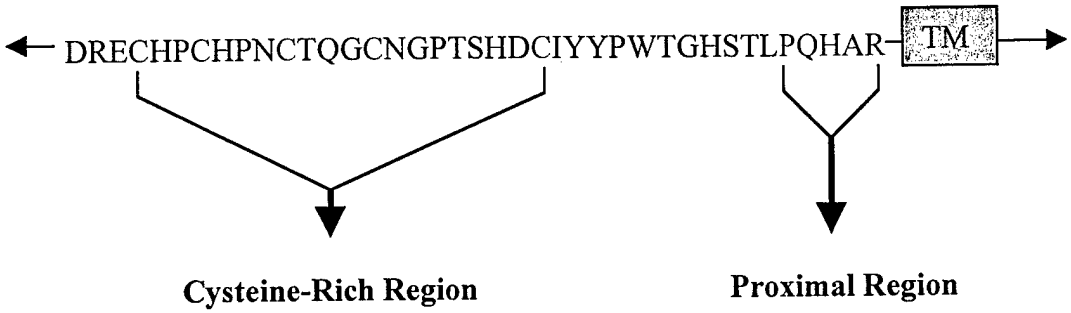

Figure 1.5 **Extracellular region of the ErbB4 receptor.** The cysteine-rich region is comprised of five cysteine residues in the wild-type receptor that were individually mutated to serine. The proximal region contains five wild-type residues that were individually mutated to cysteine.

In this work, we have generated both of these types of mutations in an attempt to generate constitutively-active ErbB4 mutants. We have produced ten distinct ErbB4 receptor mutants that create or destroy cysteine residues. Our focus is on the extracellular region comprising the cysteine-rich and the proximal regions near the transmembrane (see Figure 1.5 and Figure 1.6).

We predict that mutations in the extracellular domain of the ErbB4 receptor that either create or eliminate cysteine residues will generate constitutively-active ErbB4 homodimers. This will enable us to determine biological responses associated with ErbB4 signaling.

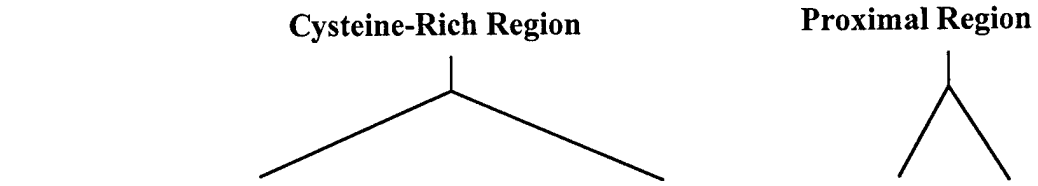

ErbB4	DRECHPCHPNCTQGCNGPTSHDCIYYPWTGHSTLPQHAR
C614S	DRESHPCHPNCTQGCNGPTSHDCIYYPWTGHSTLPQHAR
C617S	DRECHPSHPNCTQGCNGPTSHDCIYYPWTGHSTLPQHAR
C621S	DRECHPCHPNSTQGCNGPTSHDCIYYPWTGHSTLPQHAR
C625S	DRECHPCHPNCTQGSNGPTSHDCIYYPWTGHSTLPQHAR
C633S	DRECHPCHPNCTQGCNGPTSHDSIYYPWTGHSTLPQHAR
P645C	DRECHPCHPNCTQGCNGPTSHDCIYYPWTGHSTLCQHAR
Q646C	DRECHPCHPNCTQGCNGPTSHDCIYYPWTGHSTLPCHAR
H647C	DRECHPCHPNCTQGCNGPTSHDCIYYPWTGHSTLPQCAR
A648C	DRECHPCHPNCTQGCNGPTSHDCIYYPWTGHSTLPQHCR
R649C	DRECHPCHPNCTQGCNGPTSHDCIYYPWTGHSTLPQHAC

Figure 1.6 **ErbB4 site-directed mutants.** The portion of the ErbB4 extracellular domain that was mutated is shown. Blue residues indicate the residues that were mutated. Red residues indicate the substitutions that were made. The serine substitutions were made in a cysteine-rich region that encompasses amino acid 614 through 633. Cysteine substitutions were made in the proximal region that encompasses amino acids 645 through 649.

CHAPTER II
MATERIALS AND METHODS

Antibodies and Reagents

Anti-ErbB4 mouse monoclonal (SC-8050), anti-ErbB4 rabbit polyclonal (SC-283), and anti-ErbB2 rabbit polyclonal (C-18) antibodies were purchased from Santa Cruz Biotechnology. Goat anti-mouse and goat anti-rabbit horseradish peroxidase conjugated enzymes were purchased from Pierce. Enhanced chemiluminescence (ECL) Western blotting reagents, Redivue™ adenosine 5'-[γ-^{32}P] –triphosphate, and Protein-A Sepharose (CL-4B) were purchased from Amersham Pharmacia Biotech. Anti-phosphotyrosine antibodies were purchased from Upstate Biotechnology. Unless otherwise stated, all other reagents were purchased from Sigma Chemical Company.

ErbB4 Mutagenesis

The recombinant retroviral vector pLXSN-ErbB4 (Riese *et al.,* 1995) was used as the template for site-directed mutagenesis (QuikChange™ Site Directed Mutagenesis Kit, Stratagene) to construct putative gain-of-function, constitutively-active ErbB4 mutants. The mutants were constructed by substituting a novel cysteine in the region of the extracellular domain proximal to the transmembrane domain (amino acids 645, 646, 647, 648, 649). Proximal region mutants are as follows: P645C, Q646C, H647C, A648C, R649C. A second approach involved mutating individual wild-type cysteine residues located in the cysteine-rich region of ErbB4 (amino acids 614, 617, 621, 625, 633) to serine. Cysteine-rich region mutants are as follows: C614S, C617S, C621S, C625S, C633S. Ten total pLXSN-ErbB4-Neo^{R} mutants were constructed: C614S, C617S, C621S, C625S, C633S, P645C, Q646C, H647C, A648C, and R649C. A new restriction

enzyme site was also engineered in each mutant for identification purposes. The new restriction enzyme sites are listed on the Top (T) primer strands with the following sets of primers (T and B) used in site directed mutagenesis:

C614ST Pvu I @ 3812

5' – TATGCTGATCCCGATCGGGAGAGCCACCCATGC – 3'

C614SB

5' – GCATGGGTGGCTCTCCCGATCGGGATCAGCATA – 3'

C617ST Mun I @ 3836

5' – GAGTGCCACCCAAGCCATCCCAATTGCACCCAAGGG – 3'

C617SB

5' – CCCTTGGGTGCAATTGGGATGGCTTGGGTGGCACTC – 3'

C621ST XcmI @ 3852

5' – TGCCATCCAAACAGCACCCAAGGGTGTAATGGTCCCACTAGT – 3'

C621SB

5' – ACTAGTGGGACCATTACACCCTTGGGTGCTGTTTGGATGGCA – 3'

C625ST XcmI @ 3852

5' – TGCACCCAAGGGAGTAATGGTCCCACTAGT – 3'

C625SB

5' – ACTAGTGGGACCATTACTCCCTTGGGTGCA – 3'

C633ST Age I @ 3894

5' – CCCACTAGTCATGACTCCATTTACTACCCATGGACCGGTCATTCCACTT

TACCA – 3'

C633SB

5' – TGGTAAAGTGGAATGACCGGTCCATGGGTAGTAAATGGAGTCATGACTA

GTGGG – 3'

P645CT Age I @3894

5' – ATTTACTACCCATGGACCGGTCATTCCACTTTATGCCAACATGCTAGA

ACTCCC – 3'

P645CB

5' – GGGAGTTCTAGCATGTTGGCATAAAGTGGAATGACCGGTCCATGGGTA

GTAAAT – 3'

Q646CT Age I @ 3894

5' – TACTACCCATGGACCGGTCATTCCACTTTACCATGCCATGCTAGAACTC

CCCTG – 3'

Q646CB

5' – CAGGGGAGTTCTAGCATGGCATGGTAAAGTGGAATGACCGGTCCATGGG

TAGTA – 3'

H647CT Age I @ 3894

5' – CATTTACTACCCATGGACCGGTCATTCCACTTTACCACAATGTGCTAGAC

TCCCCT – 3'

H647CB

5' – AGGGGAGTTCTAGCACATTGTGGTAAAGTGGAATGACCGGTCCATGGGTAG

TAAATG – 3'

A648CT BseRI @ 3919

5' – TCCACTTTACCACAACATTGTAGAACTCCTCTGATTGCAGCTGGA – 3'

A648CB

5' – TCCAGCTGCAATCAGAGGAGTTCTACAATGTTGTGGTAAAGTGGA – 3'

Each site directed mutagenesis reaction contained the following: 5 µl of 10X reaction buffer (supplied with kit), 50 ng of pLXSN-ErbB4, 125 ng of the appropriate "T"-type primer, 125 ng of the appropriate "B"-type primer, 1 µl of dNTP mix (supplied with kit), 1 µl Pfu Turbo DNA polymerase (2.5 U/µl), and dIH_2O to a final volume of 50 µl. Reactions were overlaid with 30 µl of mineral oil and the reaction parameters were as follows: Step #1: 95°C for 30 seconds. Step #2: 95°C for 30 seconds, 55°C for 1 minute, and 68°C for 20 minutes. Step #2 was repeated 18 times. The reactions were then incubated on ice for 10 minutes. After chilling, 1 µl of Dpn I (NewEngland Biolabs) was added to the aqueous layer and the reactions were incubated at 37°C for 1 hour. Standard techniques (Sambrook and Russell, 2001) were utilized for *E. coli* transformation by electroporation. Small scale plasmid DNA preparations were generated using the Wizard® Plus Miniprep DNA purification system (Promega). Minipreps were screened for the new restriction enzyme site and *E. coli* harboring the plasmid with the appropriate mutations were expanded and large-scale plasmid isolation and purification were performed using standard techniques (Sambrook and Russell, 2001). The presence of the appropriate mutations and the absence of any additional mutations were confirmed by DNA sequencing.

Cell Lines

The Ψ2, PA317, and FR3T3 cell lines were gifts from Daniel DiMaio, Yale University. All cell lines were propagated in Dulbecco's modified Eagle's medium (DMEM) supplemented with 10% fetal bovine serum (FBS), 50 IU/ml penicillin, 50 μg/ml streptomycin (Mediatech), and 0.25 μg/ml fungizone (Amphotericin B; Gibco/BRL). Recombinant cell lines generated in the course of the following experiments were propagated in the media described above supplemented with 200 μg/ml G418 (Mediatech).

Retroviral Infections

The retroviral vector pLXSN (RV-Neo^R) is derived from the Moloney Murine Sarcoma Virus, and the Moloney Leukemia Virus, and was obtained from Dan DiMaio, Yale University. pLXSN contains an SV40 early promoter that controls the transcription of the aminoglycoside 3'-phosphotransferase gene (Neo^R gene) and the Ψ packaging signal (Miller and Rosman, 1989). The Neo^R gene confers resistance to the aminoglycoside antibiotic G418 (geneticin, Gibco/BRL). In eukaryotic cells G418 interferes with the function of the 80S ribosome and kills cells by blocking protein synthesis (Southern and Berg, 1982).

The ψ2 ecotropic retrovirus packaging cell line (Mann *et al.,* 1983) was transfected for stable expression of the pLXSN-ErbB4 mutants using standard techniques (Sambrook and Russell, 2001). These transfected Ψ2 cells were also used to package recombinant retroviruses expressing the Neo^R gene. Retroviral particles were harvested from the media conditioned by the Ψ2 cells and were used to infect PA317 and FR3T3 cell lines. Ψ2 ecotropic retrovirus packaging cell lines produce replication-defective, helper-free retrovirus stocks with titers ranging from 10^3 to 10^6 colony-forming units/ml (Mann *et al.,* 1983; Miller and Buttimore, 1986).

The PA317 amphotropic packaging cell line (Miller and Buttimore, 1986) was infected with the ecotropic recombinant retroviruses harvested from Ψ2 cells. Cells were seeded in 60 mm dishes and were infected when the cells were at approximately 75% confluence. The medium was aspirated from each plate of cells and approximately 200

μl of harvested retrovirus was added to each plate along with 900 μl DMEM supplemented with 5 μg/ml polybrene. Following incubation for 2 hours at 37°C, 4 ml of DMEM containing 2% FBS and 5 μg/ml polybrene was added to each dish. Approximately 16-24 hours later, the cells were detached from the plates with trypsin and suspended in a total volume of 9 ml of fresh medium. The cells were aliquoted into three 100 mm dishes and medium was added to a final volume of 10 ml per plate. Approximately 24 hours later, the medium on these plates was replaced with medium containing 900 μg/ml G418 to select for infected cells. Colonies of drug resistant cells were isolated and pooled into cell lines that were subsequently screened for ErbB4 receptor expression. Media conditioned by the transfected PA317 cells were harvested. They are high-titer amphotropic retrovirus stocks.

The FR3T3 cell line was infected as described earlier, except 200 Cfu (titered in PA317 cells) of each Ψ2 ecotropic retrovirus stock was used instead of 200 μl.

Immunoprecipitation and Immunoblotting

The analysis of ErbB4 and ErbB2 receptor tyrosine phosphorylation by immunoprecipitation and anti-phosphotyrosine immunoblotting has been described previously (Riese *et al.,* 1995; Riese *et al.,* 1998). Briefly, cell lysates were generated and quantified for protein content by Bradford Assay (Coomassie® Protein Assay Reagent-Pierce; Bradford, 1976) and equal amounts of protein extract were immunoprecipitated with antibodies specific for ErbB2 or ErbB4. The samples were resolved by electrophoresis on a 7.5% acrylamide, 0.17% bisacrylamide, 0.1% SDS gel and electrotransferred onto nitrocellulose. The blots were probed with the anti-phosphotyrosine monoclonal antibody 4G10 (Upstate Biotechnology, Inc.) Antibody binding was detected with a goat anti-mouse horseradish peroxidase coupled antibody (1:3,000 in TBS-T) and enhanced chemiluminescence.

The amounts of receptor tyrosine phosphorylation and expression (in PA317 cells) were quantified by digitizing the chemilumigrams using a Linotype-Hell Jade 2-dimensional scanning densitometer set at 600 dpi resolution. The bands on the images

were quantified using NIH Image for Macintosh v1.6 software. Values are expressed as arbitrary units. Background levels were computed using the vector control lanes and were subtracted from the gross values to produce net receptor expression and tyrosine phosphorylation values. The digitized images were also cropped and annotated using Adobe Photoshop for Macintosh v3.0.5 software.

Dimerization Assay

Detection of ErbB4 dimer formation was performed as described previously (Siegel and Muller, 1996) except that EBC buffer (Irusta and DiMaio, 1998) containing 10 mM Iodoacetamide, 1 mM Na_3VO_4, and 1% Aprotinin was used for cell lysis and for washing immunoprecipitates. Briefly, cells were lysed in EBC containing Iodoacetamide, Na_3VO_4, and Aprotinin. The protein content of the lysates was quantified by Bradford Assay and ErbB4 receptors were immunoprecipitated from samples containing equal amounts of protein. The immunoprecipitates were then boiled for 5 minutes in SDS loading buffer in the absence of 2- mercaptoethanol (62.5 mM Tris-HCl, 2% SDS, 5% glycerol, 0.25% bromophenol blue), resolved by electrophoresis on a 4-12 % acrylamide-0.19 to 0.56% bisacrylamide gradient gel (Burke and Stern, 1998), and electrotransferred to nitrocellulose at 200 mA overnight. Membranes were probed with an anti-ErbB4 mouse monoclonal antibody (1:300). Antibody binding was detected with a goat anti-mouse horseradish peroxidase coupled antibody (1:2,500 in TBS-T) and enhanced chemiluminescence.

In Vitro Kinase Assay

ErbB2 and ErbB4 were immunoprecipitated from protein extracts from PA317 cells as described earlier (Riese *et al.*, 1995). Immune complex kinase reactions were performed as previously described (Cohen *et al.*, 1996a). Briefly, ErbB2 or ErbB4 was immunoprecipitated from protein extracts using 35 µl Protein-A Sepharose and 5 µl of anti-ErbB2 or anti-ErbB4 rabbit polyclonal antibodies. Samples were washed five times

in 500 µl kinase buffer (20 mM Tris-HCl, pH 7.4, 5 mM $MgCl_2$, 3 mM $MnCl_2$). After the last wash, the samples were resuspended in 100 µl kinase buffer supplemented with 10 µCi of [γ-^{32}P]ATP and were incubated for 10 minutes at room temperature. The beads were then washed two times in NET-N (Irusta and DiMaio, 1998), boiled for 5 minutes in 2X Laemmli sample buffer, and the samples were resolved by electrophoresis on an SDS-7.5% acrylamide-0.17% bisacrylamide gel. The gel was then dried overnight and exposed to X-ray film for approximately 20 hours. The autoradiograms were digitized using a Linotype-Hell Jade 2-dimensional scanning densitometer set at 600 dpi resolution. The bands on the images were quantified using NIH Image for Macintosh v1.6 software. Values are expressed as arbitrary units. Background levels were computed using the vector control lanes and were subtracted from the gross values to produce net kinase activity values. The digitized images were also cropped and annotated using Adobe Photoshop for Macintosh v3.0.5 software.

Focus Forming Assay

FR3T3 cell were infected with Ψ2 ecotropic recombinant retroviruses as stated earlier and described previously (Burke and Stern, 1998). Approximately 24 hours after infection, cells were split into three 60 mm dishes. Cells were maintained in DMEM supplemented with 10% FBS until foci appeared. The medium was changed every three days. Cells were fixed in methanol and stained with Giemsa (1:25 in PBS; Fisher) to visualize the foci.

Anchorage Independency Assay

FR3T3 cells were seeded at a density of 2 x 10^4 cells in 60 mm dishes containing 2.5 ml of 0.3% Low Melting Point Agarose (LMP-agarose; Gibco/BRL) as described previously (Hwang *et al.*, 1993). Every three days DMEM supplemented with 10% FBS and 0.3% LMP-agarose was added to each plated. The cells were incubated at 37°C for 10 days and fields were photographed with an Olympus OM-10 camera attached to an

Olympus CK-2 phase-contrast inverted microscope. Photographs represent fields from three independent experiments.

Growth Rate/Saturation Density

Stable FR3T3 cell lines expressing the wild-type ErbB4 receptor, ErbB2*, or the ErbB4 mutants (Q646C, H647C, A648C) were plated in ten 60 mm dishes at a density of 2×10^4 cells per dish. Cells were incubated from one to ten days at 37°C. Cells were counted (Coulter Counter® ZM) each day for a total of ten days. The mean and standard error of the mean (SEM) are representative of three independent experiments.

CHAPTER III
RESULTS

Cysteine mutations initially discovered in the neu (ErbB2*) proto-oncogene and fibroblast growth factor receptors demonstrate that a single point mutation in the extracellular region may result in a constitutively-dimerized and -active receptor. We were interested in assessing whether ErbB4 receptors harboring analogous mutations were also constitutively active. To test our hypothesis, cysteine residues were either introduced or eliminated in the extracellular region of the ErbB4 receptor. We constructed ErbB4 mutants in which individual cysteine residues were converted to serine (C614S, C617S, C621S, C625S, C633S). We also constructed ErbB4 mutants that contained a novel cysteine residue (P645C, Q646C, H647C, A648C, R649C).

ErbB4 mutant receptors have increased signaling

Since a single unpaired cysteine residue might interfere with protein folding and export to the cell surface, we were concerned that our mutants might not be stably expressed. We analyzed the expression and tyrosine phosphorylation of the ErbB4 mutants in the Ψ2 ecotropic retrovirus packaging cell line. Ψ2 cells were transfected as described in Chapter II. These cells efficiently express genes from recombinant retroviral vectors.

As shown in Figure 3.1, Ψ2 cells transfected with the retroviral vector control LXSN, or the retroviral vectors containing wild-type ErbB4 (ErbB4 lane), mutant ErbB2* (ErbB2* lane) or the three mutant receptors (Q646C, H647C, A648C) were analyzed for receptor phosphorylation and expression. Cells transfected with vector alone do not exhibit any receptor expression or phosphorylation (LXSN lane). ErbB2* was used as a positive control throughout our experiments because this mutant is

constitutively-dimerized and -active (Bargmann and Weinberg, 1988). Although it is unclear how ErbB2* maintains an activated dimeric complex in conditions that would normally disrupt non-covalent receptor interactions, ErbB2* is constitutively phosphorylated in Ψ2 cells (Figure 3.1 top panel, ErbB2* lane).

Anti-ErbB4 immunoblotting recognizes 180-kDa proteins in Ψ2 cells transfected with retroviral vectors containing wild-type ErbB4 or the three mutant receptor constructs (bottom panel), but not in cells transfected with the vector alone or with retroviral vectors containing ErbB2*. Moreover, levels of ErbB4 expression are roughly equivalent in cells transfected with wild-type ErbB4 or with the ErbB4 mutants (bottom panel).

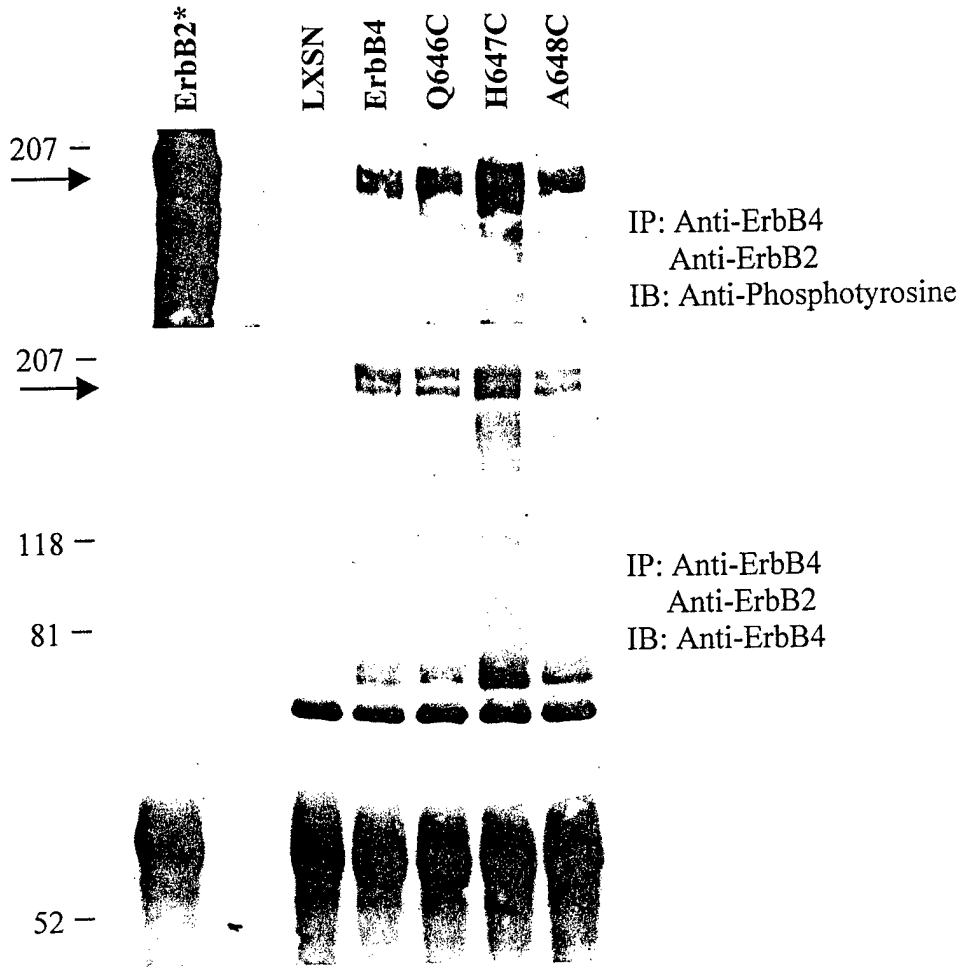

Figure 3.1 **Expression and phosphorylation of ErbB4 mutant receptors in Y2 cells.** Receptors were immunoprecipitated from lysates containing equal amounts of protein (250 μg) prepared from Ψ2 cells transfected with recombinant retroviral vectors containing wild-type ErbB4, ErbB2*, LXSN, or the ErbB4 mutants (Q646C, H647C, A648C). Cells transfected with the LXSN vector serve as a negative control. Immunoprecipitations were resolved by SDS-PAGE, electroblotted to nitrocellulose, and immunoblotted with an anti-phosphotyrosine antibody (top panel). The blot was then stripped and reprobed with an anti-ErbB4 rabbit polyclonal antibody (bottom panel). The arrows indicate bands corresponding to ErbB receptors.

Our initial results demonstrate that the ErbB4 mutants are tyrosine phosphorylated in transfected Ψ2 cells. However, wild-type ErbB4 exhibits a similar level of tyrosine Phosphorylation as the ErbB4 mutant receptors. Previous observations indicate that ErbB4 overexpression results in tyrosine phosphorylation in the absence of ligand (Cohen *et al.,* 1996a). Therefore, the ErbB4 tyrosine phosphorylation seen in Figure 3.1 could be a result of overexpression. To further explore the possibility that the ErbB4 mutants are constitutively active, we harvested ecotropic retroviruses from Ψ2 cell lines for infection of the amphotropic retroviral packaging PA317 cell line.

Retroviral-mediated gene transfer offers a number of advantages over other gene transfer strategies, including high transduction efficiencies and stability of the integrated DNA in the infected cells (Gerstmayer *et al.,* 1999). However, transfection of viral vectors into Ψ2 cells results in ecotropic retroviruses with a limited host range. Moreover, the titers of these retroviral stocks are typically low. Therefore, PA317 cells were infected to produce high-titer amphotropic retroviral stocks and to assay the biochemical properties of the ErbB4 mutants.

PA317 cells infected with retroviruses that direct the expression of wild-type ErbB4 or the ErbB4 mutants were assayed for ErbB4 expression and phosphorylation in Figure 3.2. As expected, cells infected with the LXSN vector control retrovirus do not exhibit ErbB4 expression (right panel) or tyrosine phosphorylation (left panel). Cells infected with wild-type or mutant ErbB4 retroviruses exhibit ErbB4 expression (Figure 3.2, right panel). However, cells infected with the mutant ErbB4 retroviruses exhibit abundant tyrosine phosphorylation, whereas cells infected with the wild-type ErbB4 retrovirus exhibit minimal ErbB4 tyrosine phosphorylation (Figure 3.2, left panel).

Quantification of the chemilumigrams shown in Figure 3.2 suggests that the expression levels of the three ErbB4 mutants is less than three times greater the amount of wild-type ErbB4 expression (Table 3.1). In contrast, the amounts of tyrosine phosphorylation of the three ErbB4 mutants appear to be much greater than the amount of wild-type ErbB4 tyrosine phosphorylation. Moreover, the ratios of ErbB4 tyrosine phosphorylation to ErbB4 expression for the three ErbB4 mutants appear to be at least four times greater than the ratio for wild-type ErbB4. These data suggest that the three

ErbB4 mutants exhibit greater amounts of tyrosine phosphorylation on a per molecule basis than does wild-type ErbB4. This data suggests that the three mutants are constitutively active for signaling. Although, it is unclear if the increased tyrosine phosphorylation seen in the ErbB4 mutants is caused by increased half-life of the protein on the cell surface. Indeed, if the receptors are not down regulated from the cell surface the activated state of the receptor might be maintained in an active configuration for signaling.

Table 3.1 **The Q646C, H647C, and A648C ErbB4 mutants exhibit increased normalized tyrosine phosphorylation.**

Cell Line	ErbB4 Tyrosine Phosphorylation	ErbB4 Expression	Ratio
Wild-type ErbB4	212867	1831340	0.116
ErbB4 Q646C	1860472	3329432	0.558
ErbB4 H647C	2944443	4659376	0.631
ErbB4 A648C	3981658	4509147	0.883

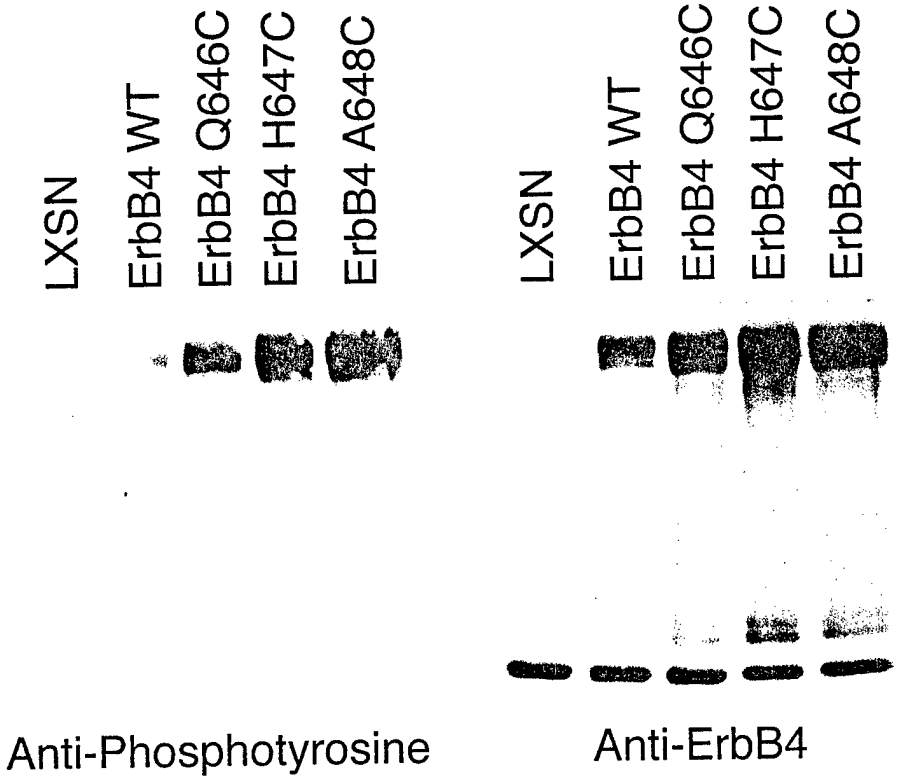

Figure 3.2 **ErbB4 mutants are constitutively tyrosine phosphorylated.** ErbB4 expression and tyrosine phosphorylation was assayed in PA317 cells infected with retroviruses that direct the expression of wild-type ErbB4 or the ErbB4 mutants. Cells infected with the LXSN recombinant retrovirus served as the negative control. Lysates were prepared from each of the cell lines and ErbB4 was immunoprecipitated from 1000 μg of each lysate. Samples were resolved by SDS-PAGE, electroblotted to nitrocellulose, and immunoblotted with an anti-phosphotyrosine antibody (left panel). The blot was then stripped and probed with an anti-ErbB4 rabbit polyclonal antibody (right panel). ErbB4 is represented by the band at the top of the blots.

Corresponding titers were determined for each retroviral stock to analyze the efficiency of infection. Ecotropic retrovirus stocks were titered by infecting FR3T3 cells and counting colonies of cells resistant to G418. Table 3.2 summarizes the titers obtained in colony-forming units per ml of retroviral stock. No significant differences in retroviral titers were observed to account for the difference in wild-type ErbB4 expression as compared to the ErbB4 mutants in the PA317 cell lines. These retroviral titers confirm that similar numbers of infectious particles were used to generate the PA317 cell lines. Therefore, we have concluded that the increased tyrosine phosphorylation of the three ErbB4 mutants reflects the increased signaling activity of these mutants rather than simple gross overexpression of the mutants.

Table 3.2 **Titers of Ψ2 retroviral particles**. Approximately 200 Cfu of each ecotropic retrovirus stock was used to infect 60 mm dishes of subconfluent FR3T3 cells. Approximately 20 hours later, 60 mm dishes were split into three 100mm dishes and allowed to grow for 2 weeks in the presence of DMEM supplemented with 10% FBS and 900 μg/ml G418. The medium was changed every three days and G418 resistant colonies were counted when uninfected cells had died. Ecotropic stocks were titered three times in FR3T3 cells. Standard Error of the Mean (SEM) represents three trials.

Ψ2 Retroviral Stock	Target Cell	Titer (Cfu/ml)	SEM
LXSN	FR3T3	NA	NA
ErbB2*	FR3T3	3.43×10^3	7.3×10^2
ErbB4	FR3T3	4.33×10^3	9.5×10^2
Q646C	FR3T3	1.19×10^3	1.6×10^2
H647C	FR3T3	2.56×10^3	5.6×10^2
A648C	FR3T3	1.79×10^3	4.0×10^2

ErbB4 mutant receptors are constitutively-dimerized

In order to ascertain whether the ErbB4 mutants are constitutively form dimers, we resolved ErbB4 immunoprecipitates by SDS-PAGE in the absence of reducing agents and analyzed the samples by immunoblotting. As shown in Figure 3.3, stable ErbB4 receptor dimers could not be detected in cells infected with the retroviral vector control (LXSN lane) or in cells that were infected with the retroviral vector containing wild-type ErbB4 (ErbB4 lane). ErbB4 is expressed in PA317 cells as shown previously (Figure 3.2; ErbB4 lane), but is not efficiently recognized by the anti-ErbB4 mouse monoclonal antibody used in this experiment (Figure 3.3; ErbB4 lane). It is unclear whether the markedly higher ErbB4 monomeric and dimeric mutant expression levels are due to increased protein stability. Nonetheless, our data suggests that the ErbB4 mutant receptors readily form dimers in the absence of ligand.

To determine whether the receptors active for signaling occur primarily as monomers or as dimers, we prepared samples as described earlier and analyzed them by anti-phosphotyrosine immunoblotting. Figure 3.4 indicates that the tyrosine phosphorylated ErbB4 mutant receptors are both monomeric and dimeric. Moreover, the total amount of tyrosine-phosphorylated ErbB4 was much greater in cells that express the ErbB4 mutants than in cells that express wild-type ErbB4. Furthermore, it is unclear how ErbB2* maintains an activated dimeric complex in conditions that would normally disrupt non-covalent receptor interactions. ErbB2* is not predicted to form disulfide bonds, but is well documented to be constitutively active and dimerized in the absence of ligand (Bargmann and Weinberg, 1988; Stern *et al.,* 1988). Finally, monomeric and dimeric ErbB4 mutants appear to be active for signaling in both the monomeric and dimeric states.

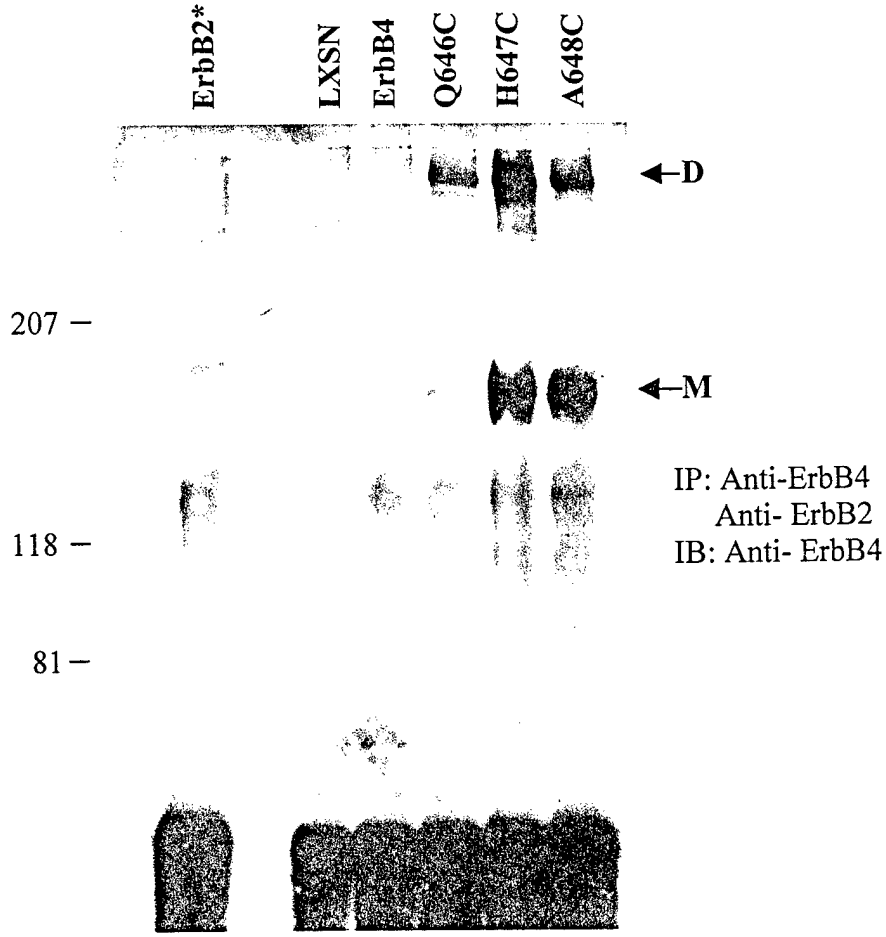

Figure 3.3 **Constitutively-dimerized ErbB4 mutant receptors.** PA317 cells stably expressing wild-type ErbB4, ErbB2*, or the receptor mutants (Q646C, H647C, A648C) were lysed in EBC buffer containing 10 mM Iodoacetamide. ErbB receptors were immunoprecipitated from approximately 2000 μg of cell lysate using anti-ErbB2 (ErbB2* lane only) or anti-ErbB4 rabbit polyclonal antibodies. Immunoprecipitated proteins were resolved under nonreducing conditions by SDS-PAGE on a 4-12% acrylamide gradient gel and electroblotted to nitrocellulose. Immunoblotting was performed with an anti-ErbB4 mouse monoclonal antibody. The arrows indicate the position of monomeric (M) and dimeric (D) ErbB4 receptors.

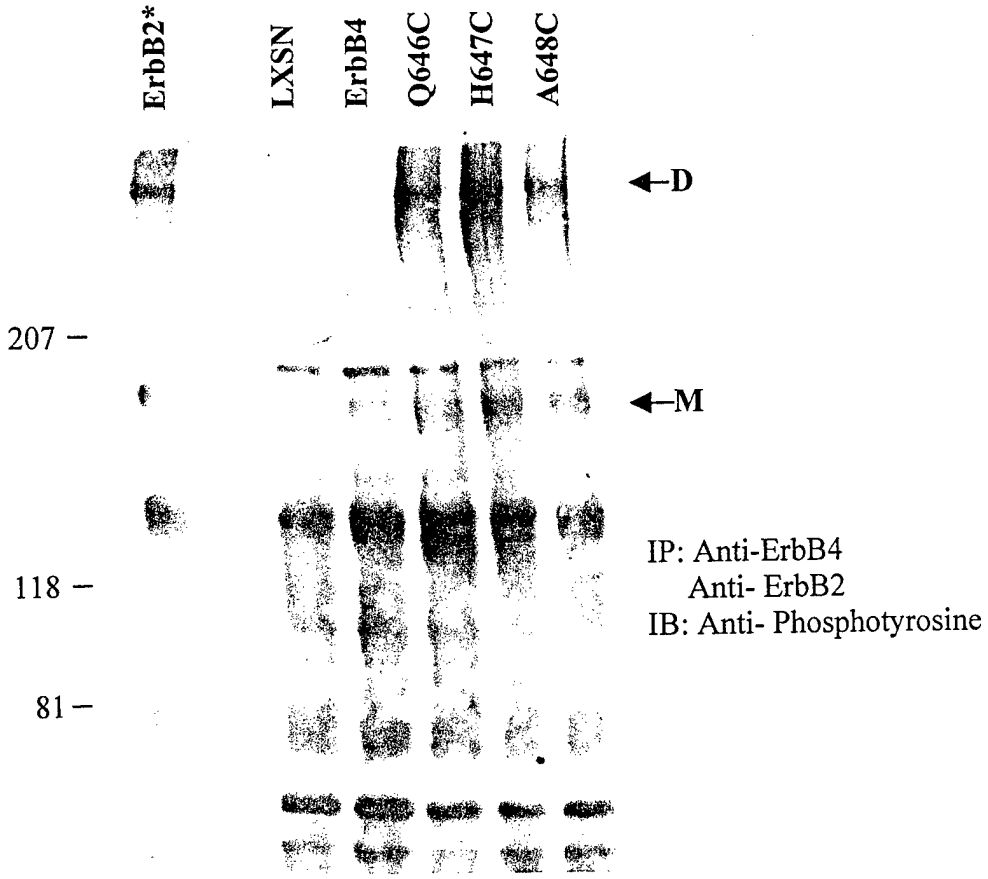

Figure 3.4 **Phosphorylation of constitutively-dimerized ErbB4 mutant receptors.** PA317 cells stably expressing wild-type ErbB4, ErbB2*, or the receptor mutants (Q646C, H647C, A648C) were lysed in EBC buffer containing 10 mM Iodoacetamide. ErbB receptors were immunoprecipitated from approximately 2000 μg of cell lysate using anti-ErbB2 (ErbB2* lane only) or anti-ErbB4 rabbit polyclonal antibodies. Immunoprecipitated proteins were resolved under nonreducing conditions by SDS-PAGE on a 4-12% acrylamide gradient gel and electroblotted to nitrocellulose. Immunoblotting was performed with an anti-phosphotyrosine antibody. The arrows indicate the position of monomeric (M) and dimeric (D) ErbB4 receptors.

ErbB4 mutant receptors have increased *in vitro* kinase activity

We have demonstrated that the Q646C, H647C, and A648C ErbB4 mutants exhibit greater ligand-independent tyrosine phosphorylation than wild-type ErbB4. Next, we assessed whether the increased tyrosine phosphorylation of the mutants correlates with increased kinase activity. To measure the levels of intrinsic kinase activity, equal amounts of protein extracts were immunoprecipitated with an anti-ErbB4 polyclonal antibody. Kinase reactions were then performed in the presence of [γ-^{32}P] ATP. The reaction products were resolved by electrophoresis. The gels were dried and the reaction products were visualized by autoradiography.

In Figure 3.5 we show that PA317 cells infected with the LXSN vector control retrovirus lack detectable ErbB4 kinase activity. Moreover, PA317 cells that express the three constitutively-active ErbB4 mutants exhibit greater ErbB4 tyrosine kinase activity than cells that express wild-type ErbB4. Quantification of the bands on the autoradiogram indicates that the Q646C and H647C ErbB4 mutants exhibit approximately 5-fold more kinase activity than does wild-type ErbB4, whereas the A648C ErbB4 mutant exhibits approximately 9-fold more kinase activity than does wild type ErbB4. Given that the expression of the ErbB4 mutants is somewhat greater than the expression of wild-type ErbB4 (Table 3.1), it appears that the intrinsic kinase activity of the three ErbB4 mutants is approximately 2-fold greater than the intrinsic kinase activity of wild-type ErbB4. This data suggests that the ErbB4 mutants Q646C, H647C, and A648C are constitutively active for signaling.

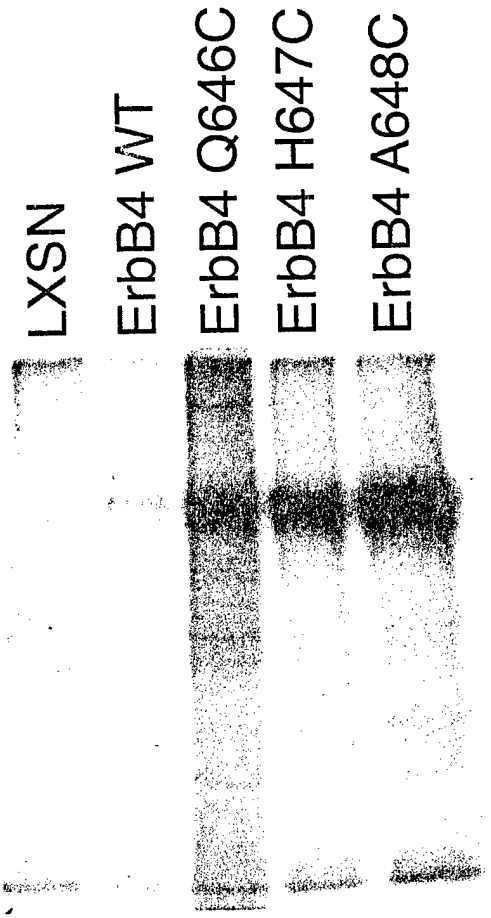

Figure 3.5 **Q646C, H647C, and A648C mutants exhibit increased *in vitro* kinase activity.** Equal amounts of protein lysates from PA317 cells that stably express wild-type ErbB4 or the ErbB4 mutants (Q646C, H647C, A648C) were immunoprecipitated with an anti-ErbB4 rabbit polyclonal antibody. Lysates from PA317 cells that express the LXSN vector served as the negative control. Kinase reactions were performed on the immunoprecipitates in the presence of [γ-^{32}P]ATP. The products were resolved by SDS-PAGE. The gel was dried overnight and exposed to X-ray film for approximately 20 hours to visualize the products of the kinase reactions.

Constitutively-active ErbB4 mutant receptors lack transforming activity

Conflicting results are seen in assays for growth transformation by ErbB4. ErbB4 induces a loss of contact inhibition (foci) in NIH 3T3 clone 7 cells in the absence of ligand (Cohen *et al.*, 1996a). In these cells the loss of contact inhibition was further stimulated with an ErbB4 ligand, neuregulin 2β. In contrast to these results, NIH 3T3 clone 7d cells transfected with wild-type ErbB4 did not form foci in the presence or absence of neuregulin 1β (Cohen *et al.*, 1996b; Zhang *et al.*, 1996).

To try to resolve this dichotomy, we next determined if increased ErbB4 phosphorylation and kinase activity correlates with loss of contact inhibition. FR3T3 rat fibroblasts were infected with 200 Cfu of each ecotropic retrovirus stock (vector, ErbB2*, wild-type ErbB4, Q646C, H647C, A648C) and assayed for focus formation.

FR3T3 cells that express ErbB2* form foci 9 days after infection, whereas cells infected with the vector control did not (Figure 3.6). Moreover, cells that express wild-type ErbB4 or the constitutively-active ErbB4 mutants did not form foci. Eighteen days after infection, cells that express the constitutively-active ErbB4 mutants formed a few foci; however, the number of foci was comparable to those seen when cells express wild-type ErbB4. Thus, we conclude that the constitutively-active ErbB4 mutants do not induce a significant loss of contact inhibition in FR3T3 fibroblasts.

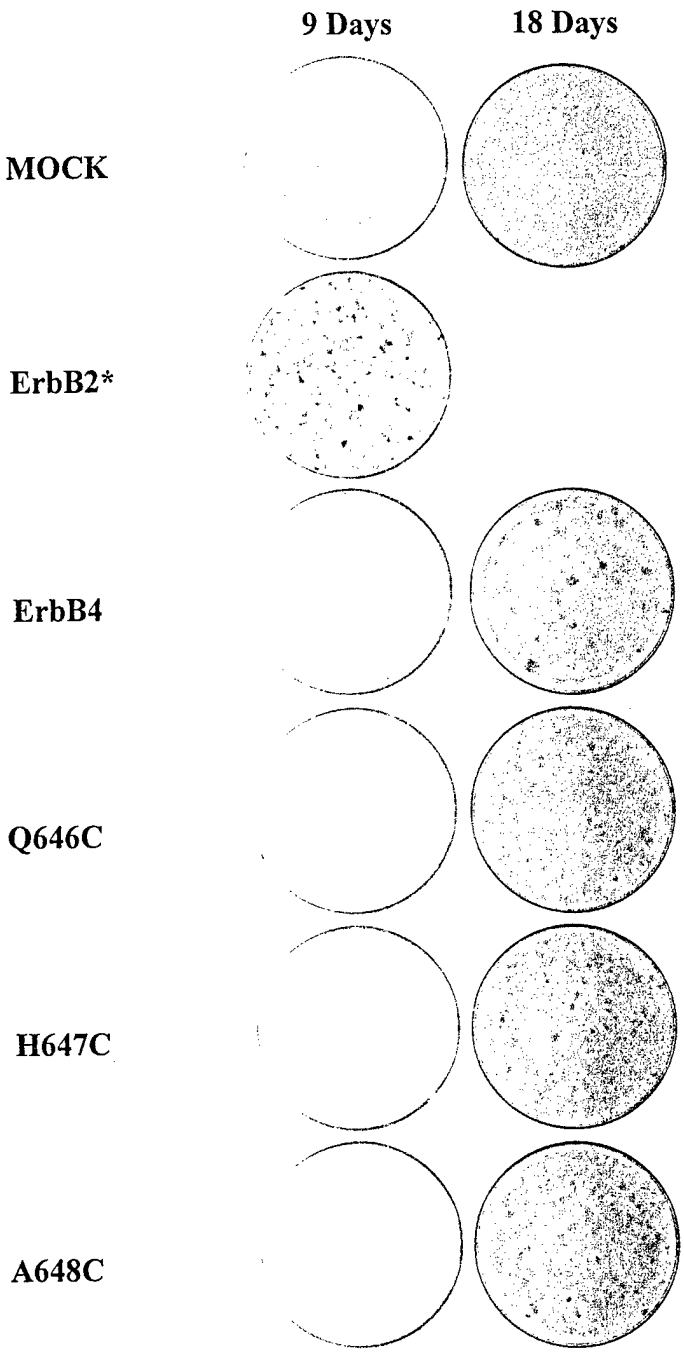

Figure 3.6 **Constitutively-active ErbB4 receptors do not induce a significant loss of contact inhibition.** FR3T3 fibroblasts infected with the vector control retrovirus, the ErbB4 retrovirus, the ErbB2* retrovirus, or the ErbB4 mutant retroviruses were assayed for loss of contact inhibition.

Constitutive ErbB4 signaling does not induce anchorage-independent growth

Next, we investigated whether the increased phophorylation and kinase activity of the constitutively-active ErbB4 mutants induced anchorage-independent growth of FR3T3 fibroblasts. Infected FR3T3 cells were seeded at a density of 2 x 10^4 cell per 60 mm dish in medium containing 0.3% LMP-agarose and cells were incubated for 10 days. Fresh medium (DMEM/10% FBS) containing LMP-agarose was added every three days and photographs were taken of representative fields.

Cells that express ErbB2* exhibit anchorage-independent growth (Figure 3.7). In contrast, cells that were infected with the vector control and cells that express wild-type ErbB4 or the ErbB4 mutants did not exhibit anchorage-independent growth. The results of this assay are consistent with the results of the focus formation assay; both assays indicated that the constitutively-active ErbB4 mutants do not oncogenically transform the growth of FR3T3 fibroblasts.

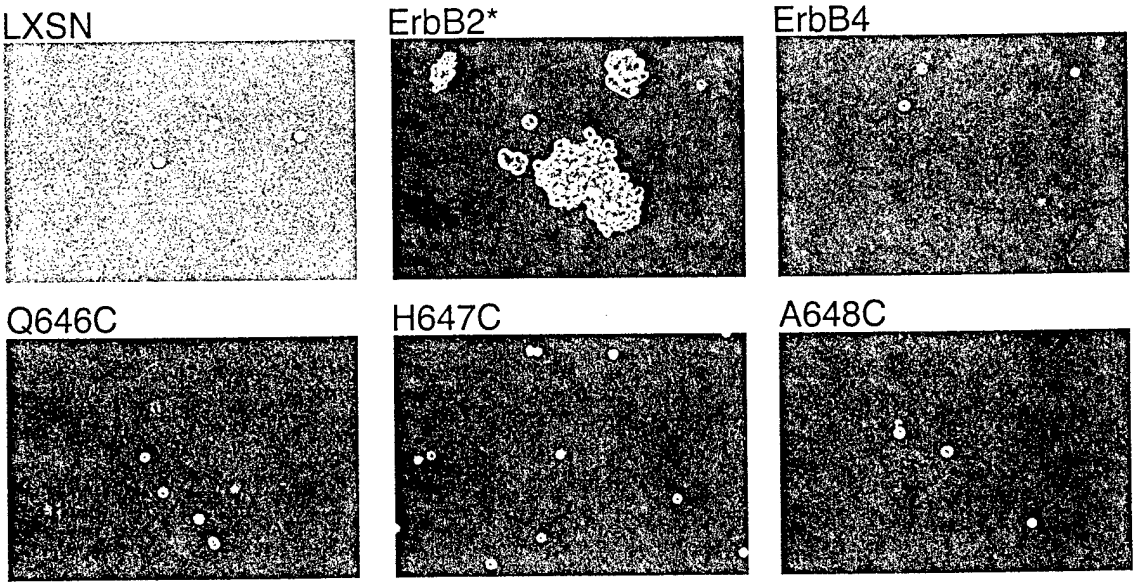

Figure 3.7 **Constitutively-active ErbB4 receptors do not induce growth in soft agar.** Infected FR3T3 cells expressing vector, ErbB2*, or the receptor mutants (Q646C, H647C, A648C) were seeded in semi-solid medium at a density of 2 x 10^4 cell per 60 mm dish. The cells were incubated for 10 days and fields were photographed. Figures shown are representative of three independent experiments.

Constitutive ErbB4 signaling does not increase the growth rate or saturation density of cells

Constitutive ErbB2* signaling is coupled to increased growth rates and saturation densities in fibroblasts (Hynes and Stern, 1994). Thus, we assessed whether the constitutively-active ErbB4 mutants affected the growth rate or saturation density of FR3T3 fibroblasts. The FR3T3 cell lines described earlier were seeded in 60 mm dishes at a density of 2×10^4 cells per dish. Cells were incubated for 10 days to permit growth. During this period cells were counted every twenty-four hours.

The results of this experiment are shown in Figure 3.8. The growth rate of the cells that express ErbB2* is slightly greater than the growth rates of the other cell lines. Note that the growth rates of the cells that express the constitutively-active ErbB4 mutants are indistinguishable from the growth rates of cell lines that express wild-type ErbB4 or the vector control.

The saturation densities for the six cell lines are shown in Table 3.3. Again, note that the saturation density of the cell line that express ErbB2* is higher than the saturation densities of the other cell lines. Moreover, the saturation densities of the cell lines that express the ErbB4 mutants are not markedly higher than the saturation densities of the vector control cell line or the cell line that expresses wild-type ErbB4. Once again, these data suggest that constitutive ErbB4 signaling does not oncogenically transform the growth of fibroblasts.

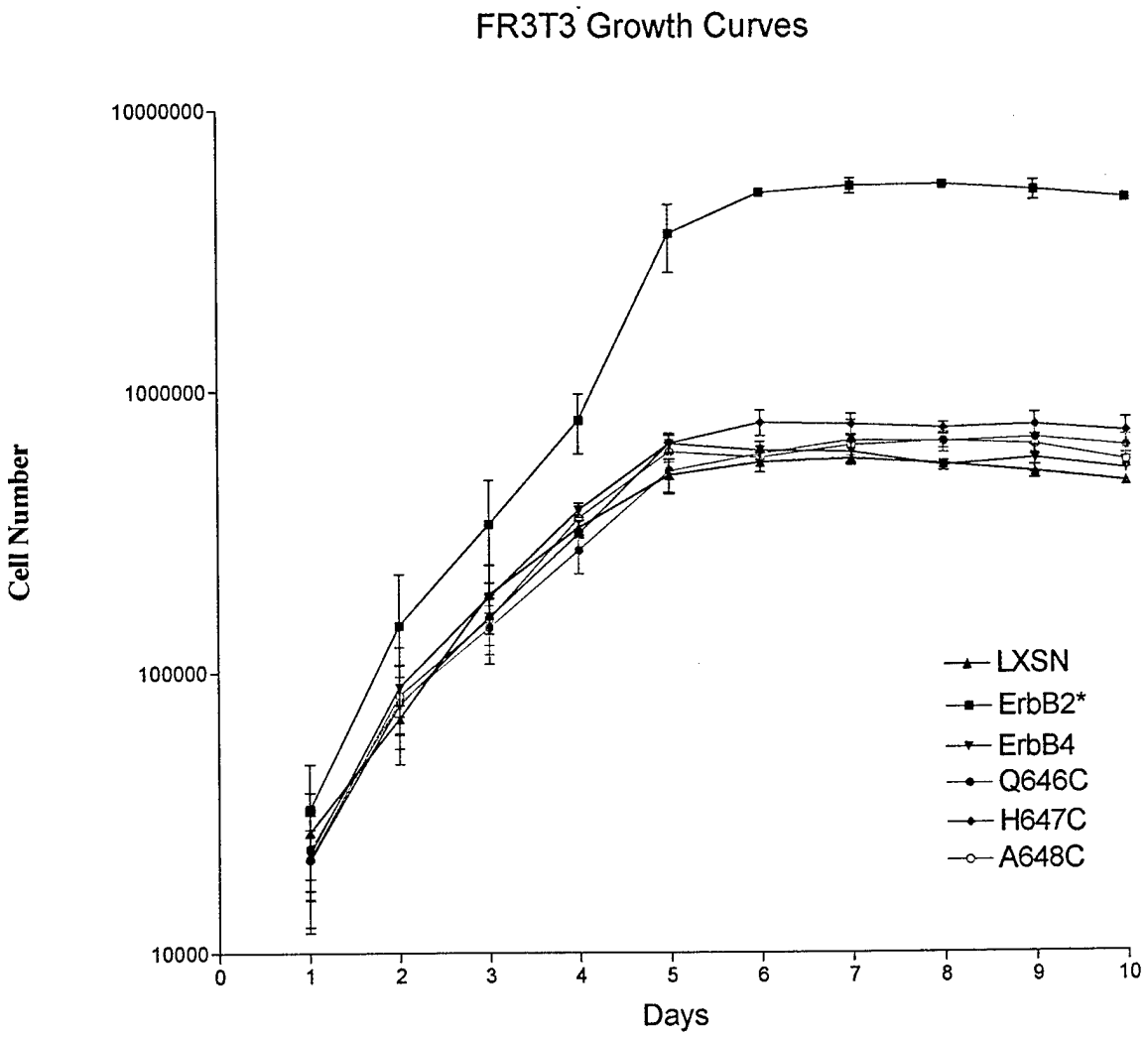

Figure 3.8 **Growth curves of constitutively-active ErbB4 mutant receptors parallel the wild-type ErbB4 receptor.** FR3T3 cells that express the vector control, ErbB2*, wild-type ErbB4, or the receptor mutants (Q646C, H647C, A648C) were plated at a density of 2 x 10^4 cells in 60 mm dishes and allowed to proliferate from one to ten days. Cells were counted daily to assess growth rates and saturation densities. The mean for three experiments is shown with error bars representing the standard error of the mean.

Table 3.3 **Saturation densities of FR3T3 cells expressing constitutively-active ErbB4 receptors.** FR3T3 cells infected with vector alone, ErbB2*, wild-type ErbB4, or the receptor mutants (Q646C, H647C, A648C) were plated at a density of 2×10^4 cells in 60 mm dishes and allowed to proliferate from one to ten days. Cells were counted daily to identify the saturation density for each cell line.

Saturation Densities	
LXSN	$5.8 \pm 0.3 \times 10^5$
ErbB2*	$5.4 \pm 0.1 \times 10^6$
ErbB4	$6.1 \pm 0.5 \times 10^5$
Q646C	$6.6 \pm 0.6 \times 10^5$
H647C	$7.6 \pm 0.7 \times 10^5$
A648C	$6.6 \pm 0.4 \times 10^5$

CHAPTER IV
DISCUSSION

In this report, we show that introducing a cysteine residue in the proximal region of ErbB4 causes constitutive dimerization and signaling by the receptor. We found that mutating any one of three different sites in the extracellular region of ErbB4 causes ligand-independent tyrosine phosphorylation and increased kinase activity. However, we were not able to show that the constitutively-active ErbB4 mutants induce increased proliferation, loss of contact inhibition, or anchorage-independent growth in fibroblasts. These results suggest that increased signaling by ErbB4 homodimers is not sufficient to promote tumorigenesis.

ErbB4 has not been shown to function independently in the progression to metastatic disease. Our results support this hypothesis. Unlike other ErbB family members, ErbB4 appears to be associated with differentiation. Multiple studies are in agreement with this conclusion. An agonistic anti-ErbB4 antibody induces differentiation of cultured MCF-7 breast cancer cells (Chen *et al.,* 1996). Neuregulin, a ligand for ErbB3 and ErbB4, induces branching and differentiation of the mammary epithelium into milk protein-secreting lobuloalveolar structures *in vivo* (Peles *et al.,* 1992; Jones *et al.,* 1996). Higher ErbB4 expression levels are associated with a more differentiated phenotype in breast cancer (Bacus *et al.,* 1996; Kew *et al.,* 2000). Furthermore, ErbB4 activation during late pregnancy is responsible for inducing Stat5 activity (an important mediator of differentiation in mammary epithelium), which regulates differentiation (Jones *et al.,* 1999).

While ErbB4 receptor expression or signaling is observed in a number of differentiated tissues, ErbB4 is overexpressed along with other ErbB family members in malignant tissues (Haugen, *et al.,* 1996; Gilbertson, *et al.,* 1997). ErbB1 or ErbB2

overexpression is associated with aggressive behavior in a wide range of solid tumors including tumors of the breast, ovary, and prostate (Hynes and Stern, 1994). ErbB3 is predominately overexpressed in a subset of human mammary and gastric cancers (Kraus *et al.,* 1989; Sanidas *et al.,* 1993). Finally, overexpression of ErbB4 is observed in a series of ovarian (up to 90%), childhood medulloblastoma, thyroid, breast, and gastric cancers (Gilbertson *et al.,* 1997; Haugen *et al.,* 1996; Kew *et al.,* 2000; Kato, 1998). From these observations we cannot rule out that increased ErbB4 signaling contributes to tumorigenesis or the malignant phenotype.

Indeed, the functional consequences of ErbB4 expression and signaling may depend on many factors. For instance, ErbB family members have dynamic patterns of expression in various organs and tissues and each ErbB family member may require complex interactions with other ErbB family members to specify a cellular response (Yarden and Sliwkowski, 2001). Thus, it is thought that the biological specificity of ErbB4 signaling is defined by the combination of both homo- and hetero-dimeric ErbB receptor complexes formed upon ligand binding (Ferguson et al., 2000). Depending on the cell type, any one of the four ErbB receptors may predominate in heterodimer complexes. Thus, ErbB4 may require heterodimerization with another ErbB family member or may require signaling by another ErbB family receptor to couple to tumorigenesis or the malignant phenotype.

Moreover, ErbB4 homodimers may couple to different cellular responses than do heterodimers of ErbB4. ErbB4 homodimers are biologically active (couple to downstream pathways) and represent naturally occurring signaling entities (Sweeney *et al.,* 2000). One caveat to our analysis of signaling by ErbB4 homodimers is that the biological responses associated with heterodimeric complexes are not seen. Indeed, multiple lines of evidence suggest that the oncogenic potential of ErbB4 is a result of heterodimeric and not homodimeric complexes (Gilbertson *et al.,* 1997). Moreover, malignant growth transformation by ErbB4 has been shown to require co-expression with other ErbB family members, as well as an ErbB receptor ligand (Cohen *et al.,* 1996b). Interestingly, cells that overexpress ErbB1 form tumors in nude mice, whereas co-expression of ErbB1 with ErbB2 in nude mice enhances tumor formation. In contrast,

cells that co-express ErbB4 with ErbB1 were unable to form tumors. In fact, ErbB4 co-expression with ErbB1 reduces the tumorigenic potential of ErbB1 alone (Cohen *et al.*, 1996b). Together, all of these results indicate that ErbB4 does not couple to metastatic disease, but may regulate the oncogenic potential of other ErbB family members.

A related question is whether the three constitutively-active ErbB4 mutants couple to different cellular responses. The simplest prediction is that the Q646C, H647C, and A648C mutants are tyrosine phosphorylated at different sites. Since each cysteine mutation is predicted to be on different face of the receptor, the alignment of a receptor monomer with another receptor monomer may be different for each mutant and may define which tyrosine residues are phosphorylated. Our results are consistent with this model for receptor signaling. Only three of the ErbB4 mutants that were constructed were effectively expressed and tyrosine phosphorylated in Ψ2 cells (data not shown). Dimerization experiments indicate that a cysteine mutation at amino acid 646 may cause receptors to be predominately expressed as dimers (Figure 3.3). A648C displays higher intrinsic kinase activity than Q646C and H647C (Figure 3.5 and Table 3.2). Furthermore, ErbB4 mutants are tyrosine phosphorylated at different levels in monomeric and dimeric states (Figure 3.2 and 3.4). Thus, each cysteine mutation may force the alignment of the kinase domain on one receptor with different phosphorylation sites on the other receptor. As a result, proper alignment of receptor interfaces, possible through disulfide bonds, may differentially phosphorylate tyrosine residues to couple to downstream pathways. Therefore, we purpose that the constitutively-active ErbB4 receptors are not generic in their signaling capabilities. Indeed, further investigation is still needed to identify potential phosphorylation sites responsible for ErbB4 activation.

We hypothesize that our mutants mimic the ligand-activated state of the receptor and are differentially tyrosine phosphorylated. Recent observations indicate that different ligands induce differential ErbB4 tyrosine phosphorylation (Sweeney *et al.*, 2000). Ligand discrimination by the ErbB4 receptor results in differential coupling to intracellular signaling pathways. For example, BTC and NRG1β preferentially stimulate the recruitment of Shc to ErbB4, whereas NRG1β and NRG2β stimulate the recruitment of p85 to ErbB4. In MDA-MB-468 cells, differentially spliced variant of neuregulin

(NRG1β and NRG2β) were found to elicit distinct phosphorylation patterns responsible for recruiting SH2 and PTB domain-containing proteins (Crovello *et al.,* 1998). Furthermore, different ligands may induce different oligomeric states of the receptor. NRG1β has been shown to induce the formation of ErbB4 oligomers that are larger than dimers (Ferguson *et al.,* 2000). These results indicate that ErbB4 ligands induce differential patterns of receptor phosphorylation and oligomeric states that are capable of activating different biological responses.

We believe that the ErbB4 mutants Q646C, H647C, and A648C provide powerful tools for assessing the biological roles played by activated ErbB4 receptors. Until now, receptor cross-talk through multiple combinatorial interaction between ErbB family members has been problematic in studying ErbB4 receptor function. The generation of constitutively-active ErbB4 mutants provides a ligand-independent mechanism for examining the biological responses of ErbB4 activation. More generally, our observations significantly modify the understanding of signaling through the ErbB4 receptor and point to a number of possible models for its function, namely, differentiation or tumor suppression. Unfortunately, we were not able to ascertain the biological roles played by ErbB4 in the context of ligand-independent activation. Indeed, multiple studies suggest that ErbB4 has functional roles in differentiation. Our work supports those suggestions and has laid the groundwork for further investigation of the physiological outcomes of ErbB4 signaling.

LIST OF REFERENCES

LIST OF REFERENCES

Alroy, I., and Yarden, Y. The ErbB signaling network in embryogenesis and oncogenesis: signal diversification through combinatorial ligand-receptor interactions. *FEBS* 410: 83-86, 1997.

Bacus, S.S., Chin, D., Yarden, Y., Zelnick, C.R., and Stern, D.F. Type 1 receptor tyrosine kinases are differentially phosphorylated in mammary carcinoma and differentially associated with steroid receptors. *Am. J. Pathol.* 148: 549-558, 1996.

Bacus, S.S, Zelnick, C.R., Plowman, G., and Yarden, Y. Expression of the erbB-2 family of growth factor receptors and their ligands in breast cancer: implications for tumor biology and clinical behavior. *Am. J. Clin. Pathol.* 102: S13-S24, 1994.

Bargmann, C.I., and Weinberg, R.A. Oncogenic activation of the neu-encoded receptor protein by point mutation and deletion. *EMBO J.* 7: 2043-2052, 1988.

Braakman, I., Helinus, J., and Helinus, A. Manipulating disulfide bond formation and protein folding in the endoplasmic reticulum. *EMBO J.* 11: 1717-1722, 1992.

Bradford, M. A rapid and sensitive method for the quantification of microgram quantities of protein utilizing the principle of protein dye-binding. *Anal. Biochem.* 72: 248-254, 1976.

Burke, C.L., and Stern, D.F. Activation of Neu (ErbB-2) mediated by disulfide bond-induced dimerization reveals a receptor tyrosine kinase dimer interface. *Mol. Cell. Biol.* 18: 5371-5379, 1998.

Chen, X., Levkowitz, G., Tzahar, E., Karunagaran, D., Lavi, S., Ben-Baruch, N., Leitner, O., Ratzkin, B.J., Bacus, S.S., and Yarden, Y. An immunological approach reveals biological differences between the two NDF/Heregulin receptor, ErbB-3 and ErbB-4. *J. Biol. Chem.* 271: 7620-7629, 1996.

Cohen, B.D., Green, J.M., Foy, L., and Fell, H.P. HER4 mediated biological and biochemical properties in NIH 3T3 cells. *J. Biol. Chem.* 271: 4813-4818, 1996a.

Cohen, B.D., Kiener, P.A., Green, J.M., Foy, L., Perry Fell, H., and Zhang, K. The relationship between human epidermal growth-like factor receptor expression and cellular transformation in NIH3T3 cells. *J. Biol. Chem.* 271: 30897-30903, 1996b.

Crovello, C.S., Lai, C., Cantley, L.C., and Carraway, K.L. III. Differential signaling by the epidermal growth factor-like growth factors neuregulin-1 and neuregulin-2. *J. Biol. Chem.* 273: 26954-26961, 1998.

d'Avis, P.Y., Robertson, S.C., Meyer, A.N., Bardwell, W.M., Webster, M.K., and Donoghue, D.J. Constitutive activation of fibroblast growth factor receptor 3 by mutations responsible for the lethal skeletal dysplasia thanatophoric dysplasia type I. *Cell Growth Differ.* 9: 71-78, 1998.

Darcy, K.M., Zangani, D., Wohlhueter, A.L., Huang, R., Vaughan, M.M., Russell, J.A., and Ip, M.M. Changes in ErbB2 (Her-2/neu), ErbB3, and ErbB4 during growth, differentiation, and apoptosis of normal rat mammary epithelial cells. *J. Histochem. Cytochem.* 48: 63-80, 2000.

Elenius, K., Choi, C.J., Paul, S., Santiestevan, E., Nishi, E., and Klagsbrun, M. Characterization of a naturally occurring ErbB4 isoform that does not bind or activate phosphatidyl inositol 3-kinase. *Oncogene* 18: 2607-2615, 1999.

Elenius, K., Corfas, G., Paul, S., Choi, C., Rio, C., Plowman, G.D., and Klagsbrun, M. A novel juxtamembrane domain isoform of HER4/ErbB4. *J. Biol. Chem.* 272: 26761-26768, 1997.

Ferguson, K.M., Darling, P.J., Mohan, M.J., Macatee, T.L., and Lemmon, M.A. Extracellular domains drive homo- but not hetero-dimerization of erbB receptors. *EMBO J.* 19: 4632-4643, 2000.

Galvin, B.D., Hart, K.C., Meyer, A.N., Webster, M.K., and Donoghue, D.J. Constitutive receptor activation by crouzon syndrome mutations in fibroblasts growth factor receptor (FGFR) 2 and FGFR2/Neu chimeras. *PNAS* 93: 7894-7899, 1996.

Gassmann, M., Casagranda, F., Orioli, D., Simon, H., Lai, C., Klein, R., and Lemke, G. Aberrant neuronal and cardiac development in mice lacking the ErbB4 neuregulin receptor. *Nature* 378: 390-394, 1995.

Gerstmayer, B., Groner, B., Wels, W., and Schnierle, B.S. Stable expression of the ecotropic retrovirus receptor in amphotropic packaging cells facilitates the transfer of recombinant vectors and enhances the yield of retroviral particles. *J. Virological Methods* 81: 71-75, 1999.

Gilbertson, R.J., Perry, R.H., Kelly, P.J., Pearson, A.D.J., and Lunec, J. Prognostic significance of HER2 and HER4 coexpression in childhood medulloblastoma. *Cancer Res.* 57: 3272-3280, 1997.

Haugen, D.R., Akslen, L.A., Varhaug, J.E., and Lillehaug, J.R. Expression of c-erbB-3 and c-erbB-4 proteins in papillary thyroid carcinomas. *Cancer Res.* 56: 1184-1188, 1996.

Hwang, E., Riese, D.J. II, Settlemen, J., Nilson, L.A., Honig, J., Flynn, S., and DiMaio, D. Inhibition of cervical carcinoma cell line proliferation by the introduction of a bovine papillomavirus regulatory gene. *J. Virol.* 67: 3720-3729, 1993.

Hynes, N.E., and Stern, D.F. The biology of erbB-2/neu/HER-2 and its role in cancer. *Biochemica et Biophysica Acta.* 1198: 165-184, 1994.

Irusta, P.M., and DiMaio, D. A single amino acid substitution in a WW-like domain of diverse members of the PDGF receptor subfamily of tyrosine kinases causes constitutive receptor activation. *EMBO J.* 17: 6912-6923, 1998.

Jones, F.E., Jerry, D.J., Guarino, B.C., Andrews, G.C., and Stern, D.F. Heregulin induces *in vivo* proliferation and differentiation of mammary epithelium into secretory lobuloalveoli. *Cell Growth Diff.* 7: 1031-1038, 1996.

Jones, F.E., Welte, T., Fu, X., and Stern, D.F. ErbB4 signaling in the mammary gland is required for lobuloalveolar development and stat5 activation during lactation. *J. Cell Biol.* 147: 77-87, 1999.

Kainulainen, V., Sundvall, M., Maatta, J.A., Santiestevan, E., Klagsbrun, M., and Elenius, K. A natural ErbB4 isoform that does not activate phosphoinositide 3-kinase mediates proliferation but not survival or chemotaxis. *J. Biol. Chem.* 275: 8641-8649, 2000.

Kato, T. Expression of mRNA for heregulin and its receptor, ErbB-3 and ErbB-4, in human upper gastrointestinal mucosa. *Life Sci.* 63: 553-564, 1998.

Keilhack, H., Tenev, T., Nyakatura, E., Godovac-Zimmermann, J., Nielsen, L., Seedorf, K., and Bohmer, F.D. Phosphotyrosine 1173 mediates binding of the protein-tyrosine phosphatase SHP-1 to the epidermal growth factor receptor and attenuation of receptor signaling. *J. Biol. Chem.* 273; 24839-24846, 1998.

Kew, T.Y., Bell, J.A., Pinder, S.E., Denley, H., Srinivasan, R., Gullick, W.J., Nicholson, R.I., Blamey, R.W., and Ellis, I.O. c-ErbB-4 protein expression in human breast cancer. *Br. J. Cancer* 82: 1163-1170, 2000.

King, C.R., Borrello, I., Bellot, F., Comoglio, P., Schlessinger, J. Egf binding to its receptor triggers a rapid tyrosine phosphorylation of the erbB-2 protein in the mammary tumor cell line SK-BR-3. *EMBO J.* 7: 1647-1651, 1988.

Knowlden, J.M., Gee, J.W., Seery, L.T., Farrow, L., Gullick, W.J., Ellis, I.O., Blamey, R.W., Robertson, J.R., and Nicholson, R.I. c-erbB3 and c-erbB4 expression is a feature of the endocrine responsive phenotype in clinical cancer. *Oncogene* 17: 1949-1957, 1998.

Kraus, M.H., Issing, W., Miki, T., Popescu, N.C., and Aaronson, S.A. Isolation and characterization of ERBB3, a third member of the ERBB/epidermal growth factor receptor family: evidence for overexpression in a subset of human mammary tumors. *PNAS* 86: 9193-9197, 1989.

Kritzik, M.R., Krahl, T., Good, A., Gu, D., Lai, C., and Fox, H. Expression of ErbB receptors during pancreatic islet development and regrowth. *J. Endocrinol.* 165: 67-77, 2000.

Lee, K., Simon, H., Chen, H., Bates, B., Hung, M., and Hauser, C. Requirement for neuregulin receptor erbB2 in neuronal and cardiac development. *Nature* 378: 394-398, 1995.

Mann, R., Mulligan, R.C., and Baltimore, D. Construction of a retrovirus packaging mutant and its use to produce helper-free defective retrovirus. *Cell* 33: 153-159, 1983.

Miettinen, P.J., Berger, J.E., Meneses, J., Werb, Z., and Derynck, R. Epithelial immaturity and multiorgan failure in mice lacking epidermal growth factor receptor. *Nature* 376: 337-344, 1995.

Miller, D.A., and Buttimore, C. Redesign of retrovirus packaging cell lines to avoid recombination leading to helper virus production. *Mol. Cell. Biol.* 6: 2895-2902, 1986.

Miller, D.A., Rosman, G.J. Improved retroviral vectors for gene transfer and expression. *BioTechniques* 7: 980-990, 1989.

Meyer, D. and Birchmeier, C. Multiple essential functions of neuregulin in development. *Nature* 378: 386-390, 1995.

Olayioye, M.A., Neve, R.M., Lane, H.A., and Hynes, N.E. The ErbB signaling network: receptor heterodimerization in development and cancer. *EMBO J.* 19: 3159-3167, 2000.

Peles, E., Bacus, S.S., Koski, R.A., Lu, H.S., Wen, D., Ogden, S.G., Ben Levy, R., and Yarden, Y. Isolation of the Neu/HER-2 stimulatory ligand: a 44 kd glycoprotein that induces differentiation of mammary tumor cells. *Cell* 69: 205-216, 1992.

Plowmann, G.D., Culouscou, J., Whitney, G.S., Green, J.M., Carlton, G.W., Foy, L., Neubauer, M.G., and Shoyab, M. Ligand-specific activation of HER4/p180erbB4, a fourth member of the epidermal growth factor receptor family. *PNAS* 90: 1746-1750, 1993.

Riese, D.J. II, Bermingham, Y., van Raaij, T.M., Buckley, S., Plowman, G.D., and Stern, D.F. Betacellulin activates the epidermal growth factor receptor and erbB-4 and induces cellular response patterns distinct from those stimulated by epidermal growth factor or neuregulin-β. *Oncogene* 12: 345-353, 1996a.

Riese, D.J. II, Kim, E.D., Elenius, K., Buckley, S., Klagsbrun, M., Plowman, G.D., and Stern, D.F. The epidermal growth factor receptor couples transforming growth factor-α, heparin-binding epidermal growth factor-like factor, and amphiregulin to Neu, ErbB-3, and ErbB-4. *J. Biol. Chem.* 271: 20047-20052, 1996b.

Riese, D.J. II, Komurasaki, T., Plowman, G.D., and Stern, D.F. Activation of ErbB4 by the bifunctional epidermal growth factor family hormone epiregulin is regulated by ErbB2*. *J. Biol. Chem.* 273: 11288-11294, 1998.

Riese, D.J. II, Van Raaij, T.M., Plowman, G.D., Andrews, G.C., and Stern, D.F. The cellular response to neuregulins is governed by complex interactions of the erbB receptor family. *Mol. Cell. Biol.* 15: 5770-5776, 1995.

Riethmacher, D., Sonnenberg-riethmacher, E., Brinkmann, V., Yamaai, T., Lewin, G.R., and Birchmeier, C. Severe neuropathies in mice with targeted mutations in the ErbB3 receptor. *Nature* 389: 725-730, 1997.

Sambrook, J., and Russel, D.W. Molecular cloning a laboratory manuel. Cold Springs Harbor, New York: Cold Springs Harbor Labortory Press, 2001.

Sanidas, E.E., Filipe, M.I., Linehean, J., Lemoine, N.R., Gullick, W.J., Rajkumar, T., and Levinson, D.A. Expression of the c-erbB-3 gene product in gastric cancer. *Int. J. Cancer* 54: 935-940, 1993.

Sawyer, C., Hiles, I., Page, M., Crompton, M., and Dean, C. Two erbB-4 transcripts are expressed in normal breast and in most breast cancers. *Oncogene* 17: 919-924, 1998.

Schlessinger, J. Cell signaling by receptor tyrosine kinases. *Cell* 103; 211-225, 2000.

Schroeder, J.A., and Lee, D.C. Dynamic Expression and activation of ERBB receptors in the developing mouse mammary gland. *Cell Growth Diff.* 9: 451-464, 1998.

Sepp-Lorenzino, L., Eberhard, I., Ma, Z., Cho, C., Serve, H., Liu, F., Rosen, N., and Lupu, R. Signaling transduction pathways induced by heregulin in MDA-MB-453 breast cancer cells. *Oncogene* 12: 1679-1687, 1996.

Sibilia, M., and Wagner, E.F. Strain-dependent epithelial defects in mice lacking the EGF receptor. *Science* 269: 234-238, 1995.

Siegel, P.M., and Muller, W.J. Mutations affecting conserved cysteine residues within the extracellular domain of Neu promotes receptor dimerization and activation. *PNAS* 93: 8878-8883, 1996.

Slamon, D.J., Clark, G.M., Wong, S.G., Levin, W.J., Ullrich, A., and McGuire, W.L. Human breast cancer: correlation of relapse and survival with amplification of HER-2/neu oncogene. *Science* 235: 177-182, 1987.

Sorkin, A., Lemmon, M.A., Ulrich, A., and Schlessinger, J. Stabilization of an active dimeric form of the epidermal growth factor receptor by introduction of an inter-receptor disulfide bond. *J. Biol. Chem.* 269: 9752-9759, 1994.

Southern, P.J., and Berg, P. Transformation of mammalian cells to antibiotic resistance with a bacterial gene under control of the SV40 early region promoter. *J. Mol. Appl. Genetics* 1: 327-341, 1982.

Srinivasan, R., Poulsom, R., Hurst, H.C., and Gullick, W.J. Expression of the c-erbB-4/HER4 protein and mRNA in normal human fetal and adult tissues in a survey of nine solid tumor types. *J. Pathol.* 185: 236-245, 1998.

Stern, D.F., and Kamps, M.P. Egf-stimulated tyrosine phosphorylation of p185neu: A potential model for receptor interactions. *EMBO J.* 7: 995-1001, 1988.

Stern, D.F., Kamps, M.P., and Cao, H. Oncogenic activation of p185neu stimulates tyrosine phophorylation *In vivo*. *Mole. Cell. Biol.* 8; 3969-3973, 1988.

Sweeney, C., Lai, C., Riese, D.J. II, Diamonti, A.J., Cantley, L.C., and Carraway, K.L. III. Ligand discrimination in signaling through an ErbB4 receptor homodimer. *J. Biol. Chem.* 275: 19803-19807, 2000.

Tang, C.K., and Lippman, M.E. EGF family receptors and their ligands in human cancer. *Hormones and Signaling*. Academic Press, San Diego, CA, Vol I: 113-165, 1998.

Threadgill, D.W., Dlugosz, A.A., Hansen, L.A., Tennenbaum, T., Lichti, U., Yee, D., LaMantia, C., Mourton, T., Herrup, K., Harris, R.C., Barnard, J.A., Yuspa, S.H., Coffey, R.J., and Magnuson, T. Targeted disruption of mouse EGF receptor: effects of genetic background on mutant phenotype. *Science* 269: 230-234, 1995.

Ullrich, A., and Schlessinger, J. Signaling transduction by receptors with tyrosine kinase activity. *Cell* 61: 203-212, 1990.

Webster, M.K., and Donoghue, D.J. FGFR activation in skeletal disorders: too much of a good thing. *TIG* 13: 178-182, 1997.

Yang, Y., Spitzer, E., Meyer, D., Sachs, M., Niemann, C., Hartmann, G., Weidner, K.M., Birchmeier, C., and Birchmeier, W. Sequential requirement of hepatocyte growth factor neuregulin in the morphogenesis and differentiation of the mammary gland. *J. Cell Biol.* 131: 215-226, 1995.

Yarden, Y., and Sliwkowski, M.X. Untangling the ErbB signaling network. *Mol. Cell Biol.* 2: 127-137, 2001.

Zang, K., Sun, J., Liu, N., Wen, D., Chang, D., Thomason, A., and Yoshinaga, S.K. Transformation of NIH3T3 cells by HER3 or HER4 receptors requires the presence of HER1 or HER2*. *J. Biol. Chem.* 271: 3884-3890, 1996.

Zimonjic, D.B., Alimandi, M., Miki, T., Popescu, N.C., and Kraus, M.H. Localization of the human HER4/erbB-4 gene to chromosome 2. *Oncogene* 10: 1235-1237, 1995.

APPENDICES

Appendix A

Diagrammatic Representation of Specific Phosphotyrosine Residues and Signaling Molecules For The ErbB Family of Receptor Tyrosine Kinases

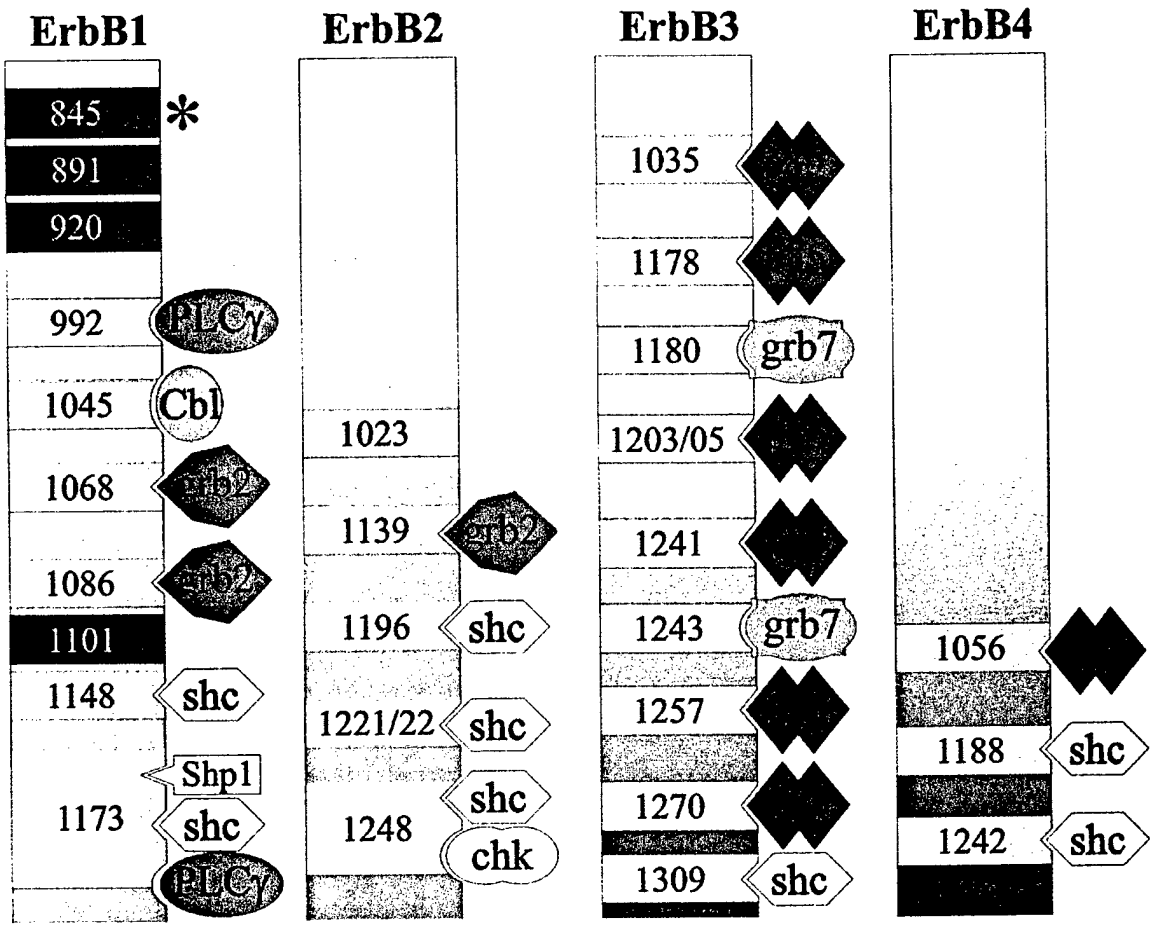

(Reproduced from Olayioye *et al.*, 2000)

Cytoplasmic domains of the four ErbB RTKs are shown. Tyrosine residues that have been identified as autophosphorylation sites are numbered and sites for the Src kinase are indicated in black. Adapter proteins are shown bond to their respective sites. The asterisk represents a tyrosine in the T loop of the kinase domain of ErbB1.

Appendix B

The ErbB Signaling Network

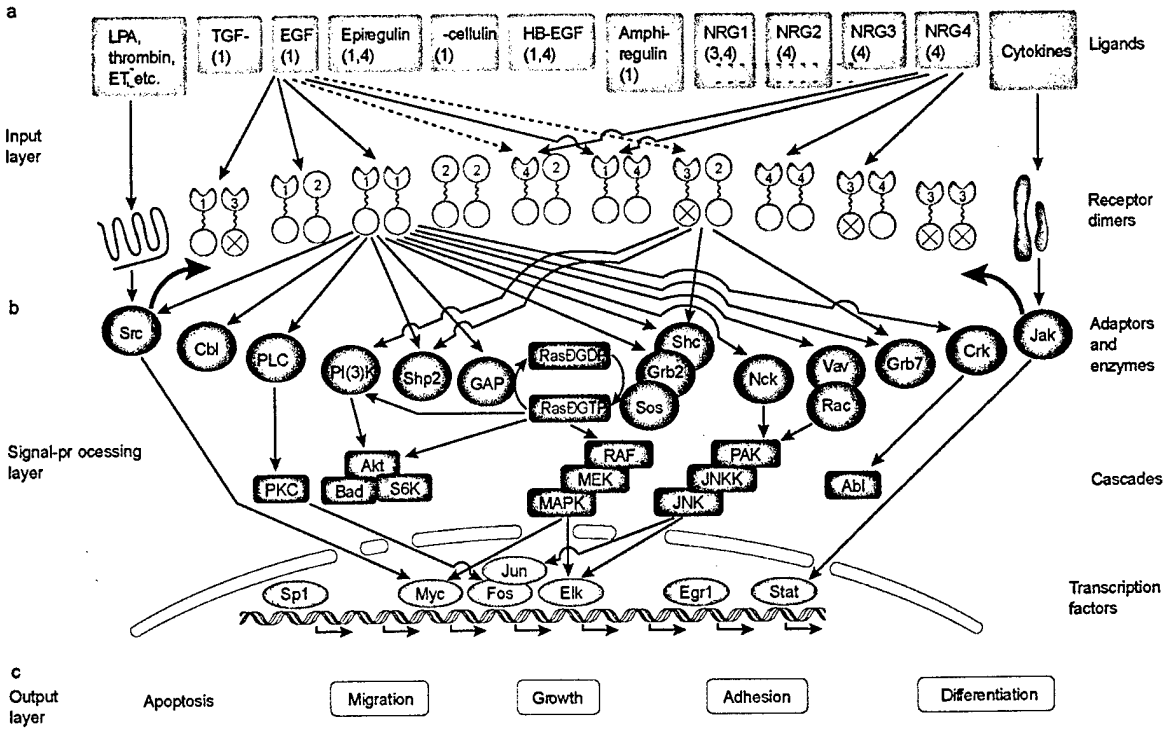

(Reproduced from Yarden and Sliwkowski, 2001)

a. Ligands and the ten dimeric receptor combinations comprise the input layer. Numbers in each ligand block indicate the respective high-affinity ErbB receptors. ErbB2 binds no ligand with high affinity, and ErbB3 homodimers are catalytically inactive (crossed kinase domains). **b.** Signaling to the adaptor layer, only some of the transcription factors are represented in this layer. **c.** Signaling to the output layer is poorly understood at present.

Appendix C

ErbB4 Isoforms

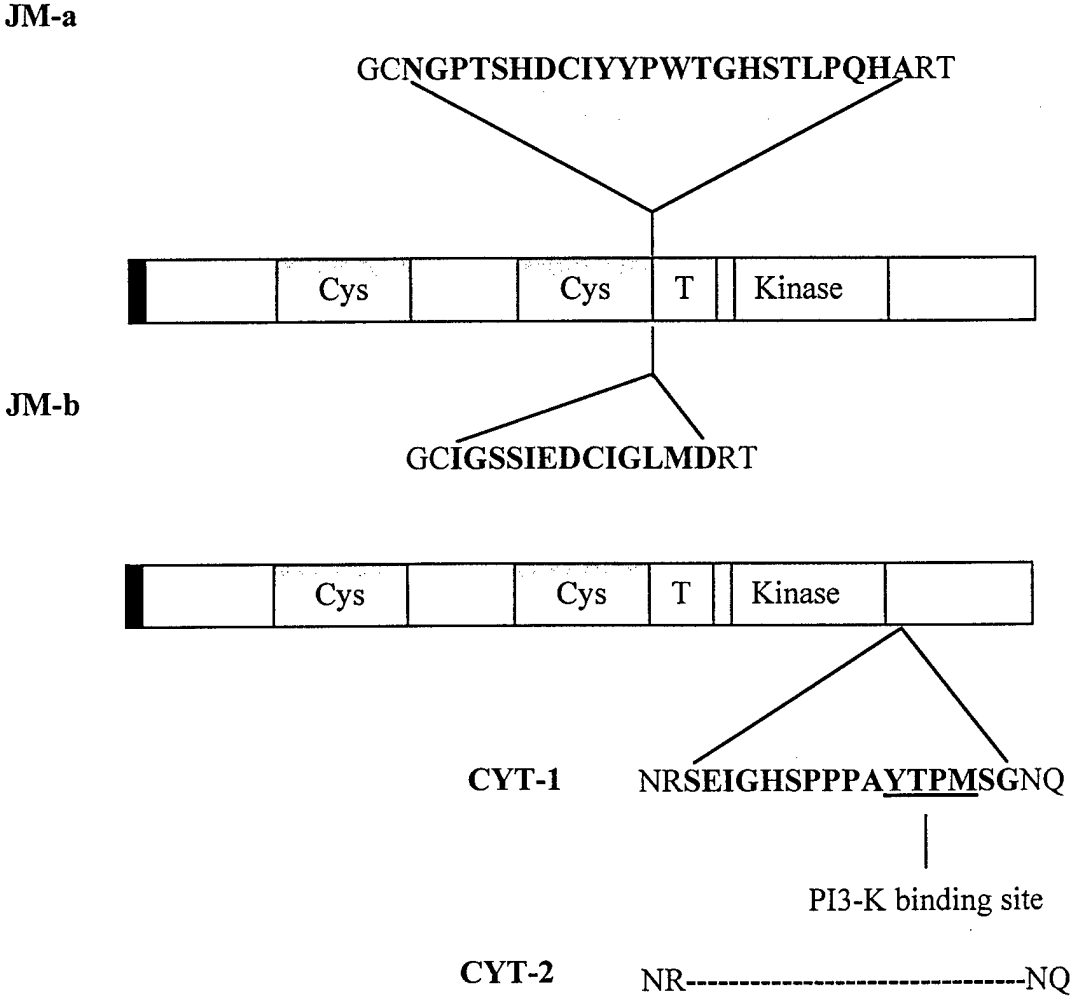

The deduced amino acid sequences of the alternative extracellular juxtamembrane (JM-a and JM-b) and cytoplasmic (CYT-1 and CYT-2) domains of the ErbB4 receptor. JM-a contains a 23 amino acid form, whereas JM-b contains a 13 amino acid form. CYT-1 contains the only PI3-K binding site in ErbB4, isoform CYT-2 does not. JM-a and CYT-1 are identical forms of the ErbB4 receptor. The alternative sequences are in boldface. *Cys*, cysteine-rich domains; *T*, transmembrane domain; *Kinase*, tyrosine kinase domain. (JM isoforms – Elenius *et al.,* 1997; CYT isoforms – Elenius *et al.,* 1999)

Figure 1. Neuregulin2α and Neuregulin2β stimulate ErbB3 signaling, but Neuregulin3 and Neuregulin4 do not.

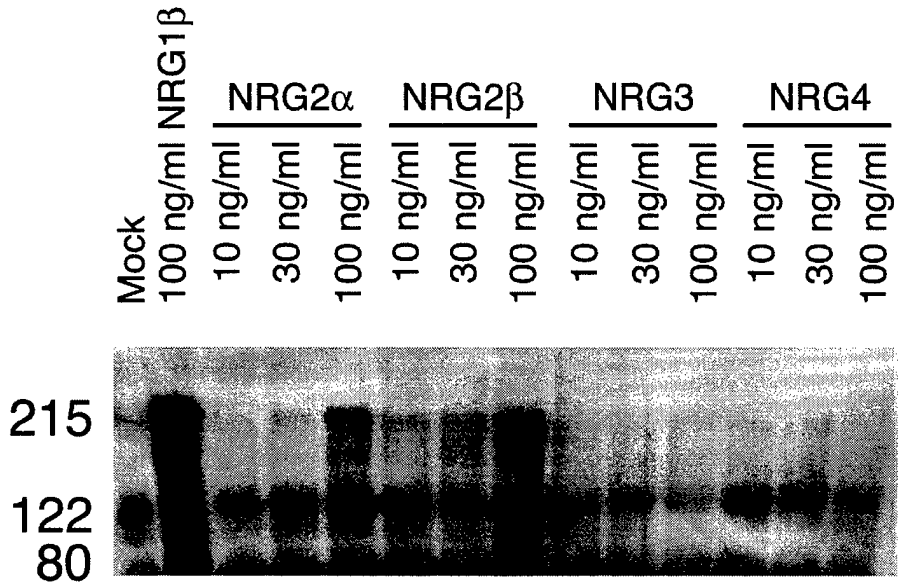

BaF3/ErbB2+ErbB3 Cell Line
ConA-Sepharose Precipitation
Anti-Phosphotyrosine Immunoblot

Figure 2. Neuregulin2 β is a potent ErbB4 agonist, whereas Neuregulin3 and Neuregulin4 are weaker agonists and Neuregulin2α does not stimulate ErbB4 signaling.

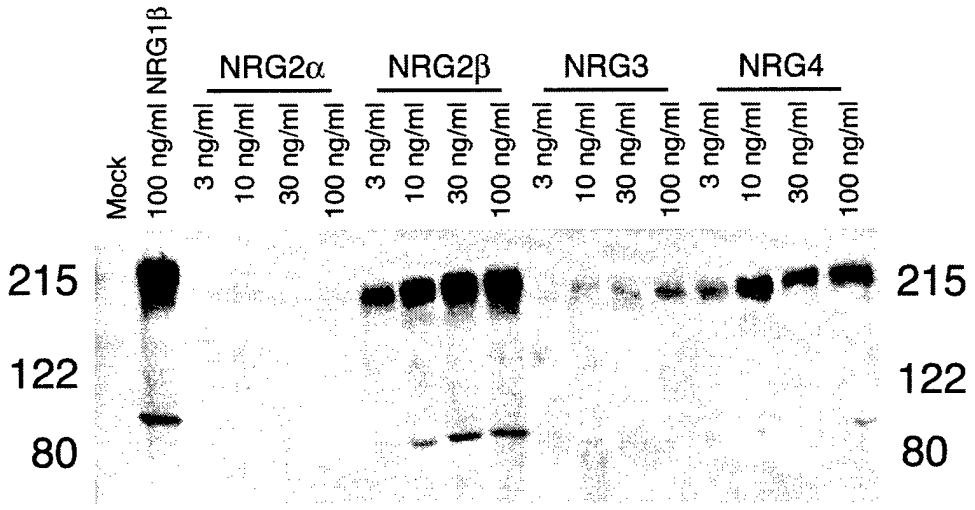

CEM/ErbB4 Cell Line
ConA-Sepharose Precipitation
Anti-Phosphotyrosine Immunoblot

Figure 3. Phenylalanine45 of NRG2β is required for activation of ErbB4 tyrosine phosphorylation by NRG2β.

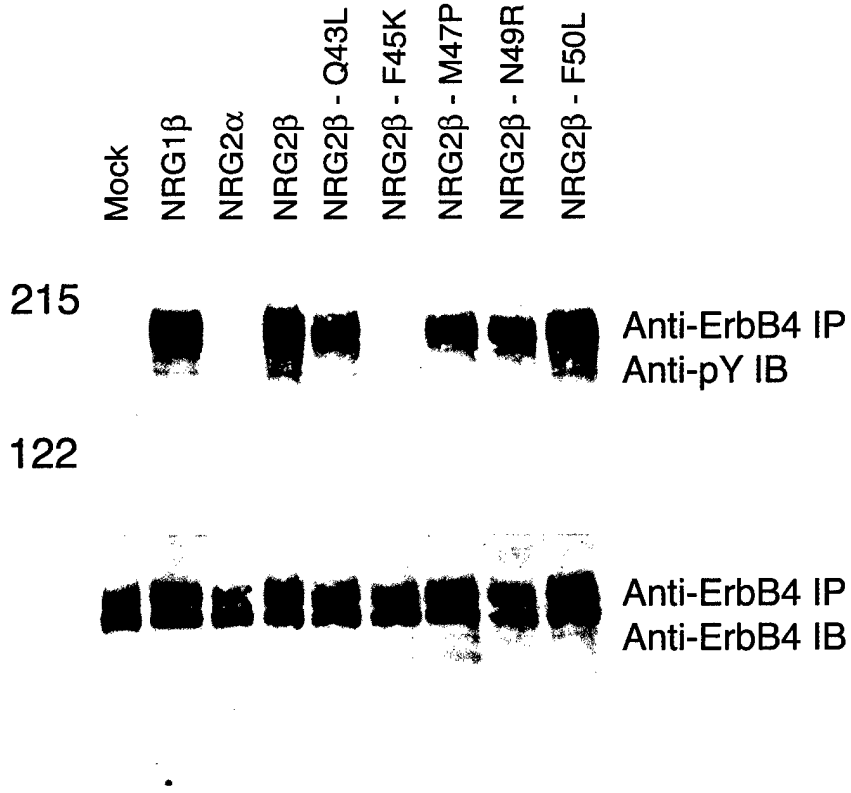

Figure 4. Phenylalanine45 of NRG2β is sufficient for activation of ErbB4 tyrosine phosphorylation by NRG2α.

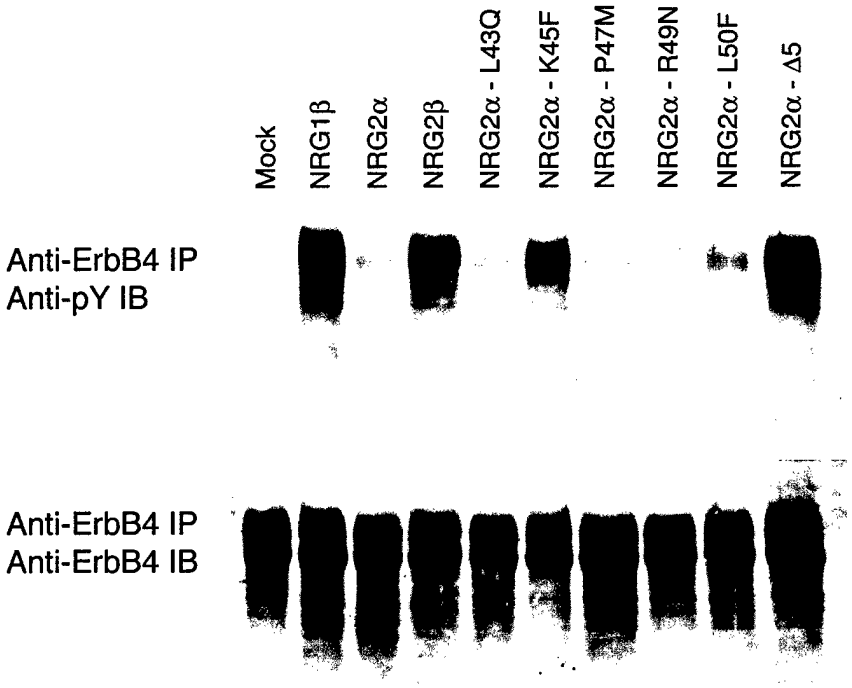

Generation and Validation of a Reagent Suitable for the Isolation of Aptamer Ligands for the ErbB2/HER2/Neu Receptor Tyrosine Kinase

David J. Riese II*†, Christie Denson*, Samin Sajan*, Jennifer Vanderpoel*, Timothy Vortherms*, Andrew Morris*, Sarah Slavik*, Stephanie Coffing*, Robert P. Hammer★, and Douglas Beussman*

*Department of Medicinal Chemistry and Molecular Pharmacology
Purdue University School of Pharmacy and Pharmacal Sciences

★Department of Chemistry
Louisiana State University

Running Title: Method for ErbB2 Aptamer Isolation

† Corresponding Author:
David J. Riese II
1333 RHPH, Room 225
Purdue University School of Pharmacy and Pharmacal Sciences
West Lafayette, IN 47907
Tel: 765-494-6091 FAX: 765-494-1414

Draft Date: 7/23/01 2:36 PM
To be submitted to *Biochemical and Biophysical Research Communications*

Abstract

The ErbB2 (HER2/Neu) receptor tyrosine kinase is overexpressed in a significant fraction of breast tumors, where it correlates with increased tumor cell proliferation, metastasis, and chemoresistance. Consequently, we want to generate oligodeoxynucleotide (aptamer) ErbB2 ligands and antagonists. The SELEX *in vitro* strategy for selecting targeted aptamers is well established. Key prerequisites include the generation of a suitable target and the identification of conditions for aptamer selection. Here we describe the expression, characterization, and use of the recombinant ErbB2 extracellular domain (s-ecErbB2). We describe the strategy for s-ecErbB2 expression, purification, and quantification. We demonstrate that s-ecErbB2 retains at least some of the binding epitopes present in native ErbB2. Finally, we use Chg5For, a low-affinity oligodeoxynucleotide ligand for s-ecErbB2, to demonstrate aptamer elution from immobilized s-ecErbB2 and aptamer amplification following recovery. Therefore, in this work we describe a reagent and experimental procedures that should permit identification of ErbB2 aptamer ligands.

Introduction

ErbB2 (HER2/Neu) is a member of the ErbB family of receptor tyrosine kinases, a family that also includes the Epidermal Growth Factor Receptor (EGFR/ErbB1), ErbB3/HER3, and ErbB4/HER4 [Reviewed in 1]. Deregulated signaling by ErbB2 plays a critical role in human tumorigenesis, tumor cell invasiveness and metastasis, and tumor chemoresistance. For example, ErbB2 is overexpressed in approximately 30% of breast tumors. Moreover, this overexpression, which causes constitutive signaling by ErbB2, correlates with increased tumor metastasis, reduced response to chemotherapy, and poorer patient prognosis [Reviewed in 2-10].

There has been significant interest in the development of agents that target ErbB2. Such molecules hold promise as tumor diagnostic or staging agents (by detecting ErbB2 overexpression) and as chemotherapeutics (by disrupting ErbB2 function). Unfortunately, there are no naturally occurring ligands for ErbB2 that could be used as a starting point for the design of synthetic ErbB2 ligands. However, antibodies specific for ErbB2 are available and some of these can be used in immunohistochemistry to assess ErbB2 expression levels in sections of tumor biopsies [11]. Furthermore, a "humanized" anti-ErbB2 monoclonal antibody (Herceptin) that binds to the ErbB2 extracellular domain and stimulates ErbB2 turnover and down-regulation from the cell surface is being used as a breast cancer therapy [Reviewed in 12-16].

However, there are drawbacks to antibodies as therapeutics. One of the fundamental problems is that antibodies must be "humanized" in order to avoid anti-isotypic immune responses to the antibody in the patient. This is typically achieved by replacing the antibody Fc domain and all of the variable domains save the complementarity determining regions (CDR) with corresponding sequences from generic human IgG heavy and light chains. This is not entirely straightforward, however, because in some antibodies the antigen-binding domain

extends beyond the CDR. Moreover, this process does not necessarily eliminate anti-idiotypic immune responses to the humanized antibody. While the Herceptin "humanized" chimeric mouse-human antibody retains high-affinity binding to human ErbB2 as well as cytotoxicity against tumor cells that overexpress ErbB2 [17], Herceptin still appears to elicit anti-idiotypic immune responses (chills, fever, flu-like symptoms) in patients [15]. Moreover, a substantial percentage of women treated with Herceptin develop congestive heart failure. While the molecular mechanism of this ailment has yet to be established, it is reasonable to hypothesize that the congestive heart failure may be the result of an anti-idiotypic immune response to Herceptin [18].

Other factors contribute to the reduced therapeutic efficacy of monoclonal antibodies [Reviewed in 19]. Monoclonal antibodies are large proteins (Herceptin is 148 kDa); consequently, these molecules exhibit slower kinetics of distribution and limited tissue penetration compared to smaller molecules. Moreover, uniform delivery of therapeutic monoclonal antibodies is dependent upon blood supply. Thus, monoclonal antibodies exhibit reduced ability to penetrate tumors, particularly solid tumors.

A final drawback is that it is difficult to screen the large numbers of monoclonal antibodies needed to ensure that a high-affinity ligand for the target protein can be identified. Typically, no more than 10,000 hybridomas are screened for the production of a high-affinity, monoclonal antibody ligand. Furthermore, immunodominance can reduce the number of distinct antibody species expressed by a population of hybridomas, thereby reducing the likelihood that a high-affinity ligand will be identified.

The therapeutic limitations of monoclonal antibodies have led to efforts to develop new strategies for generating ligands for target proteins. Some of the most exciting recent

developments in drug discovery have been advances in the area of drugs that are based on nucleic acids. The discoveries of self-splicing introns in *Tetrahymena* and other catalytic RNAs have led to the realization that small, single-stranded nucleic acids can form stable, three-dimensional structures through intramolecular base pairing. Furthermore, the ease of synthesizing a random oligonucleotide library and of amplifying selected members of this library have led to the development of general strategies for selecting and amplifying synthetic oligonucleotide ligands (SELEX) for a given target [20-23; Reviewed in 24-29]. These strategies have been used to develop high affinity ligands for a number of proteins, including thrombin [22], T4 DNA polymerase [21], and HIV-1 integrase [30] and reverse transcriptase [31].

As therapeutics, aptamers have several theoretical advantages over monoclonal antibodies. Since they are smaller in mass (typically 6 – 10 kDa) than monoclonal antibodies, they should exhibit more rapid kinetics of diffusion and greater tissue penetration. Moreover, aptamers should be less antigenic than monoclonal antibodies and should be less likely to elicit undesired immune responses. Finally, because aptamers can be readily synthesized, screened, and amplified *in vitro*, a library of as many as 10^{13} aptamers can be screened for ligands in a matter of weeks.

Here we describe our efforts to develop a system for isolating single-stranded DNA molecules that bind to the extracellular domain of ErbB2. Furthermore, we describe experiments that use this system to characterize a single-stranded DNA molecule that appears to bind to ErbB2. Thus, our results suggest that we have developed a system that may enable us to develop novel cancer diagnostic and therapeutic agents.

Materials and Methods

Construction of s-ecErbB2 expression plasmid. The insect cell expression plasmid pMT/BiP/V5-HisB was purchased from Invitrogen. This plasmid contains a Drosophila metallothionein promoter as well as segments encoding the BiP secretion signal, a V5 epitope tag, and a hexahistidine epitope tag. The plasmid cDNeu, which contains the full-length human ErbB2 cDNA, was the generous gift of Dr. Gregory Plowman (Sugen). A segment of this clone that encodes the ErbB2 extracellular domain (Thr23 to Pro650 [32]) was amplified by PCR using primers 2For and 2Rev and subcloned into pMT/BiP/V5-HisB between the BiP signal sequence and the epitope tags using the KpnI and SacII restriction enzyme sites. The segment was inserted in frame with the BiP signal sequence and the epitope tags. The resulting plasmid is called pMT-s-ecErbB2. This plasmid was predicted to encode a secreted, epitope-tagged recombinant protein of 663 amino acids, with a molecular weight of approximately 74,900 Da.

Cells and cell culture. S2 Schneider insect cells were purchased from the American Type Culture Collection (ATCC) and were propagated according to ATCC instructions. Fetal bovine serum was purchased from Gemini Bioproducts and Schneider's insect cell culture medium was purchased from Sigma. Serum-free insect cell culture medium was purchased from Gibco/BRL-Life Technologies.

Generation of S2 cells that express s-ecErbB2. S2 cells were co-transfected with 19 μg pMT-s-ecErbB2 and 1 μg pCoHygro (Invitrogen), which expresses the hygromycin resistance gene. The transfection was performed using a calcium phosphate transfection kit according to manufacturer's instructions (Invitrogen). Two days after transfection, cells were transferred to medium containing 300 μg/ml hygromycin B (Calbiochem) to select for stable transformants.

Drug-resistant cells began appearing approximately 10 days after transfection. Once the drug-resistant cells reached saturation density ($1x10^7$ cells/ml), they were transferred into larger volume culture flasks and frozen in liquid nitrogen for archival purposes.

Induction of s-ecErbB2 expression and s-ecErbB2 purification. S2 cells transfected with s-ecErbB2 were seeded at a density of $2x10^6$ cells/ml in a 2 L Erlenmeyer flask containing 1 L of s-ecErbB2 induction medium. This medium consists of serum-free insect cell culture medium supplemented with 0.1% (w/v) Pluronic F-68 (Sigma) and 10 U/ml heparin (Sigma) to reduce cell clumping and supplemented with 1 mM $CuSO_4$ to induce s-ecErbB2 expression from the Drosophila metallothionein promoter. Cells were incubated for five days at 22°C at 100 rpm in a refrigerated shaking incubator (New Brunswick) to permit maximal s-ecErbB2 expression.

The recovery and purification of s-ecErbB2 is facilitated by the fact that more than 90% of the s-ecErbB2 expressed by the insect cells is secreted into the culture medium (data not shown). Following induction with copper sulfate, the cells were recovered from the culture by centrifuging the culture at 1000x g for 20 minutes at 4°C. The culture medium supernatant was decanted into a fresh container and the cells were discarded. The culture medium supernatant was then filtered using a 0.22 μM filter to remove residual cells and other large contaminants. The filtrate was then concentrated approximately 30-fold by ultrafiltration at 4°C using a stirred cell apparatus and a 5000 MWCO filter (Amicon). The filtrate was discarded and the retentate (~30 ml) was dialyzed using a 3,500 MWCO membrane (Pierce) against 5 changes of 2 L phosphate-buffered normal saline (PBS) over a 48 hour period. The recombinant s-ecErbB2 protein contains a carboxyl-terminal hexahistidine epitope tag, which binds a nickel cation. Thus, the s-ecErbB2 was then purified from this concentrated, desalted crude protein preparation by nickel ion affinity chromatography. The affinity chromatography matrix (ProBond –

Invitrogen) was prepared and the affinity chromatography was performed according to manufacturer's instructions. The s-ecErbB2 was eluted from the nickel ion beads using three 25 ml aliquots of 500 mM imidazole (Sigma). The eluate was concentrated 20-fold by ultrafiltration using a stirred cell apparatus and a 5000 MWCO filter (Amicon). The filtrate was discarded and the retentate (~ 4 ml) was dialyzed using a 3,500 MWCO (Pierce) membrane against 5 changes of 2 L PBS over a 48 hour period. The purified protein was then divided into 100 μl aliquots and stored at –80°C until needed.

Analysis of s-ecErbB2 concentration by anti-V5 immunoblotting. A small amount of the purified s-ecErbB2 was resolved by SDS-PAGE on a 12% acrylamide gel. The resolved material was electroblotted onto nitrocellulose (Gelman Sciences) using a tank electroblotter (Hoefer/Amersham/Pharmacia). Non-specific antibody binding to the blot was blocked by incubating the blot for forty-five minutes at room temperature with gentle (100 rpm) shaking in 5% Bovine Serum Albumin (BSA – Sigma) dissolved in TBS-T (Tris-buffered normal saline with 0.05% Tween-20). The blot was then incubated for two hours at room temperature with rocking in an anti-V5 monoclonal antibody (Invitrogen), diluted 1:10,000 in TBS-T supplemented with 5% BSA. The blot was then washed by incubating in 200 ml TBS-T at room temperature with gentle shaking (100 rpm). The blot was washed five times for six minutes each time.

Primary antibody binding was detected by incubating the blot for one hour at room temperature with rocking in a goat anti-mouse antibody conjugated with horseradish peroxidase (Pierce). This secondary antibody was diluted 1:5000 in TBS-T supplemented with 5% milk. The blot was then washed by incubating in 200 ml TBS-T at room temperature with gentle shaking (100 rpm). The blot was washed twelve times for ten minutes each time. Antibody

binding was visualized by enhanced chemiluminescence (ECL – Amersham) according to manufacturer's instructions.

The resulting chemilumigrams were scanned on a Linotype-Hell Jade flatbed scanner at 600 dpi resolution. The bands present in the digitized image were quantified using NIH Image (National Institutes of Health) software. A standard curve of signal versus protein concentration was constructed using known quantities of the recombinant Positope protein (Invitrogen), which contains the same V5 epitope tag as s-ecErbB2. This standard curve was used to quantify the amount of s-ecErbB2 represented by a band. A correction factor of 1.5 was used to adjust for the difference in the mass of s-ecErbB2 (75 kDa) versus the mass of Positope (50 kDa).

s-ecErbB2 immunoprecipitation. Three samples were prepared containing 1 μg s-ecErbB2 (10 μl), dissolved in 500 μl PBS supplemented with 5% (w/v) non-fat dry milk (Carnation) to prevent non-specific antibody binding and 1% Aprotinin (Sigma) to inhibit proteolysis. To one sample 500 ng of an anti-ErbB2 mouse monoclonal antibody (Ab-5, Calbiochem) was added, followed by 2 ul of a rabbit anti-mouse bridging antibody (31188; Pierce) and 35 μl of a 50% (v/v) slurry of Protein A sepharose (Amersham/Pharmacia). To another sample 500 ng of an anti-EGFR mouse monoclonal antibody (528, Santa Cruz Biotechnology) was added, followed by rabbit anti-mouse bridging antibody and Protein A sepharose. A third sample received only rabbit anti-mouse bridging antibody and Protein A sepharose. Both the anti-ErbB2 monoclonal antibody and the anti-EGFR monoclonal antibody recognize the extracellular domain of the appropriate receptor. Previous experiments have demonstrated that these antibodies are specific for the appropriate receptor [Riese, *et al.*, 1995].

One blot was probed with an anti-ErbB2 antibody (Ab-5, Calbiochem; diluted 1:1000 in TBS-T/5% BSA), while the other was probed with an anti-EGFR antibody (528, Santa Cruz Biotechnology; diluted 1:1000 in TBS-T/5% BSA). Primary antibody binding to the immobilized antigens was detected using a goat anti-mouse antibody coupled to horseradish peroxidase (Pierce; diluted 1:5000 in TBS-T/5% milk) and ECL (Amersham) as described earlier. The washes following incubation in primary and secondary antibodies were performed as described earlier.

DNA oligonucleotides. The oligonucleotides 2For, 2Rev, Chg5For, Chg5Up, and Chg5Dn were all synthesized and purified by Integrated DNA Technologies. Chg5Up and Chg5Dn were purified by HPLC, while Chg5For was PAGE purified. The sequence of the oligonucleotides are as follows: 2For, 5'- CTC GAG GGT ACC CAC CCA AGT GTG CAC C -3'; 2Rev, 5'-CTC GAG CCG CGG AGG GCT GGC TCT CTG-3'; Chg5For, 5'- CGG ATT CTT CGG ACA GAG ATG TCA GGA GTT CCT GAT GTT GAA CTT CTA CAT GCC AGA TCC TAA GCA AAG TG -3'; Chg5Up, 5'- CGG ATT CTT CGG ACA GAG –3'; Chg5Dn, 5'- CAC TTT GCT TAG GAT CTG GC –3'.

s-ecErbB2 aptamer binding assay. The s-ecErbB2 aptamer was immobilized on beads by incubating 250 μg s-ecErbB2 with 50 μl of a 50% slurry of washed nickel ion beads (ProBond – Invitrogen). Excess s-ecErbB2 was washed away and the washed beads were stored at 4°C until use. Beads lacking s-ecErbB2 were prepared in parallel. Beads were stored for no more than 1 hour before use. Typically 50 μg s-ecErbB2 bound to the nickel ion beads (data not shown).

The Chg5For deoxynucleotide was radiolabeled with ^{32}P-phosphate at the 5' end using T4 DNA kinase (New England Biolabs) and [γ-^{32}P]-rATP (Amersham) according to

manufacturer's instructions. The labeled oligonucleotide was purified away from the unincorporated radiolabel by column chromatography (ProbeQuant G50 MicroColumns - Amersham) and the specific activity of the radiolabeled oligonucleotide was determined by scintillation counting. Typically, 10 pmoles of Chg5For were radiolabeled using 50 μCi [γ-^{32}P]-rATP to a specific activity of 0.6 Ci/μmol.

Chg5For binding to immobilized s-ecErbB2 was assayed by adding 1 pmole of radiolabeled Chg5For diluted in 200 μl TE to the nickel ion beads coated with 50 μg s-ecErbB2. The sample was incubated 30 minutes at 4°C with rocking. The beads were collected by centrifugation and washed three times with 100 μl ice-cold TE. The beads were suspended in 100 μl TE and the amount of Chg5For bound to the beads was assayed by scintillation counting.

Elution and Recovery of Chg5For From Beads Coated With s-ecErbB2. Eight samples of Chg5For bound to nickel beads coated with s-ecErbB2 were prepared as described earlier, with the exception that at the end of the assay the beads were not suspended in TE nor assayed by scintillation counting. Instead, the samples were incubated for 5 minutes at room temperature in 100 μl deionized water, 200 mM NaCl, 300 mM NaCl, 400 mM NaCl, 500 mM NaCl, 6 M LiCl, 20% acetic acid, or 100 mM glycine, pH 2.5. Following elution, the beads were collected by centrifugation and the eluate was transferred to a fresh tube. Each sample was eluted three times and the eluates were pooled and assayed by scintillation counting. The beads were suspended in 200 μl TE and the Chg5For that remained bound to the beads was assayed by scintillation counting. Elution efficiency was calculated by dividing the amount of radiolabeled Chg5For

eluted from the beads by the total amount of Chg5For present (amount eluted plus the amount remaining bound to the beads).

The Chg5For eluted from the beads by 500 mM NaCl was recovered by first desalting the oligonucleotide solution using a SepPak C-18 cartridge (Waters). The oligonucleotide was eluted from the cartridge with five 1 ml aliquots of 30% acetonitrile in 100 mM TAEB. The Chg5For was recovered from the eluate by vacuum evaporation in a centrifuge (Savant SpeedVac). The recovered Chg5For was dissolved in 100 µl TE and assayed by scintillation counting.

Amplification of Recovered Chg5For. The polymerase chain reaction (PCR) was used to amplify the recovered Chg5For. Roughly one-fourth of the recovered Chg5For was amplified using Deep Vent DNA polymerase (New England Biolabs) and the oligonucleotide primers Chg5Up and Chg5Dn. Chg5For was amplified by 30 cycles of denaturation at 94°C for 30 seconds, annealing at 55°C for 30 seconds, and elongation at 72°C for 30 seconds. A control reaction was performed in the absence of Chg5For template. Reactions were assayed by PAGE on a 10% Acrylamide/TBE gel. The DNA products were stained with ethidium bromide and the gel was photographed using a Polaroid instant film camera.

Results and Discussion

There are a number of reagents that must be developed and validated and experimental conditions that must be identified prior to successfully screening an oligonucleotide library for aptamer ligands for a target of interest. Here we show that we have developed and validated reagents and identified experimental conditions suitable for screening an oligonucleotide library for aptamer ligands for the ErbB2/HER2/Neu receptor tyrosine kinase.

s-ecErbB2 expression and quantification. One key prerequisite for screening aptamers is to acquire the appropriate target protein. We subcloned the portion of the human ErbB2 cDNA that encodes the extracellular domain (Thr23 to Pro650) into the insect cell expression vector pMT/BiP/V5-HisB, resulting in the plasmid pMT-s-ecErbB2. The insert encoding the ErbB2 extracellular domain was cloned in frame and downstream of a BiP secretion signal and in frame and upstream of V5 and hexahistidine epitope tags. Thus, pMT-s-ecErbB2 was predicted to direct the expression of a recombinant, secreted, epitope-tagged form of the ErbB2 extracellular domain. The pMT-s-ecErbB2 plasmid was cotransfected using calcium phosphate into S2 Schneider (*D. melangaster*) cells along with pCoHygro, a plasmid that directs the expression of the hygromycin resistance gene. Transfected cells were selected using hygromycin; the resulting drug-resistant cells were pooled and expanded.

The resulting cell line was treated with copper sulfate for five days to induce s-ecErbB2 expression. The conditioned medium (which contained s-ecErbB2) was recovered, concentrated by ultrafiltration, and desalted by dialysis against PBS. The s-ecErbB2 was isolated by nickel ion affinity chromatography, and the purified s-ecErbB2 was again concentrated by ultrafiltration and desalted by dialysis against PBS. The s-ecErbB2 yield was quantified by anti-V5 immunoblotting (**Figure 1**). Here we show that anti-V5 immunoblotting predominantly detects a

single band of apparent molecular weight of approximately 79,000 Da. The molecular weight of s-ecErbB2 as determined by mass spectrometry is between 78,600 Da and 79,100 Da depending on the buffer (data not shown). Because the predicted molecular weight of s-ecErbB2 is 74,900 Da, it appears that s-ecErbB2 expressed by insect cells is glycosylated. While full-length ErbB2 expressed by mammalian cells is also glycosylated, the post-translational modifications to s-ecErbB2 may not be identical to the modifications of native, full-length ErbB2 expressed by mammalian cells. Finally, immunoblot analysis of a purified, V5-epitope-tagged recombinant protein (Positope; Invitrogen) suggests that the concentration of s-ecErbB2 in our final, concentrated preparation is approximately 1 μg/μl. Additional calculations indicate that our yield of s-ecErbB2 was approximately 5 mg per liter of cultured S2 cells. Other preparations have had yields ranging from 1 mg per liter to 20 mg per liter.

s-ecErbB2 retains binding affinity. Given that the post-translational modifications to s-ecErbB2 may not be identical to the modifications of native, full-length ErbB2 expressed by mammalian cells, we were concerned that s-ecErbB2 lacks epitopes present in native ErbB2. Consequently, we assayed whether an antibody specific for the extracellular domain of native, human ErbB2 precipitated s-ecErbB2. As shown in **Figure 2**, s-ecErbB2 used in excess binds to an anti-ErbB2 antibody, but does not bind to an antibody specific for the extracellular domain of the EGFR.

We also tested whether an antibody specific for the extracellular domain of human ErbB2 bound to s-ecErbB2 immobilized on a nitrocellulose filter. We spotted s-ecErbB2 onto two nitrocellulose filters using a slot blot apparatus. One blot was probed with an antibody specific for the extracellular domain of human ErbB2, while the other blot was probed with an antibody specific for the extracellular domain of human EGFR. These antibodies were also spotted onto

the nitrocellulose filters as controls. As shown in **Figure 3**, the antibody specific for the extracellular domain of human ErbB2 binds to immobilized s-ecErbB2, while the antibody specific for the extracellular domain of human EGFR does not. Both of these experiments suggest that s-ecErbB2 retains the binding specificity of full-length native ErbB2 expressed by human cells. Thus, we predict that molecules that bind to s-ecErbB2 will also bind to the extracellular domain of full-length ErbB2 expressed by human cells.

Identification of an aptamer ligand for s-ecErbB2. We then wished to use s-ecErbB2 to develop the methodologies for screening an oligonucleotide library for ErbB2 aptamers. Such reconstruction experiments require an oligonucleotide ligand for s-ecErbB2, even if this ligand has poor affinity for s-ecErbB2. Consequently, we tested selected oligonucleotides already present in the laboratory (not a library of random oligonucleotides) for binding to s-ecErbB2. We immobilized s-ecErbB2 on nickel beads, then labeled oligonucleotides with ^{32}P-Phosphate on their 5' end using T4 DNA kinase. We incubated the labeled oligonucleotides with the immobilized s-ecErbB2 to permit oligonucleotide binding, washed away unbound oligonucleotide, and assayed the amount of bound oligonucleotide by scintillation counting. Specific oligonucleotide binding to s-ecErbB2 was calculated by dividing the amount of oligonucleotide bound to immobilized s-ecErbB2 by the amount of oligonucleotide binding to nickel beads lacking s-ecErbB2. As shown in **Table 1**, approximately three times more of the oligonucleotide Chg5For binds to nickel beads coated with s-ecErbB2 than binds to nickel beads lacking s-ecErbB2. This suggests that Chg5For is a ligand for s-ecErbB2. Unfortunately, the binding affinity of Chg5For for s-ecErbB2 is not sufficient to permit quantification, nor can we detect Chg5For binding to full-length human ErbB2 expressed on the surface of cultured cells.

Nonetheless, Chg5For is an important tool that we used to develop conditions for screening for s-ecErbB2 aptamers.

Elution and recovery conditions for s-ecErbB2 aptamers. Important steps in the *in vitro* selection of aptamer ligands for a target protein are the elution and recovery of the bound aptamers. The Chg5For oligonucleotide was radiolabeled with ^{32}P-Phosphate on the 5' end and was bound to s-ecErbB2 immobilized on nickel ion beads. The samples were then incubated in several different solutions to identify the optimal elution buffer. The amount of Chg5For oligonucleotide that was eluted was quantified by scintillation counting, as was the amount of Chg5For oligonucleotide that remained bound to the beads. The relative elution efficiency was calculated by dividing the amount of oligonucleotide present in the eluate by the total amount of oligonucleotide.

As shown in **Table 2**, a 500 mM NaCl solution is the most efficient for eluting the radiolabeled Chg5For oligonucleotide from beads coated with s-ecErbB2. However, other elution buffers, including 300 mM NaCl, 400 mM NaCl, and 6 M LiCl, also appear to be efficient at eluting Chg5For. In contrast, a number of buffers, including 20% acetic acid and 100 mM glycine, are inefficient at eluting Chg5For. Following elution, the Chg5For oligonucleotide was desalted using a SepPak C18 cartridge and recovered from the C18 eluate by simple evaporation. Approximately 70% of the Chg5For oligonucleotide that was eluted from the beads coated with s-ecErbB2 was recovered in this manner (data not shown).

The next step in our proposed strategy for screening oligonucleotide libraries for aptamer ligands for s-ecErbB2 involves amplifying the recovered selected oligonucleotides in preparation for another cycle of selection using the beads coated with s-ecErbB2. Consequently, we wished to establish whether the Chg5For oligonucleotide eluted from the beads coated with s-ecErbB2

could be amplified by PCR. We used the desalted, recovered Chg5For oligonucleotide as template and the oligonucleotides Chg5Up and Chg5Dn as primers. A control PCR reaction was performed in the absence of template. As shown in **Figure 4**, the PCR reaction containing the Chg5For oligonucleotide as template yielded a product of between 67 and 76 base pairs. This apparent size corresponds with the predicted length of the Chg5For oligonucleotide (71 bases). In contrast, the PCR reaction performed in the absence of template did not yield this fragment.

To recap, we have generated a reagent and established methodologies suitable for screening an oligodeoxynucleotide library for aptamer ligands for the ErbB2 receptor tyrosine kinase. We have expressed and purified s-ecErbB2, the extracellular domain of ErbB2. We have shown that s-ecErbB2 shares epitopes with native ErbB2, validating s-ecErbB2 as a target. We have identified Chg5For, a low affinity aptamer ligand for s-ecErbB2. This molecule has enabled us to identify conditions for eluting aptamer ligands bound to immobilized s-ecErbB2, as well as conditions for recovering and amplifying the eluted aptamers. Consequently, we are now positioned to begin screening oligodeoxynucleotide libraries for ErbB2 aptamers.

Acknowledgments

This work was supported by grants from the USAMRMC BCRP (DAMD17-00-1-0415 & DAMD17-00-1-0416 to D.J.R.), NIH/NCI (CA80770 to D.J.R. & CA85049 to R.P.H.), the Showalter Trust, the Indiana Elks Foundation, and the Carroll County (Indiana) Cancer Association. Support from an American Cancer Society Institutional Research Grant to the Purdue Cancer Center (IRG-58-006-40) is also gratefully acknowledged.

References

1. Prigent, S.A., and Lemoine, N.R. (1992). The type I (EGFR-related) family of growth factor receptors and their ligands. *Prog. Growth Factor Res.* **4**, 1-24.
2. Hynes, N.E. and Stern, D.F. (1994). The biology of erbB-2/neu/Her-2 and its role in cancer. *Biochim. Biophys. Acta* **1198**, 165-184.
3. Earp, H.S., Dawson, T.L., Li, X., and Yu, H. (1995). Heterodimerization and functional interaction between EGF receptor family members: a new signaling paradigm with implications for breast cancer research. *Breast Cancer Res. Treat.* **35**, 115-132.
4. Lupu, R., Cardillo, M., Harris, L., Hijazi, M., and Rosenberg, K. (1995). Interaction between erbB-receptors and heregulin in breast cancer tumor progression and drug resistance. *Sem. Cancer Biol.* **6**, 135-145.
5. Ravdin, P.M. and Chamness, G.C. (1995). The c-erbB2 proto-oncogene as a prognostic and predictive marker in breast cancer: a paradigm for the development of other macromolecular markers - a review. *Gene* **159**, 19-27.
6. Mendelsohn, J. and Fan, Z. (1997). Epidermal growth factor receptor family and chemosensitization. *J. Natl. Cancer Inst.* 89, 341-343.
7. Gullick, W.J., and Srinivasan, R. (1998). The type I growth factor receptor family: new ligands and receptors and their role in breast cancer. *Breast Cancer Res. Treat.* **52**, 43-53.
8. Mehigan, B.J., and Kerin, M.J. (1999). The HER-2/neu story: from oncogene through prognostic marker to therapeutic strategy determinant and monoclonal therapy. *Eur. J. Surg. Onc.* **25**, 111-112.
9. Hung, M.-C., and Yu, D. (2000). Role of ErbB2 in breast cancer chemosensitivity *Bioessays* **22**, 673-680.
10. Menard, S., Tagliabue, E., Campiglio, M., and Pupa, S.M. (2000). Role of HER2 gene overexpression in breast carcinoma. *J. Cellular Phys.* **182**, 150-162.
11. Slamon, D.J., Godolphin, W., Jones, L.A., Holt, J.A., Wong, S.G., Keith, D.E., Levin, W.J., Stuart, S.G., Udove, J., Ullrich, A., and Press, M.F. (1989). Studies of the HER2/Neu proto-oncogene in human breast and ovarian cancer. *Science* **244**: 707-712.
12. Cohen, R.L. (1999). Herceptin: Breaking new ground. *Cancer Biother. Radiopharm.* **14**, 1-4.

13. Dillman, R.O. (1999). Perceptions of Herceptin: A monoclonal antibody for the treatment of breast cancer. *Cancer Biother. Radiopharm.* **14**, 5-10.
14. Goldenberg, M.M. (1999). Trastuzumab, a recombinant DNA-derived humanized monoclonal antibody, a novel agent for the treatment of metastatic breast cancer. *Clin. Therapeutics* **21**, 309-318.
15. Perry, C.M., and Wiseman, L.R. (1999). Trastuzumab. *Biodrugs* **12**, 129-135.
16. Albanell, J., and Baselga, J. (1999). Trastuzumab, a humanized anti-HER2 monoclonal antibody, for the treatment of breast cancer. *Drugs of Today* **35**, 931-946.
17. Carter, P., Presta, L., Gorman, C.M., Ridgway, J.B.B., Henner, D., Wong, W.L.T., Rowland, A.M., Kotts, C., Carver, M.E., and Shepard, H.M. (1992). Humanization of an anti-p185HER2 antibody for human cancer therapy. *Proc. Natl. Acad. Sci. USA* **89**, 4285-4289.
18. Feldman, A.M., Lorell, B.H., and Reis, S.E. (2000). Trastuzumab in the treatment of metastatic breast cancer. *Circulation* **102**, 272-274.
19. Breedveld, F.C. (2000). Therapeutic monoclonal antibodies. *Lancet* **355**, 735-740.
20. Ellington, A.D., and Szostak, J.W. (1990) *In vitro* selection of RNA molecules that bind specific ligands. *Nature* **346**, 818-822.
21. Tuerk, C., and Gold, L. (1990). Systematic evolution of ligands by exponential enrichment: RNA ligands to bacteriophage T4 DNA polymerase. *Science* **249**, 505-510.
22. Bock, L.C., Griffin, L.C., Latham, J.A., Vermaas, E.H., and Toole, J.J. (1992). Selection of single-stranded DNA molecules that bind and inhibit human thrombin. *Nature* **355**, 564-566.
23. Ellington, A.D., and Szostak, J.W. (1992) Selection *in vitro* of single-stranded DNA molecules that fold into specific ligand-binding structures. *Nature* **355**, 850-852.
24. Ciesiolka, J., Illangasekare, M., Majerfeld, I., Nickles, T., Welch, M., Yarus, M., and Zinnen, S. (1996). Affinity selection-amplification from randomized ribooligonucleotide pools. *Meth. Enz.* **267**, 315-335.
25. Conrad, R.C., Giver, L., Tian, Y., and Ellington, A.D. (1996). *In vitro* selection of nucleic acid aptamers that bind proteins. *Meth. Enz.* **267**, 336-367.
26. Fitzwater, T., and Polisky, B. (1996). A SELEX primer. *Meth. Enz.* **267**, 275-301.

27. Breaker, R.R.. (1997). DNA aptamers and DNA enzymes. *Curr. Opin. Chem. Biol.* **1**, 26-31.

28. Famulok, M., and Jenne, A. (1998). Oligonucleotide libraries – *variatio delectat. Curr. Opin. Chem. Biol.* **2**, 320-327.

29. Wilson, D.S., and Szostak, J.W. (1999). *In vitro* selection of functional nucleic acids. *Ann. Rev. Biochem.* **68**: 611-647.

30. Mazumder, A., Neamati, N., Ojwang, J.O., Sunder, S., Rando, R.F., and Pommier, Y. (1996). Inhibition of the human immunodeficiency virus type I integrase by guanosine quartet structures. *Biochemistry* **35**, 13762-13771.

31. Tuerk, C., MacDougal, S., and Gold, L. (1992). RNA pseudoknots that inhibit human immunodeficiency virus type I reverse transcriptase. *Proc. Natl. Acad. Sci. USA* **89**, 6988-6992.

32. Yamamoto, T., Ikawa, S., Akiyama, T., Semba, K., Nomura, N., Miyajima, N., Saito, T., and Toyoshima, K. (1986). Similarity of protein encoded by the human c-erbB-2 gene to epidermal growth factor receptor. *Nature* **319**, 230-234.

Table 1. Oligonucleotide Chg5For binding to s-ecErbB2 immobilized on nickel beads and to nickel beads lacking bound protein.

Trial	Beads Lacking Protein	Beads With s-ecErbB2	Ratio
Trial #1	2837	7235	2.550
Trial #2	9383	32238	3.436
Trial #3	3598	5748	1.598
Trial #4	24619	40540	1.647
Trial #5	56837	237094	4.171
		Mean Ratio =	2.680
		Standard Error =	0.450
		t Value =	3.738
		$P < 0.025$ (one tailed)	

Table 2. Elution of oligonucleotide Chg5For from s-ecErbB2 immobilized on nickel beads.

Elution Buffer	% Elution
Water	59.5%
200 mM NaCl	77.2%
300 mM NaCl	90.9%
400 mM NaCl	94.5%
500 mM NaCl	97.5%
20% Acetic Acid	33.6%
6 M LiCl	94.2%
100 mM Glycine	32.6%

Figure 1. Quantification of s-ecErbB2 by anti-V5 immunoblotting.

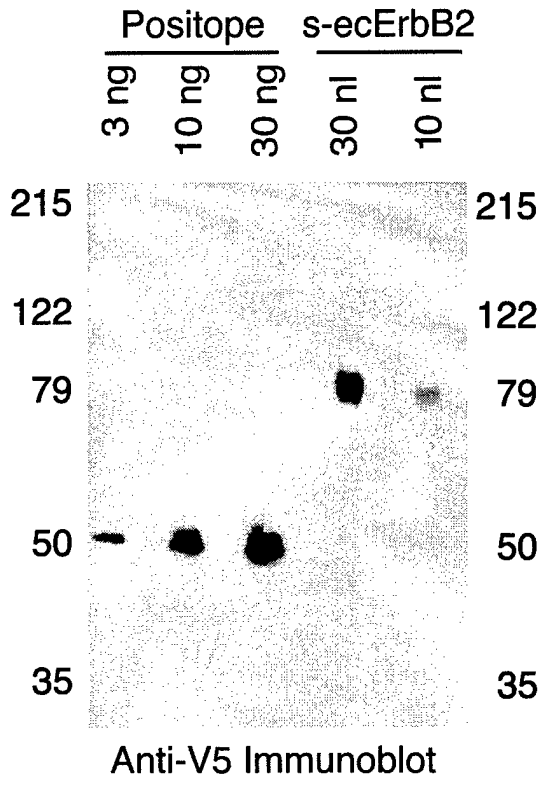

Legend:
The indicated amounts of Positope positive control peptide and purified s-ecErbB2 were resolved by SDS-PAGE on a 12% acrylamide gel. The resolved proteins were electrotransferred onto nitrocellulose. Non-specific antibody binding to the resulting blot was blocked by incubating the blot in 5% BSA, afterwhich the blot was probed with an anti-V5 mouse monoclonal antibody. Primary antibody binding was detected by probing the blot with a goat anti-mouse antibody conjugated to HRP. Secondary antibody binding was visualized by ECL.

Figure 2. An anti-ErbB2 antibody precipitates s-ecErbB2.

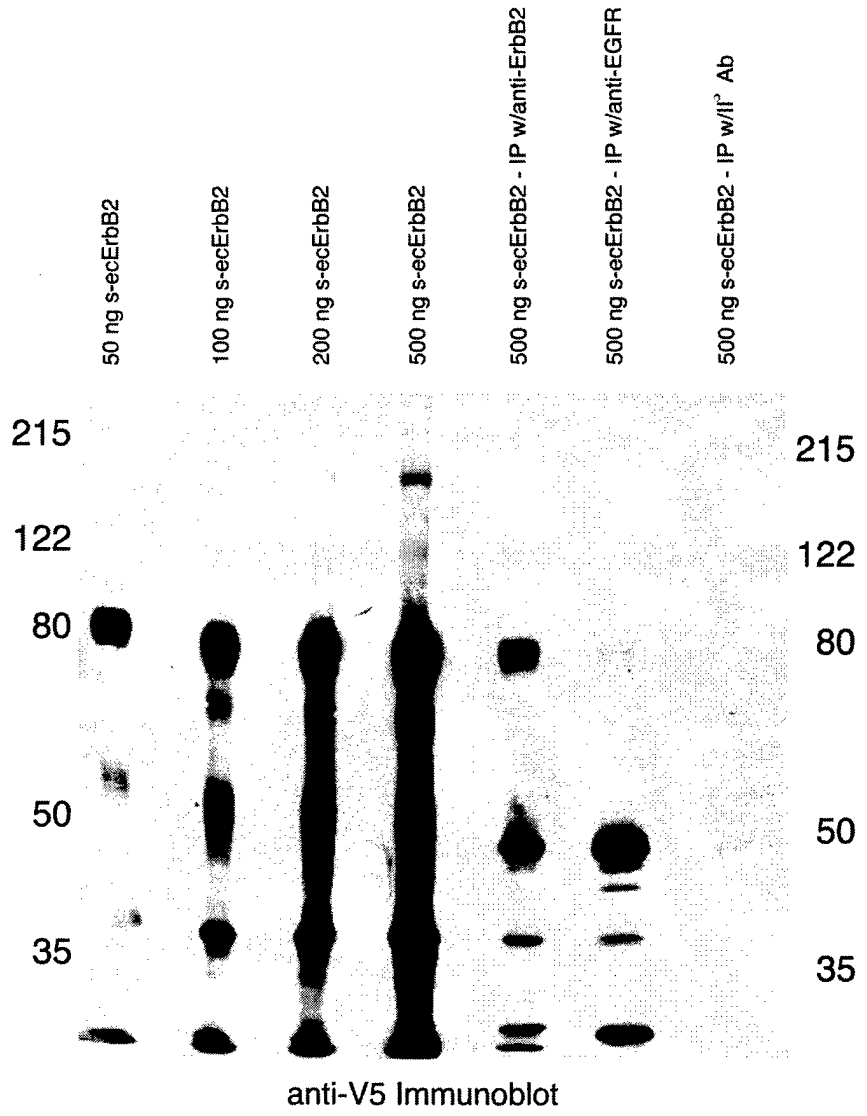

Legend:
Three immunoprecipitations were prepared that included 1 μg s-ecErbB2, a rabbit anti-mouse secondary (bridging) antibody, and protein A-sepharose. One immunoprecipitation also contained an anti-ErbB2 mouse monoclonal antibody that recognizes the extracellular domain of native ErbB2, while another immunoprecipitation contained an anti-EGFR mouse monoclonal antibody that recognizes the extracellular domain of native EGFR. Following incubation to permit complex formation, the immunoprecipitates were washed and the complexes were eluted from the beads by boiling in reducing-SDS protein sample buffer. One-half of each eluate was resolved by SDS-PAGE on a 12% acrylamide gel. As controls, 50-500 ng of s-ecErbB2 were resolved on the same gel. The resolved proteins were electrotransferred onto nitrocellulose. The resulting blot was probed with an anti-V5 antibody to visualize s-ecErbB2 present in the immunoprecipitates. The procedure was as described earlier.

Figure 3. An anti-ErbB2 antibody binds s-ecErbB2 immobilized on nitrocellulose.

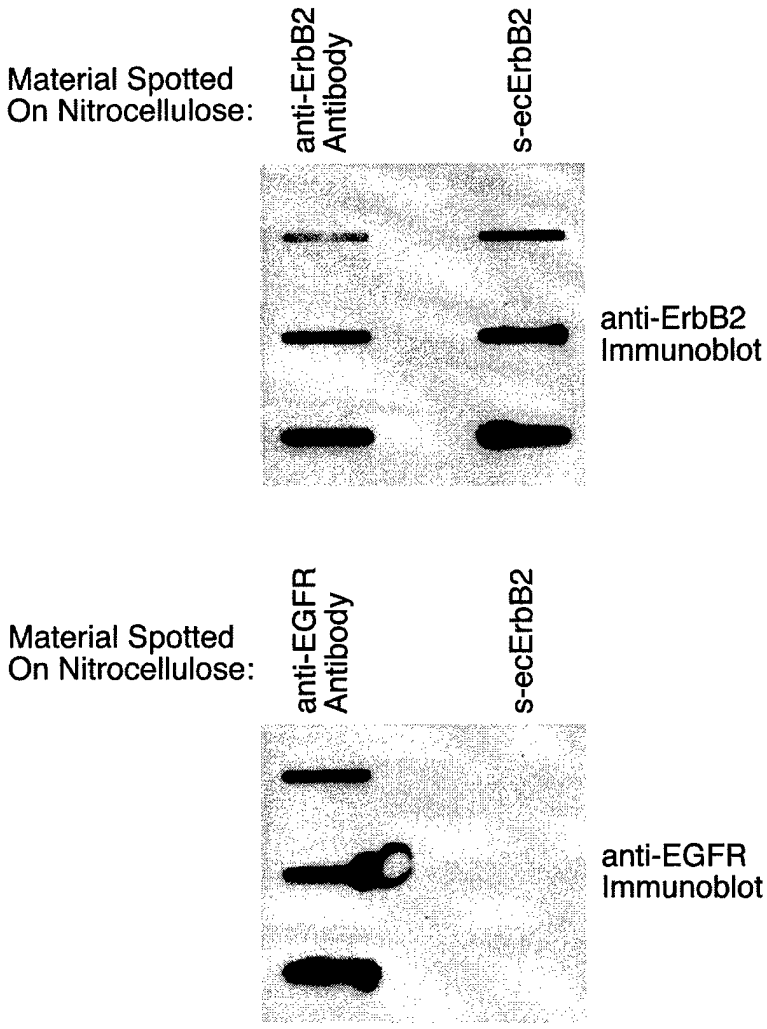

Legend:
One, three, and ten nanograms of s-ecErbB2, an anti-EGFR mouse monoclonal antibody, and an anti-ErbB2 mouse monoclonal antibody were blotted onto nitrocellulose as indicated using a slot blotter. As indicated, one of the resulting blots was probed with an anti-ErbB2 mouse monoclonal antibody, while the other was probed with an anti-EGFR mouse monoclonal antibody. Primary antibody binding was detected by probing the blots with an anti-mouse secondary antibody conjugated to HRP. Secondary antibody binding was visualized by ECL.

Figure 4. Amplification of Chg5For oligonucleotide recovered from s-ecErbB2.

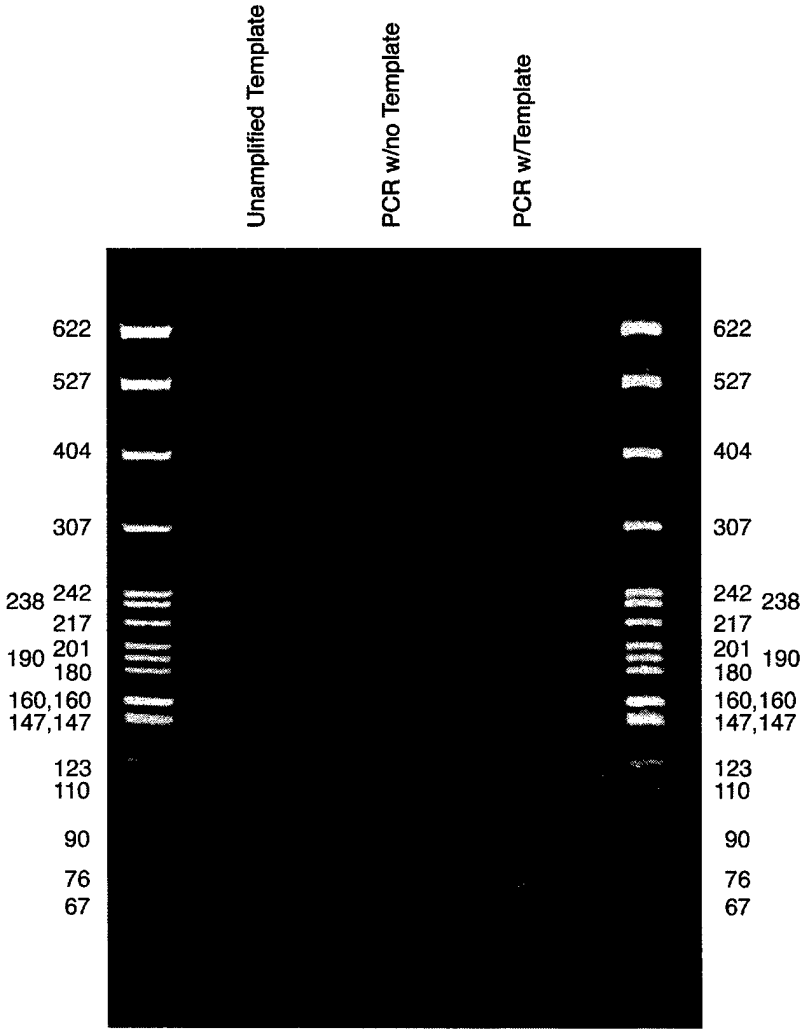

Legend:
Chg5For oligonucleotide recovered from s-ecErbB2 was amplified by PCR using the oligonucleotides Chg5Up and Chg5Dn. Thirty cycles of amplification were performed using the following parameters: incubation at 95°C for 1 minutes to denature the template; incubation at 50°C for 1 minutes to permit primer annealing; and incubation at 72°C for 30 seconds to permit elongation. A PCR reaction was also performed in the absence of template. One-fifth of each reaction was resolved by PAGE using a 10% acrylamide gel. Plasmid pBR322 DNA digested with MspI served as size markers. The length of each marker fragment (in base pairs) is indicated.